«ELECTRICAL ENGINEERING & ELECTROMECHANICS»

SCIENTIFIC & PRACTICAL JOURNAL

Journal was founded in 2002

Founders:

National Technical University «Kharkiv Polytechnic Institute» (Kharkiv, Ukraine)

State Institution «Institute of Technical Problems of Magnetism of the NAS of Ukraine» (Kharkiv, Ukraine)

ISSUE 3/2017

TABLE OF CONTENTS

Editorial office address: Dept. of Electrical Apparatus, NTU «KhPI», Kyrpychova Str., 2, Kharkiv, 61002, Ukraine

phones: +380 57 7076281, +380 67 3594696, **e-mail:** a.m.grechko@gmail.com (**Grechko O.M.)**

ISSN (print) 2074-272X

ISSN (online) 2309-3404

Printed 30.06.2017. Format 60 x 90 ⅛. Paper – offset. Laser printing. Edition 200 copies. Order no.66/172-03-2017.

Printed by Printing house «Madrid Ltd» (11, Maksymilianivska Str., Kharkiv, 61024, Ukraine)

UDC 621.3: 537.8: 910.4 **doi: 10.20998/2074-272X.2017.3.01**

M.I. Baranov

AN ANTHOLOGY OF THE DISTINGUISHED ACHIEVEMENTS IN SCIENCE AND TECHNIQUE. PART 38: NOBEL PRIZE LAUREATES IN PHYSICS FOR 2005-2010

Purpose. Implementation of brief analytical review of the distinguished scientific achievements of the world scientists-physicists, awarded the Nobel Prize in physics for period 2005-2010 yy. Methodology. Scientific methods of collection, analysis and analytical treatment of scientific and technical information of world level in area of modern theoretical and experimental physics. Results. The brief analytical review of the scientific openings and distinguished achievements of scientists-physicists is resulted in area of modern physical and technical problems which were marked by the Nobel Prizes in physics for the period 2005-2010. Originality. Systematization is executed with exposition in the short concentrated form of the known scientific and technical materials, devoted creation of quantum theory of optical coherentness by scientists-physicists, development of laser exact spectroscopy, opening form of spectrum for a black body and anisotropy of space microwave base-line radiation, opening of effect of giant magnetoresistance, opening of mechanism of spontaneous violation of symmetry in subatomic physics, development of new technology of transmission of light in optical fibres, invention of a semiconductor circuit for registration of images and results of innovative experiments on research of 2D material of graphen. Practical value. Popularization and deepening of scientific and technical knowledges for students, engineers and technical specialists and research workers in area of modern theoretical and experimental physics, extending their scientific range of interests and collaboration in further development of scientific and technical progress in human society. References 31, figures 25.

Key words: **modern physics, achievements, quantum theory of optical coherentness, laser overexact spectroscopy, space microwave base-line radiation, effect of giant magnetoresistance, spontaneous violation of symmetry, transmission of light in optical fibres, semiconductor circuit for registration of images, 2D material of graphen.**

Приведен краткий аналитический обзор выдающихся научных достижений ученых мира, отмеченных Нобелевской премией по физике за период 2005-2010 гг. В число таких достижений вошли создание квантовой теории оптической когерентности, развитие лазерной точной спектроскопии, открытие чёрнотельной формы спектра и анизотропии космического микроволнового фонового излучения, открытие эффекта гигантского магнетосопротивления, открытие механизма спонтанного нарушения симметрии в субатомной физике, разработка новой технологии передачи света в оптических волокнах, изобретение полупроводниковой схемы для регистрации изображений и результаты новаторских экспериментов по исследованию двумерного материала графена. Библ. 31, рис. 25.

Ключевые слова: **современная физика, достижения, квантовая теория оптической когерентности, лазерная сверхточная спектроскопия, космическое микроволновое фоновое излучение, эффект гигантского магнетосопротивления, спонтанное нарушение симметрии в субатомной физике, передача света в оптических волокнах, полупроводниковая схема для регистрации изображений, двумерный материал графен.**

Introduction. As is well known, in 1900 the prominent German theoretical physicist Max Planck (1858-1947) developed the quantum theory of the thermal radiation of an absolutely black body (ABB), according to which the heat flux from the ABB contained separate discrete portions (*«quanta»*) of energy [1, 2]. Precisely for the discovery of discrete quanta of «action» (energy) M. Planck in 1918 was awarded the Nobel Prize in physics [1]. In 1905 the quantum theory of thermal radiation of M. Planck was significantly supplemented and developed by another prominent German theoretical physicist Albert Einstein (1879-1955), who extended it to light radiation and introduced the concept of the flux of *«quanta of electromagnetic radiation»* for sunlight or *«photons»* – peculiar quasiparticles without a rest mass [1, 2]. So in physics, the concept of dualism (duality) for light, which was simultaneously a flux of quasiparticles (photons) and a set of electromagnetic waves of various lengths, was introduced. The light radiation having a quantum-wave nature is of a stochastic nature. In this connection, the state of the light field is determined only statistically [3]. Light quanta are characterized by different wavelengths that are not moving in phase. The microstructure of the light field is determined by a huge number of parameters, an exact description of which can not be given. Therefore, previously, it was possible to investigate only certain particular characteristics of the light field (for example, its spectrum and average intensity [3]).

1. Quantum optics and high-precision laser spectroscopy. The Nobel Prize in physics for 2005 was awarded to an outstanding scientist working in the field of modern optics and laser technology [3]: American theoretical physicist Roy Glauber (Fig. 1) – *«for his contribution to the quantum theory of optical coherence,»* to the American experimental physicist John Hall (Fig. 2) and the German experimental physicist Theodor Hansch (Fig. 3) – *«for the development of precision laser spectroscopy, in particular, for the methods of Raman spectroscopy in the optical range.»* In 1963, R. Glauber published in print the method he developed for quantizing the electromagnetic field to calculate the structure of a light field with coherent waves. It should be recalled that the term *«coherence»* comes from the Latin word *«cohaerentia» – «cohesion»* and physically *means «the consistent flow of several oscillatory or wave processes in time, the phase difference of which is constant»* [4]. Waves of light radiation satisfy these requirements. That's

why it is considered coherent. It is the coherence of the waves of light radiation that determines the phenomenon of their *«interference» – «amplification of waves at certain points of space and their attenuation in others, depending on the phase difference of the waves»* [4]. To describe the complex picture of the light field and determine the spatial-temporal distribution of its intensity, he introduced the so-called *«correlation functions»*, which form the basis of the new division of optics – *«quantum optics»* created by R. Glauber [3]. The methods of quantum optics developed by him make it possible to investigate the subtle details of intermolecular interactions in various physical bodies from the change in the indications of several photoreceivers that record the flux of light photons and fluctuations in the light field (the deviation of its intensity from a certain average value) when light is scattered in the medium under consideration.

At present, such a physical device from the field of quantum electronics as a laser [5] has become an indispensable tool for accurate measurements. As is well known, high stability of laser radiation and its monochromaticity contribute to this.

Fig. 1. Prominent American theoretical physicist Roy J. Glauber, born in 1925, Nobel Prize Laureate in physics for 2005

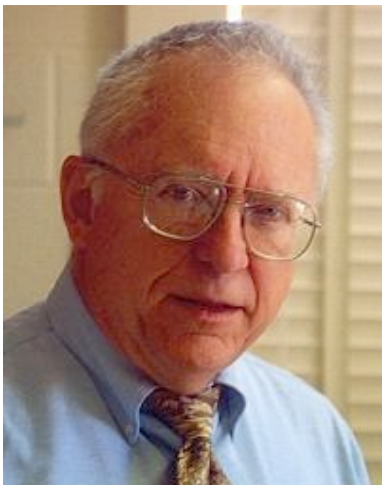

Fig. 2. Prominent American experimental physicist John L. Hall, born in 1934, Nobel Prize Laureate in physics for 2005

Fig. 3. Prominent German experimental physicist Theodor W. Hansch, born in 1941, Nobel Prize Laureate in physics for 2005

Any conventional laser operates in a very narrow frequency band of electromagnetic radiation and is always characterized by a certain frequency. J. Hall and T. Hansch in their scientific studies have shown that to achieve ultra-high accuracy of measurements requires a laser emitting a huge number of light waves with coherent frequencies (modes) [3]. When they are added, a light pulse is formed, the duration of which is shorter the more frequencies participate in its formation. According to their estimates, to obtain, for example, a light pulse with a duration of 5 femtoseconds ($5 \cdot 10^{-15}$ s), it is necessary to add a million frequencies that cover most of the visible light range [3]. Their frequency spectrum form a kind of *«comb»* with *«teeth»*, corresponding to individual frequencies. As a result of such a superposition of electromagnetic waves between the mirrors of the laser cavity [5], short light pulses will appear. Outgoing laser through the semitransparent mirror of its resonator, light will form a sort of «ruler» with fissions in the form of ultrashort light pulses [3]. Such a mode of operation of one of the lasers was obtained by T. Hansh in the 1970s. However, a real scientific breakthrough in increasing the accuracy of measurements occurred in 1999, when lasers with superfine pulses were required to measure the optical frequencies of atomic clocks operating on cesium atoms.

In the case when the measured frequency of the radiation of a microobject (for example, an atom) coincides with one of the frequency *«teeth»* for the considered *«spectral comb»* from this laser, then it is uniquely determined. The physical approach developed by the learned laureates in the field of new applications of laser spectroscopy makes it possible to measure the frequencies of radiation emitted by the atoms of a substance with unprecedented accuracy [3]. Thus, the *«frequency comb»*, formed by a new type of quantum oscillator of stimulated emission of the optical band (laser), has become an effective standard in ultra-precise measurements of atomic radiations.

2. Discovery of the black body spectral shape and the anisotropy of cosmic background microwave radiation. In 2006, one of the most notable scientific

events in world physics was the Nobel Prize to two American radiophysicists George F. Smoot (Fig. 4) and John C. Mather (Fig. 5) *«for the discovery of the equilibrium form of the cosmic background Microwave radiation and its anisotropy»* [6]. In radio astronomy this radiation is also called «cosmic relic radiation» [7]. Relic (this term comes from the Latin word *«relictum»* – *«remnant»* [4]) radiation is a microwave electromagnetic radiation, preserved in space from the early stages of the development of the universe. Note that «cosmic relic radiation» with a wavelength of about 7 cm and a temperature of about 3 K was discovered in 1965 by American experimental physicists Arn Penzias and Robert Wilson (Nobel Prize in physics for 1978 [1]). Then A. Penzias and R. Wilson observed this short-wave electromagnetic background radiation propagating in the cosmic space of the boundless universe, as «electromagnetic noise» in radio telescopes fixed on the surface of our planet, which is unavoidable for these cosmic researchers [1, 7].

Fig. 4. Prominent American radiophysicist George Fitzgerald Smoot, born in 1945, Nobel Prize Laureate in physics for 2006

Their discovery confirmed the «hot» model of the universe [1, 7]. As we know, the era of quantum physics for earthlings was discovered by the prominent German theoretical physicist Max Planck (1858-1947), who in 1900 formulated his famous quantum law of equilibrium thermal radiation for an artificially or naturally heated «absolutely black body» (ABB) [2, 8]. Let us remind the reader that the quantum theory of M. Planck, developed by him for thermal radiation of the ABB, based on the concept of the «quantum of action», which was fundamentally new in physics and appeared in the scientific world, in fact, as a revolutionary event, was awarded the Nobel Prize In physics for 1918 [1]. In the quantum theory of M. Planck, the AKT (substance) and thermal (electromagnetic) radiation from it are in an equilibrium state [8]. In astrophysics it is believed that in the early stages of the development of the universe its matter and radiation from it were also in equilibrium [7]. This assumption allows us to determine the possible spectral composition of the relic electromagnetic radiation, which in shape must correspond to the spectrum of radiation from the ABB. This spectrum of thermal radiation for the ABB (an idealized computational model) by physicists has been thoroughly studied long ago. Therefore, according to this hypothesis, in the background (relic) radiation of the Universe, the number of its electromagnetic quanta with a particular wavelength will depend only on the temperature of the matter of the Universe at an early stage of its development [7]. At a later stage of the evolution of the Universe, in the opinion of astrophysicists, its electromagnetic radiation, while maintaining its frequency spectrum, «breaks away» from its matter and adiabatically cools, uniformly penetrating the entire Universe [7].

Fig. 5. Prominent American radiophysicist John Cromwell Mather, born in 1946, Nobel Prize Laureate in physics for 2006

For greater clarity, it is necessary to indicate that this cosmic electromagnetic radiation is concentrated mainly in the microwave range (in the frequency range typical for modern domestic microwave ovens) [7]. The first measurements of the cosmic microwave background radiation were carried out by radiophysicists at high-altitude radiophysical stations. With the help of such measurements, the long-wavelength part of the relict radiation spectrum was investigated. The results of these studies made it possible to estimate the temperature T_R of a given background radiation, which amounted to about 2.7 K [7]. Conducting more accurate and large-scale measurements of the cosmic microwave background of the Universe required the use of a sophisticated instrument placed outside the Earth's atmosphere. In 1989, the US aerospace agency NASA for this purpose created and launched into the outer space satellite «COBE» (COsmic Background Explorer), whose external view is shown in Fig. 6.

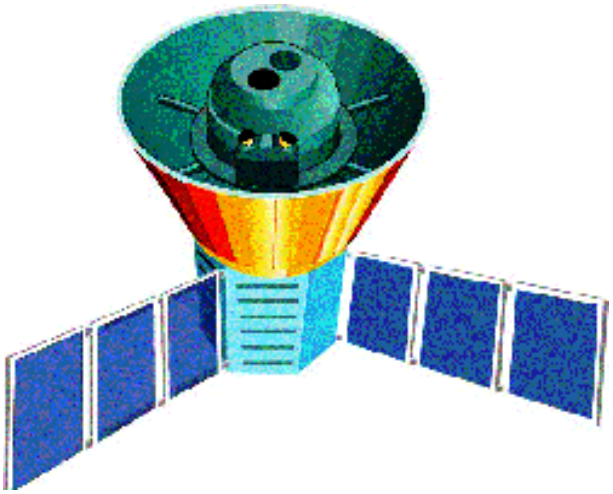

Fig. 6. External view of the American satellite «COBE» comprehensively investigated in the 1990s relic (background) radiation of our Universe [7]

On the satellite «COBE», a microwave relic radiation spectrometer with a high resolving power was installed, which makes it possible to estimate the degree of isotropy of this radiation [7]. Already the first measurements with the help of the satellite equipment «COBE» of cosmic microwave background radiation have shown that it completely corresponds to the spectrum of the equilibrium radiation of the ABB (the «spontaneous» spectrum of electromagnetic radiation). During numerous measurements on this satellite, it was established that the temperature T_R of the cosmic microwave background of the universe is (2.725±0.002) K [7]. In addition, a program of similar radiophysical studies using the satellite «COBE» contained a study of the anisotropy of this radiation – the detection of small deviations in the intensity and, correspondingly, of the temperature of cosmic relic radiation in various directions of the universe. Note that the possible deviation of this radiation from the mean temperature in different parts of the universe can testify to the places where galaxies and stars originate in it, and also indicate the regions of concentration of matter in the universe. In this part, the results of such studies are particularly interesting with respect to «dark» matter or «black holes» of the Universe [9], which can significantly change the temperature of the background radiation. As you know, such a matter can not be directly seen, but can be detected by its super-strong influence on the physical processes taking place in outer space [7]. In astrophysics it was established that in the Universe thanks to gravity there is a continuous process of formation of clumps of matter – proto-types of future planets, stars and galaxies. In the regions of matter thickening, the temperature rises locally [7]. The SOBE spectrometer made it possible to measure the temperature fluctuations T_R of background radiation at the level of $10^{-5} \cdot T_R$ in three frequency ranges corresponding to the maximum intensity of the relict radiation [7]. At the same time, its angular resolution was about 7 angular degrees for outer space. The results of the measurements carried out on the «COBE» satellite for four years showed the contribution of the «Milky Way» galaxy, which includes our solar system, to the dipole component of cosmic background radiation at the level of $\Delta T_R/T_R=10^{-3}$ [7]. Experiments on «COBE» confirmed the Gaussian character of the distribution at large angles of resolution of temperature fluctuations ΔT_R in the background radiation of the Universe. They allowed to give a rigorous justification of the cosmological model of the «Big Bang», which occurred about 12 billion years ago in the Universe.

3. Discovering the effect of giant magnetoresistance. About 150 years ago it was established experimentally that when the conductor is placed with an electric current in an external magnetic field, its reactance R_e slightly changes [10]. This phenomenon was called the magnetoresistive effect – the «magnetoresistance» of the conductor R_{em} [4, 8]. The nature of the established dependence for R_e on the level of the intensity H_m of the external magnetic field was then unknown. For more than a half-century history of the evolution of world electrical engineering, no one paid serious attention to this phenomenon for chains made of traditional conductor materials (copper, aluminum, iron, etc.). After all, changes in the resistance R_e of the conductors for them, depending on the level of the magnetic field intensity H_m, did not exceed a few percent [10]. Only after in the leading scientific laboratories of the world of materials scientists learned to artificially create special laminates with new physical properties, this dependence of R_e on H_m began to be studied more closely. In the second half of the 20th century, talented physicists – the Frenchman Albert Fert (Fig. 7) and the German Peter Grünberg (Fig. 8) experimentally recorded the appearance of the «giant magnetoresistance» R_{em} in new laminates [10]. The discovery by these physicists of the phenomenon of «giant magnetoresistance» was noted by the Nobel Prize in physics for 2007 [6, 10].

Fig. 7. Prominent French physicist Albert Fert, born in 1946, Nobel Prize Laureate in physics for 2007

The «roots» of the new physical phenomenon under consideration deeply «enter» the quantum nature of the

electric current in the conducting material, according to which this current is determined by the drifting free electrons, which have in it an energy close to their maximum energy – the Fermi energyW_F [10, 11].

Fig. 8. Prominent German physicist Peter Grünberg, born in 1939, Nobel Prize Laureate in physics for 2007

The electric current in a metal conductor of a high-current circuit at room temperature (about T_0=293 K [8]) of surrounding its air medium is a superposition of a rapid (with an average thermal velocity v_{eT} of the order of 10^5 m/s [11, 12]) of random motion in interatomic or interionic space of free electrons (elementary particles-fermions [8]) and slow (with an average velocity v_{eD} of the order of 10^{-2} m/s [11, 12]) of the directed displacement (drift) of the «electron gas» in the internal crystal structure of the conductor. It is known that electrons as quantum objects possess wave properties. For an electron moving with velocity v_e, the length of the electron wave λ_e is determined by the fundamental quantum-mechanical relation introduced by the eminent French theoretical physicist Louis de Broglie (1892-1987), of the form [8]: $\lambda_e=h/(m_e v_e)$, where h=6.626·10^{-34} J·s is the Planck constant; m_e=9.109·10^{-31} kg is the rest mass of an electron. Then, at v_{eT}=10^5 m/s, we find that for a chaotic motion of carriers of an elementary electric charge of the «electronic gas» of a conductor having a density n_e of the order of 10^{29} m^{-3} [11], at this temperature it will correspond to the average electron wavelength $\lambda_{eT}\approx$7.3·10^{-9} m. According to [8], the considered Fermi gas of a conductor is considered to be «degenerate» when an inequality of the form $n_e\lambda_e^3>>1$ is satisfied. Substituting in this inequality the given numerical values for n_e=10^{29} m^{-3} and $\lambda_{eT}\approx$7.3·10^{-9} m, we are convinced that the randomly moving free electrons of our conductor will be a purely «degenerate» Fermi gas. In the case of a drift (directional displacement) of the «electronic gas» of the conductor (n_e=10^{29} m^{-3}), the parameters sought for it will have the following numerical values: v_{eD}=10^{-2} m/s; $\lambda_{eD}\approx$7.3·10^{-2} m. After substituting the values of these parameters into the above inequality, we come to the conclusion that the drifting «electronic cloud» of the conductor, in comparison with its randomly moving free electrons, will even more satisfy the requirements of the «degeneracy» of the Fermi-gas. And if so, the quantum properties of the drifting «electron cloud» of the conductor under consideration will be significant and must be taken into account when studying the electrophysical processes in it.

The active resistance R_e of the conductor is determined by the scattering of drifting free electrons (electron de Broglie waves [11]) on the inhomogeneities of the conductor material (for example, on the defects of its crystal lattice, impurity atoms or quasiparticles, phonons, quanta of elastic thermal vibrations of atoms of this Lattice) [8]. Among other things, electrons also have such an important quantum-physical characteristic as the «spin» S_e (this term derives from the English word *«spin» – «to rotate»* and in atomic physics it denotes the intrinsic mechanical moment of the momentum of an elementary particle or atomic nucleus [4]). Quantitatively, the spin S_e of an electron is expressed in special units with respect to a constant value $h/(2\pi)$ [8, 11]. Therefore, the electron spin will be numerically equal to $2\pi S_e/h$=1/2 [8]. It is this value of the spin S_e that determines for an electron capable of rotating about its axis in two directions (for example, in the direction of the vector of intensity H_m of the acting magnetic field or against it), its spin quantum number in the form m_S=±1/2 [8]. A distinctive feature of the electron spin S_e is that it not only causes the electron to respond to the action of an external magnetic field, but also generates a similar field. For ordinary conductors (especially nonmagnetic – copper or aluminum), the spin S_e of an electron does not have a serious effect on the conductivity flow in it. Therefore, practically no one remembers this characteristic of the main carriers of negative charge in metal conductors in traditional electrical engineering. But for new layered materials, in which the phenomenon of the «giant magnetoresistance» was discovered, it turned out that it is the electron spin that plays the key role [10]. What is the role of this quantum-physical characteristic? For a more reasoned answer to this simple but complex question, let us first consider the behavior of free electrons inside a ferromagnetic material of a planar conductor (conductive bus) of a rectangular configuration with a longitudinal current. Let the magnetic induction of its pre-magnetized material also be directed along the longitudinal axis of such a conductor. In this case, the internal magnetic field of the conductor will differently affect its longitudinally drifting free electrons, the spins S_e of which differ by their orientation with respect to the indicated direction of the field vector H_m of this field (over the field or against the field). The electric current of the conductor under consideration in this case will consist of two carefully interleaved electron fluxes, one of which has electron spins S_e oriented in the direction of magnetization of its material and the other with their orientation against the direction of the internal magnetic field of the conductor [10]. The electrons of these two flows will experience a different resistance from the crystal structure of the

conductor metal in this case. It turns out that electrons with spins S_e oriented *opposite to the magnetic field* will move *more freely* along the conductor (without delay), and electrons with their spins S_e oriented *along the magnetic field – more difficult* (with a delay) [10]. In the first case (for a sort of electrons with spins S_e *opposite to the field*), the resistance R_e of the conductor will be relatively *small*, and in the second case (for a sort of electrons with spins S_e *along the field*) – *large*. We note that similar features in the flow of the conduction current for us will for the time being be characteristic only of a ferromagnetic material (diamagnetic materials such as copper and other metals do not exhibit such singularities at T_0=293 K) [10]. Similar features of the free electron drift in conductors were established relatively recently – in 1968 by a group of French physicists, which included also the future Nobel Prize winner in physics in 2007, A. Fert [10]. It was then before the researchers and the question arose about the feasibility of practical use of the revealed features of the electron drift for a sharp change in the values of the resistivity R_e of the conducting structures. Now, on the basis of the data of [10], we can briefly answer the question posed earlier by us about the role of the spin S_e of the electron. The answer can be reduced to the fact that the concentration of free electrons with the considered S_e (*along the field* or *opposite to the field*) near the level of the Fermi energy W_F depends essentially on the orientation of the spins of H_m electrons for a number of conductors relative to the direction of the intensity vector H_m of the internal (external) magnetic field, characteristic for conduction bands and determining the drift current of the conductor [10]. If there are a lot of free electrons in the material of a conductor with Fermi energy W_F, then a relatively large conduction current with *small* electric resistance R_e to it (current) can flow in it. If there are a little of free electrons in the material of the conductor with Fermi energy W_F, then comparatively weak conduction current with *large resistance* R_e to current can occur in it [10].

Having created in the 1980s artificially new ultrathin layered conductive materials (*superlattices* (Fig. 9), in which strictly alternating magnetic and nonmagnetic layers of two types of metals have a thickness of several atoms [10]), physicists learned to control not only by the magnitude of the magnetization of their layers, but also by the character of their magnetic ordering. And then through the nature of the magnetic ordering of the layers – the electrical resistance R_e of a similar conductive «puff».

In 1986, P. Grünberg's research group in the «puff» made of ultrathin layers of magnetic iron Fe and nonmagnetic Cr chromium (Fig. 10) revealed the effect of alternating magnetization orientations of such Fe iron layers in the absence of an external magnetic field H_m [10, 13]

$$H_m = 0.$$

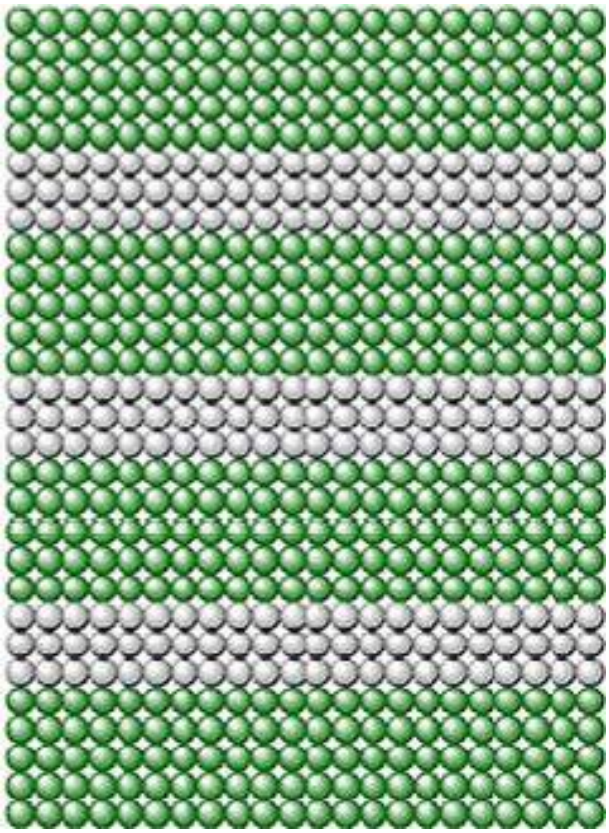

Fig. 9. Schematic view of the modern *superlattice* – strictly alternating layers of atomic thickness of two materials (for example, from 4 layers of magnetic iron Fe and 3 layers of nonmagnetic chromium Cr) with similar crystal structures [10]

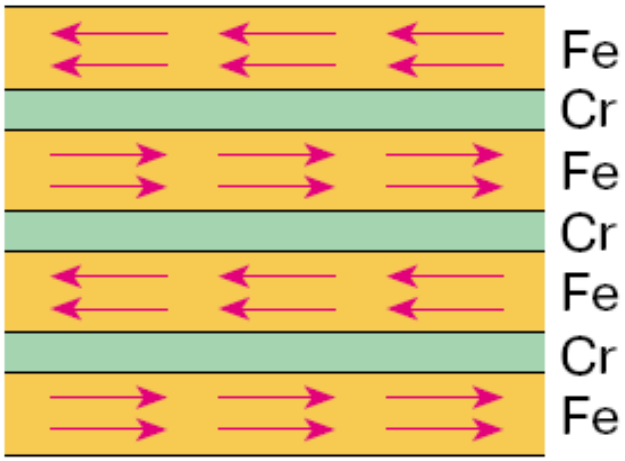

Fig. 10. Schematic representation of the order of alternation of the magnetization of hyperfine layers of iron Fe in a «puff» of iron Fe and non-magnetic chromium Cr in the absence of external constant magnetic field [10]

In the case of an external high constant magnetic field with strength H_m on the one shown in Fig. 10 the «slab» – the *superlattice* Fe-Cr, the magnetization of the layers of iron Fe was acquired due to the magnetization reversal by the field of these layers of the same spatial orientation (Fig. 11) [10, 13]

$$H = H_m.$$

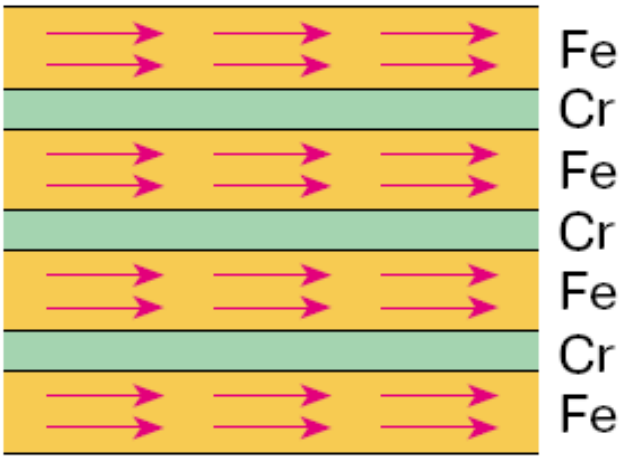

Fig. 11. Schematic representation of the magnetization of ultrathin iron Fe layers in a «puff» of iron Fe and non-magnetic chromium Cr under the action of external high constant magnetic field [10]

It is interesting to note that when the action of an external strong magnetic field with the strength H_m on the *superlattice* under consideration ceases Fe-Cr magnetization of its atomic Fe layers returned to the initial state, shown in Fig. 10. Thus, thanks to superlattices, the physicists-experimenters have a real possibility of rapidly changing the nature of the magnetic ordering of their hyperfine layers [10, 14]. And, finally, they have a real way to control the change within the noticeable limits of the electrical resistance R_e of the conductive «puff». A. Fert and P. Grünberg with their colleagues during 1988-1989, studying the passage of a constant electric current across the layers of «puff» from iron Fe and chromium Cr in the absence and impact modes of an external strong permanent magnetic field, and discovered the effect of «giant magnetoresistance» [13, 14]. In the first experiments of A. Fert, in which an experimental sample of this «puff» of Fe-Cr was placed in a cryostat with a temperature of about 4.2 K, a decrease in the value of its active resistance R_{em} for the cases H_m=0 and H=H_m from the range of high constant magnetic fields (H_m is more than 10 kOe [12]) was approximately twice [10, 14]. Initially, in analogous experiments of P. Grünberg, carried out with this «puff» only at room temperature T_0=293 K, the changes in R_{em} were only 1.5 % [10, 13]. P. Grünberg took several years of careful scientific research to bring his results to room temperature T_0=293 K to the level of reducing the values of R_{em} by two times [10, 15]. An analysis of the experimental results obtained for such a change in the values of the active resistance of the R_{em} «puff» from Fe-Cr showed that they are due to the influence of the orientation of the free electrons of the S_e considered by us above (*along the field* or *opposite to the field*) in the hyperfine layers of iron Fe. The concentration of the corresponding two types of drifting electrons (with a magnetic quantum number m_S=+1/2 or m_S=−1/2) near the Fermi energy level W_F [13-15].

Practical use of the «giant magnetoresistance» effect in computer technology immediately led to a sharp increase in the density of magnetic data recording on hard disks. «Puff» with Fe-Cr and such active resistance R_{em} appeared to be a compact, fast, sensitive and simple by design magnetic field sensor [10]. Being located above the rapidly rotating plate of the hard drive of the computer, such a «puff» tracked the magnetic fields of the information bit streams flying under it in the binary system (the term *«bit»* is derived from the English words *«binary»* and *«digit»* [4]) and immediately transferred them to the corresponding pulses of the electric current.

4**. Discovery of the mechanism of spontaneous breaking of symmetry in subatomic physics.** Nobel laureates in physics in 2008 were scientists from Japan (Makoto Kobayashi, Fig. 12; Toshihide Maskawa, Fig. 13) and the United States (Yoichiro Nambu, Fig. 14) for discoveries in elementary particle physics that explained the causes The fact that the universe we observe consists of matter, and not of antimatter and matter equally, and also the mechanism of the appearance of matter in matter [16]. The studies of these theoretical physicists concern the breaking of symmetry in the world of elementary particles. Their works are related to different time periods, and the symmetries they are considering are related to different interactions of elementary particles [16]. In 1973, M. Kobayashi and T. Maskawa in their joint article suggested that the reason that led to the predominance of matter over antimatter in the universe may be that they participate in different ways in weak interactions (the so-called violation of CP-symmetry) [16-18].

Fig. 12. Prominent Japanese theoretical physicist Makoto Kobayashi, born in 1944, Nobel Prize Laureate in physics for 2008

The first experimental observations in the world of the Kobayashi-Maskawa asymmetry were made by physicists only in 2002 with the help of accelerators KEKB (Japan) and Stanford Linear Accelerator (USA) [16, 19].

Fig. 13. Prominent Japanese theoretical physicist Toshihide Maskawa, born in 1940, Nobel Prize Laureate in physics for 2008

The hypothesis stated in the above-mentioned paper by M. Kobayashi and T. Maskawa, «*The CP Violation in the Renormalizable Theory of Weak Interaction»* (1973), [16] postulated the existence of the third generation of «quarks», which was indirectly confirmed by experiment in four years (in 1977) with the discovery of the *b*-quark [19]. It should be recalled that a quark in the physics of elementary particles and high-energy physics is called a hypothetical particle with a fractional charge of the electron electric charge $e_0=1.602\cdot10^{-19}$ C [8, 11]. In this regard, M. Kobayashi and T. Maskawa in 2008 were awarded the Nobel Prize in physics *«for the discovery of a source of symmetry breaking, which allowed to predict the existence in nature of at least three generations of quarks»* [16-19].

Prior to the work of these theoretical physicists, hadron physics was a real impotent dark «mess» [16]. By 1960, in the experiments on proton synchrotrons by nuclear physicists, dozens of various strongly interacting hadron particles had already been discovered [8]. These hadron particles were with a wide variety of masses, charges, lifetimes and «channels» of decay [16]. Physicists at that time did not understand the «purpose» of these particles, nor their relationship with each other. At that time, there was not even a reasonable scheme for classifying these hadrons. The search for intelligent hadron systematics led scientists to the idea of quarks [16]. In the proposed Y. Nambu, together with the Italian physicist G. Jona-Lazinho, the models of the interaction of hadrons of physics saw a spontaneous breaking of the «chiral» symmetry. Owing to this violation with particles, metamorphoses took place in the developed model: mesons appeared (as bound states of fermion particles, which were analogous to «Cooper pairs» of electrons in superconductors [5]), and the fermion particles themselves became much heavier and can be was identified with protons and neutrons [16]. This led to a rethinking of the physical essence of hadrons [8].

The main investigations of Y. Nambu, who emigrated from Japan to the USA in 1952, was devoted to the development of the idea of spontaneous breaking of symmetry in subatomic physics, expressed by him in 1960 [20]. In 1965, together with M. Khan, he succeeded in creating a scheme of strong hadron-particle interactions, based on three triplets of quarks with integer charges (the well-known Hahn-Nambu model [20]).

Fig. 14. Prominent Japanese-American theoretical physicist Yoichiro Nambu, born in 1921, Nobel Prize Laureate in physics for 2008

Y. Nambu based on this model introduced the «color» interaction of elementary particles [16, 20]. By this theoretical development he laid the foundations of quantum chromodynamics. He essentially developed the quark model of hadron structure [19]. The idea of spontaneous symmetry breaking in the world of elementary particles was actively developed by theoretical physicists, and subsequently the Higgs mechanism of violation of electroweak symmetry also grew out of it. It was *«for the discovery of the mechanism of spontaneous breaking of symmetry in the physics of elementary particles»* that he won the Nobel Prize in physics in 2008 [16].

5**. Development of a new technology for the transmission of light in optical fibers.** In 2009, the first half of the Nobel Prize in Physics was awarded to the Chinese Charles Kao (Fig. 15) *«for the revolutionary achievements concerning the transmission of light in fibers for optical communications»* [21]. Historically, it happened that Ch. Kao in the field of information technology was at the source of fiber-optic data transfer. Because of the rapid development in the world of telecommunications, it has turned out that the traditional technologies for the transmission of information over long distances (with the help of coupled electromagnetic waves in metallic wires and free radio waves) have a fundamental disadvantage – the relatively low speed of the processes taking place in the transmission channels. In order to increase in them (channels) the speed of information transfer by increasing the modulation

frequency, an increase in the carrier frequency of the electromagnetic signal is required. That is why physicists turned their eyes to light pulses (signals), whose frequency is of the order of 10^{15} Hz [8, 11].

Fig. 15. Prominent Chinese experimental physicist Charles K. Kao, born in 1933, Nobel Prize Laureate in physics for 2009

At first glance, an optical fiber with thin glass filaments placed in a protective envelope had to satisfy the rigid requirements for the transmission of light pulses over large distances. However, experimental data testified that in the first half of the 20th century, in the purest glass fibers, the attenuation of the light signal was about 1000 dB/km [21]. Physicists have found that for the effective use of optical fiber as a communication information carrier, the attenuation factor of the light pulse in it should be 20 dB/km or less [21]. In the 1960s, after the graduation from the University of Greenwich (England), with a degree in electrical engineering and the subsequent defense of his doctoral dissertation, he began research at the Standard Telephones and Cables (Harlow) on fiber technology [22]. Here he made his innovative physical and technical discovery, explaining the strong attenuation of light pulses in ordinary glass fibers. He in 1966 found that the reason for this are the impurities present in the glass fibers. In this regard, Ch. Kao, for the efficient use of fiberglass in the transmission of information, proposed carrying it out of thin quartz filaments (Fig. 16) [22]. It was in quartz glass lenses that the lowest level of attenuation of the transmitted light pulse was observed.

Ch. Kao was the first in the world to use fiber-optic cables to transmit telecommunication information over long distances. Technical difficulties in obtaining high-purity quartz glass for these purposes were overcome only in 1972 when researchers from Corning Glass Works (R. Maurer, D. Keck and P. Schulz), using the technology of chemical precipitation from the gas phase, glass fibers were obtained with an attenuation factor of up to 4 dB/km [21, 22].

Fig. 16. External view of a fragment of a bundle of optical fibers with quartz filaments in a protective shell, effectively transmitting light pulses for long distances [22]

Fig. 17 shows the dependence of the attenuation factor of the light signal in a quartz fiber-optic fiber on the length of the waves propagating along it [21].

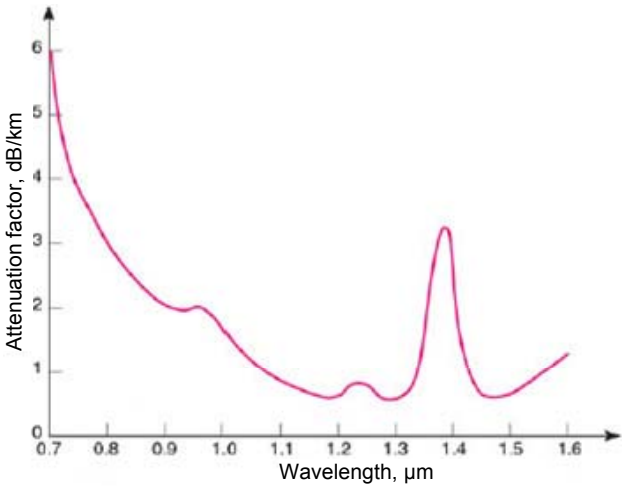

Fig. 17. Attenuation of the light pulse in quartz filaments as a function of the length of its electromagnetic waves [21]

From Fig. 17 that the loss of light intensity is least of all not in the optical but in the infrared (IR) region of the light signal spectrum [21]. This is why the minimal absorption (scattering) of light energy in quartz optical fibers occurs in separate «transparency windows» (at wavelengths of 1.3 μm and 1.45 μm) in the near infrared range of the light pulse. It is at these wavelengths (frequencies) of electromagnetic waves that modern fiber-optic communication operates [21]. Note that, according

to Fig. 17 with decreasing wavelength of the light wave, the damping coefficient increases sharply due to the scattering of light by the inhomogeneities of the refractive index of the medium under consideration (the case of «Rayleigh scattering» [8]). In the region of wavelengths of light waves of more than 1.45 μm, strong lines of absorption of the hydroxyl group OH begin to appear in quartz filaments [21]. As is known, because of Rayleigh scattering of light waves in the atmosphere, the sky on the Earth looks blue-bluish, and the sunset or sunrise is orange-reddish [8, 23]. In 1988, the first transatlantic fiber-optic communication cable was laid [21]. At present, the technology of production of such cables is constantly being improved. Now, in the prototypes of the latest developments in fiber optic cables, the decay factor of the light pulse is characterized by a level of up to 0.2 dB/km [21].

6. The invention of a semiconductor circuit for images recording. In 2009, the second half of the Nobel Prize in physics was awarded to Americans Willard Boyle (Fig. 18) and George Smith (Fig. 19) *«for the invention of a semiconductor circuit for images recording»* [21]. W. Boyle and G. Smith invented a semiconductor device that allows you to obtain digital photographs without photographic film. This semiconductor sensor device, which allows to take photographs in digital format, has been called a «Charged-Coupled Device» or a CCD-matrix [21]. In the CCD-matrix, which is part of a modern camera or digital video camera, the light stream is immediately transferred to a digital file with a color image of the object being photographed.

Before considering the operation of the CCD-matrix as a whole in this semiconductor sensory scheme for recording a color image, we need to start with its one of the main components – a semiconductor cell of digital memory, schematically depicted below in Fig. 20. In 1969, W. Boyle [24] and G. Smith [25], as employees of the famous American laboratory «Bell Labs», began to develop a new highly efficient semiconductor device for recording and reading information in which the information would be stored in the form of microscopic «charge clouds» [21].

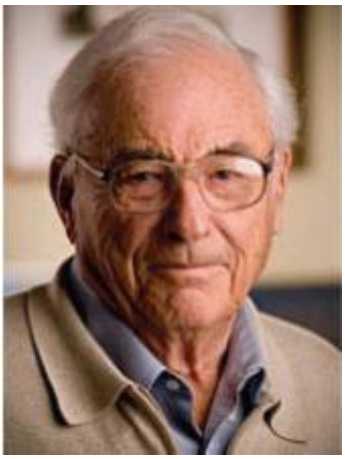

Fig. 18. Prominent American experimental physicist Willard Boyle (1924-2011), Nobel Prize Laureate in physics for 2009

Fig. 19. Prominent American experimental physicist George Elwood Smith, born in 1930, Nobel Prize Laureate in physics for 2009

As a result of research by them in 1969, a semiconductor digital memory cell was proposed, consisting according to Fig. 20 from a plane metal electrode separated by a layer of insulator (silicon dioxide SiO_2) from *p*-type semiconductor (Si silicon) [21]. The role of a bit of information in such a device was played by the «cloud» of electrons that appears in the semiconductor when it is excited.

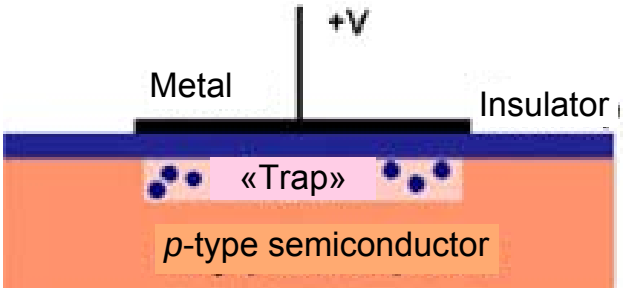

Fig. 20. Schematic representation of the elementary semiconductor cell of digital memory proposed by American physicists W. Boyle and G. Smith [21]

Recall that a semiconductor also possesses such a property as photosensitivity [8, 21]. Light photons (quanta of the electromagnetic field), falling into a semiconductor, generate in it pairs of electrons and holes. In order for such electrons not to be absorbed by holes and stored in a certain region of the semiconductor, W. Boyle and G. Smith proposed to apply an electrical potential of positive polarity to the metal electrode of this cell. Because of their positive charge, the emerging holes «left» out of the small area under this positively charged electrode, and the electrons that appeared to «sit» in it and appeared to be in this local «trap» [21]. It was this «trap» that played the role of a «custodian» of information in a semiconductor cell of digital memory. If there was a small «cloud» of electrons in this «trap», then «1» is written in the cell, if not, «0» [21]. Then, in front of W. Boyle and G. Smith, a serious question arose about reading out information from similar memory cells. For this purpose, they came up with a new method of data transmission – «charge

communication» [21]. It was this method that was realized by them in the created CCD-matrix, presented in a simplified form in Fig. 21.

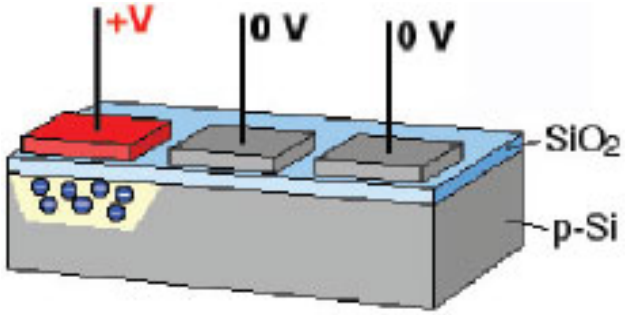

Fig. 21. Schematic representation of a one-dimensional CCD-matrix with three cells of digital memory in a row [21]

By supplying certain voltage V to the metal electrodes of the digital memory (with potential $+V$ and the presence of a small «cloud» of electrons) in the digital information memory cells adjacent to the active information cells (for initial voltage V=0 and the absence of a small «cloud» of electrons in their «traps») and then removing the electric voltage from the active cells, it was possible synchronously in a finite number of cycles to shift information in the CCD-matrix to the reader, at the edge of this matrix [21]. The reader will perceive the electric charge coming from the active cell of the digital memory and give the corresponding electrical signal. In the case that the reader will not simply detect the absence or presence of an electric charge in the «trap» of the next memory cell, but also measure the charge accumulated in it, then the output of such a semiconductor circuit produces a real optical image recorded immediately in digital form. It should be noted that some electromagnetic waves that are part of the light signal cells influencing the semiconductor and determining the colors of light emanating from the object of observation will cause the emergence of memory cells of the electrons «caught» by them in the «traps» of memory cells. The name of the «charged-coupled device» (CCD-matrix) reflects the way the electric charge is read in it by shifting from one matrix element to another, gradually filling the camera's buffer register [26]. Further, the voltage from the reader is amplified and fed to the analog-to-digital converter, after which the signal is digitally received for subsequent processing in the camera processor [26]. This matrix, the general view of which is shown in Fig. 22, in fact, is a microchip consisting of millions of photocells that react to light. CCD-matrices made a scientific and technological revolution in photography (they quickly entered our everyday life in the form of compact digital photo and video cameras) [26, 27]. They are widely used in low-dose digital X-ray units and installed on all modern telescopes [27].

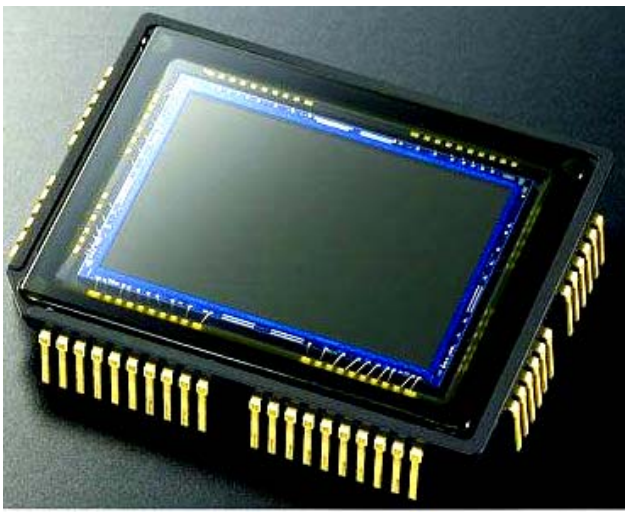

Fig. 22. External view of a modern CCD-matrix [26]

7. Implementation of innovative experiments to create a two-dimensional material graphene. Natives of Russia Andrey Konstantinovich Geim (Fig. 23) and Konstantin Sergeevich Novoselov (Fig. 24), working before his emigration at the Institute of Microelectronics Technology Problems and Highly Pure Materials of the Russian Academy of Sciences (Chernogolovka, Russia), in 2004 in the laboratory of the University of Manchester (Great Britain) opened a fundamentally new material – «graphene» [5, 28]. Graphene is a unique hyperfine material made on the basis of carbon ${}_6{}^{12}C$ with a graphite layer thickness of one atom [5]. Therefore, because of such a vanishingly small nanometric thickness (of the order of 0.1 nm), it is called a two-dimensional nanocrystalline material belonging to the second-order nanomaterials [5]. Carbon atoms in a thin graphene film are connected to a hexagonal two-dimensional crystal lattice (Fig. 25) [28].

Fig. 23. Prominent Russian-Dutch physicist Andre K. Geim, born in 1948, Nobel Prize Laureate in physics for 2010

Fig. 24. Prominent Russian-British physicist Kostya S. Novoselov, born in 1974, Nobel Prize Laureate in physics for 2010

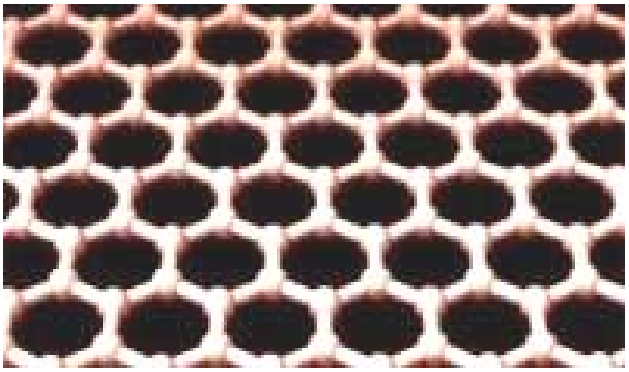

Fig. 25. External view of a fragment of a hexagonal crystal lattice of an atomic layer of graphene, in knots which contains carbon atoms $_6^{12}C$ [28]

Artificially obtained now graphene by chemical deposition of carbon vapor $_6^{12}C$ on the substrate (with its linear dimensions of several centimeters and more) showed surprising physicochemical properties. It is almost transparent material, it has incredible mechanical strength (100 times greater than that of steel) [28].

Graphene has a sufficiently high electrical conductivity (as in the widely used $2_9^{63}Cu$ copper in electrical engineering) and is characterized by high thermal conductivity [28]. In his first experiments, A.K. Game and K.S. Novoselov miniature samples of new material were obtained with a rectangular piece of electrical graphite and an ordinary adhesive tape – adhesive tape. Applying the scotch to the flat surface of graphite and tearing it off, they found it under a microscope and found plaque-monolayers of carbon [28]. It turns out that everything is simple!

The study of physicochemical properties of graphene and its behavior under external influences of various physical factors (for example, mechanical loads, electric current, electric field, etc.) on it provided a number of possibilities for its technical application. It turned out that a practically transparent graphene conductor is well suited for the production of transparent touch screens, light panels, solar cells and electrochemical current sources, as well as for manufacturing high-frequency transistors with regard to mobile phones and ultrafast optic sensors in fiber communication [28]. The creation of graphene may in the near future lead to the emergence of a new class of nanoelectronics with a record low transistor thickness – up to 10 nm. The use of graphene in computer technology can lead to an increase in the speed of computers thousands of times. He practically does not stop «flying» through him free electrons. Therefore, it has a very low active resistance to electric current [28]. Moreover, the experimental data of A.K. Geim and K.S. Novoselov, as well as ivestigations in the Russian Federation showed that graphene or superthin graphite film can change its electrical resistance (more precisely, increase the electrical conductivity) when an external electric (electro-magnetic) field is applied to them [29]. These results, in the opinion of physicists, point to promising possibilities of using such materials in semiconductor or, more precisely, graphite electronics. In addition, it was found that when stretching graphene (it can be stretched to 20 % of the increase in the original linear dimension), it can turn into a good semiconductor [28]. This is due to the formation in this way of an appropriate «semiconductor» discontinuity in the energy spectrum of its atomic structure (in fact, due to an increase in the energy gap between its valence band and the conduction band) [11]. Such a new property of graphene with its high thermal conductivity opens certain prospects for the use of this new material in converter nanoelectronics. The attempts of physicists of the use of graphene, even as a mass micro-sensor, are interesting [28]. According to preliminary estimates by physicists, such «atomic» scales are capable of weighing even one molecule of substance! Technical problems in this case, experts who try to adapt graphene to the solution of similar super-thin (for us, we can say, just fantastic) physical tasks, certainly enough [28]. At present, many nanotechnologists, in close cooperation with engineering and technical workers, carry out solutions to complex applied problems in the industrial production of graphene with geometric dimensions necessary for modern technology (in fractions, units and tens of meters). Taking into account the exceptional scientific and technical significance for the technosphere of human society of the received and studied by A.K. Geim [30] and KS. Novoslov [31] new unique material, they *«for the basic experiments on the creation of two-dimensional material graphene»* and were awarded the Nobel Prize in physics for 2010 [5, 28].

REFERENCES

1. Khramov Yu.A. *Istoriia fiziki* [History of Physics]. Kiev, Feniks Publ., 2006. 1176 p. (Rus).

2. Baranov M.I. An anthology of the distinguished achievements in science and technique. Part 34: Discovery and study of quantum-wave nature of microscopic world of matter. *Electrical engineering & electromechanics*, 2016, no.5, pp. 3-15. (Rus). **doi: 10.20998/2074-272X.2016.5.01**.

3. Available at: http://www.nkj.ru/archive/articles/3477 (accessed 15 May 2014). (Rus).
4. *Bol'shoj illjustrirovannyj slovar' inostrannyh slov* [Large illustrated dictionary of foreign words]. Moscow, Russkie slovari Publ., 2004. 957 p. (Rus).
5. Baranov M.I. *Antologiia vydaiushchikhsia dostizhenii v nauke i tekhnike: Monografiia v 2-kh tomakh. Tom 1.* [An anthology of outstanding achievements in science and technology: Monographs in 2 vols. Vol.1]. Kharkov, NTMT Publ., 2011. 311 p. (Rus).
6. Available at: http://nobelprize.org/nobel_prizes/physics (accessed 25 March 2014). (Rus).
7. Available at: http://hepd.pnpi.spb.ru/ioc/ioc/line06910/n1.htm (accessed 11 August 2012). (Rus).
8. Kuz'michev V.E. *Zakony i formuly fiziki* [Laws and formulas of physics]. Kiev, Naukova Dumka Publ., 1989. 864 p. (Rus).
9. Baranov M.I. *Antologiia vydaiushchikhsia dostizhenii v nauke i tekhnike: Monografiia v 2-kh tomakh. Tom 2.* [An anthology of outstanding achievements in science and technology: Monographs in 2 vols. Vol.2]. Kharkov, NTMT Publ., 2013. 333 p. (Rus).
10. Available at: http://elementy.ru/news/430612 (accessed 10 April 2014). (Rus).
11. Javorskij B.M., Detlaf A.A. *Spravochnik po fizike* [Handbook of physics]. Moscow, Nauka Publ., 1990. 624 p. (Rus).
12. Baranov M.I. *Izbrannye voprosy elektrofiziki. Tom 2, Kn. 2: Teoriia elektrofizicheskikh effektov i zadach* [Selected topics of Electrophysics. Vol.2, Book 2. A theory of electrophysical effects and tasks]. Kharkiv, NTU «KhPI» Publ., 2010. 407 p. (Rus).
13. Binasch G., Grünberg P., Saurenbach F., Zinn W. Enhanced magnetoresistance in layered magnetic structures with antiferromagnetic interlayer exchange. *Physical Review B*, 1989, vol.39, no.7, pp. 4828-4830. **doi: 10.1103/physrevb.39.4828**.
14. Fert A. et al. Gigant magnetoresistance of (001)Fe/(001)Cr magnetic superlattices. *Physical Review Letters*, 1988, vol.61, pp. 2472-2475.
15. Nikitin S.A. Giant magnetoresistance. *Soros educational journal*, 2004, no.2, pp. 92-98. (Rus).
16. Available at: http://elementy.ru/news/430870 (Accessed 11 July 2015). (Rus).
17. Available at: https://en.wikipedia.org/wiki/Makoto_Kobayashi_(physicist) (accessed 11 May 2010).
18. Available at: https://en.wikipedia.org/wiki/Toshihide_Maskawa (accessed 22 September 2012).
19. Available at: http://ria.ru/science/20081007/151954918.html (accessed 23 October 2014). (Rus).
20. Available at: https://en.wikipedia.org/wiki/Yoichiro_Nambu (accessed 22 June 2012).
21. Available at: http://fiz.1september.ru/view_article.php?ID=200902319 (accessed 31 May 2013). (Rus).
22. Available at: https://en.wikipedia.org/wiki/Charles_K._Kao (accessed 21 January 2013).
23. Baranov M.I. An anthology of the distinguished achievements in science and technique. Part 29: Discoverers of secrets of global natural light phenomena. *Electrical engineering & electromechanics*, 2015, no.6, pp. 3-13. (Rus). **doi: 10.20998/2074-272X.2015.6.01**.
24. Available at: https://en.wikipedia.org/wiki/Willard_Boyle (accessed 10 November 2011).
25. Available at: https://en.wikipedia.org/wiki/George_E._Smith (accessed 10 May 2010).
26. Available at: https://en.wikipedia.org/wiki/Digital_camera (accessed 10 April 2012).
27. Available at: www.ferra.ru/online/digiphoto/s27140/print (accessed 25 September 2014). (Rus).
28. Available at: http://class-fizika.narod.ru/nobel2010.htm (accessed 08 June 2015). (Rus).
29. Shakirzyanov F.N. Graphen and photoconductive effect. *Electricity*, 2011, no.1, pp. 65-66. (Rus).
30. Available at: https://en.wikipedia.org/wiki/Andre_Geim (accessed 22 October 2013).
31. Available at: http://www.people.su/81015 (accessed 10 July 2014). (Rus).

Received 27.01.2016

M.I. Baranov, Doctor of Technical Science, Chief Researcher,
Scientific-&-Research Planning-&-Design Institute «Molniya»
National Technical University «Kharkiv Polytechnic Institute»,
47, Shevchenko Str., Kharkiv, 61013, Ukraine,
phone +38 057 7076841, e-mail: eft@kpi.kharkov.ua

How to cite this article:
Baranov M.I. An anthology of the distinguished achievements in science and technique. Part 38: Nobel Prize Laureates in Physics for 2005-2010. *Electrical engineering & electromechanics*, 2017, no.3, pp. 3-15. **doi: 10.20998/2074-272X.2017.3.01.**

UDC 621.313 **doi: 10.20998/2074-272X.2017.3.02**

V. Chenchevoi, Iu. Romashykhin, Zh. Romashykhina, Atef S. Al-Mashakbeh

ANALYSIS OF THE SPECIAL FEATURES OF THE THERMAL PROCESS IN AN INDUCTION GENERATOR AT HIGH SATURATION OF THE MAGNETIC SYSTEM

Purpose. Development of the method for the assessment of the thermal operation modes of an autonomous electrical power system with an induction motor, aiming at improvement of the reliability of electricity supply and the quality of electric energy. Methodology. Induction generator mathematical modeling taking into account the magnetic system saturation was used in the research. A heat model taking into account the excess of the temperature of the induction generator units in the mode of high saturation was developed. The obtained results were compared with the experimental data. Results. The paper contains the solution to the problem of improvement of the mathematical model sand methods for steel losses determination in there search of the operation modes of an autonomous uncontrolled induction generator taking into consideration the properties of the magnetic system in the mode of high saturation. The expression for determination of steel losses in the mode of high saturation is obtained. It enables the assessment of the induction generator thermal condition. Originality. The analytical dependence for the calculation of the steel losses in the mode of magnetic system saturation has been obtained for the first time. Practical value. The obtained expression for the calculation of the steel losses can be used for determination of the admissible time of generator operation at overload. It will allow avoiding broken winding insulation and complete use of the generator overload capacity. As a result, it will reduce possible irregularities of electricity supply due to the generator preliminary cutoff. References 10, tables 2, figures 3.
Key words: **autonomous induction generator, magnetic system saturation, steel losses, thermal processes.**

Цель. Разработка методики оценки тепловых режимов работы автономной электроэнергетической системы с асинхронным генератором с целью повышения надежности электроснабжения и качества электроэнергии. Методология. Для проведения исследований использовалось математическое моделирование асинхронного генератора с учетом насыщения магнитной системы. Разработана тепловая модель, которая учитывает превышение температуры узлов асинхронного генератора в режиме высокого насыщения. Полученные результаты моделирования сравнивались с экспериментальными данными. Результаты. В работе решена задача усовершенствования математических моделей и методов определения потерь в стали при исследовании режимов работы автономного нерегулируемого асинхронного генератора с учетом свойств магнитной системы в режиме высокого насыщения. Получено выражение для определения потерь в стали в режиме высокого насыщения, которое позволяет оценивать тепловое состояние асинхронного генератора. Оригинальность. Впервые получена аналитическая зависимость для расчета потерь в стали в режиме насыщения магнитной системы. Практическое значение. Полученное выражение для расчета потерь в стали может быть использовано для определения допустимого времени работы генератора при перегрузке. Это позволит избежать повреждения изоляции обмоток и в полном объеме использовать перегрузочную способность генератора. В результате это снизит возможные перебои с электрической энергией из-за преждевременного отключения генератора. Библ. 10, табл. 2, рис. 3.
Ключевые слова: **автономный асинхронный генератор, насыщение магнитной системы, потери в стали, тепловые процессы.**

Introduction. Autonomous electrical power systems (AES) take an important place in the development of power engineering [1]. Recently AES have become widespread in electricity supply systems of both special and general purpose. The domain of application of such systems includes electric devices (stationary, mobile ones), controlled electromechanical systems (transport, small hydroelectric stations, wind energy plants), no-break power systems of important consumers. The necessity for the use of AES occurs when it is technically impossible or economically unprofitable to apply centralized electricity supply.

AES theoretical research and practical experience of their application show that there are good prospects of the use of induction generators (IG) with capacitor excitation as a power supply in them.

In spite of availability of a great number of papers related to theoretical and practical research of AES with IG the problems of these systems have not been completely solved. In particular, the thermal transient processes in IG with capacitor self-excitation at high saturation of the magnetic system are insufficiently analyzed.

The analysis of the previous research and the problem statement. Under the modern conditions there is a necessity for development of heat models for the analysis of IG operation [2]. During the choice of the heat model it is necessary to take into account the conditions of the induction machine operation [3–5]. The analysis of literature [1, 2] revealed that the thermal processes in IG are essentially influenced by steel losses. The method of thermal equivalent circuits is widely used for thermal calculations of electric machines in the solution of general problems of heating.

Losses dependences on the squared frequency and voltage are used as the basis for the classical methods of steel losses calculation [6, 7]. Moreover, it is shown in [8] that at high saturation of the magnetic system an abnormal increase of steel losses can be observed. This increase is much bigger than the values calculated by the conventional methods.

Usually, in induction machine thermal models the steel losses under the steady-state condition are not taken into consideration due to their small values. Taking into account the steel losses as a value proportional to the value of squared magnetic induction [9] results in a considerable error as such a relation is only true for an unsaturated magnetic circuit. Steel losses, having achieved rather high values, essentially influence the process of IG windings heating. That is why their neglect causes noticeable errors in determination of IG thermal state and is often inadmissible.

As a consequence, when dynamic thermal processes developing unequally at different degrees of magnetic system saturation are analyzed, there appears a necessity for a specified taking into account the steel losses in a heat model. So, the research of thermal transient processes in IG with capacitor self-excitation at the magnetic system high saturation is of both theoretical and practical interest.

Purpose of the paper. Working out the methods for assessment of the thermal operating modes of AES with IG.

Material and results of research. For the specified verification of IG element heating the non-stationary thermal processes are researched taking into account the real distribution of temperature and thermal flows in the machine. A three-mass mathematical model of an induction machine is analyzed in the paper. Apart from the stator and rotor windings the influence of the stator steel is taken into consideration in the model. However, in the analysis it is assumed that every active element represents a homogeneous body with an infinitely high internal thermal conductivity.

An induction motor (IM) is used as an IG. An IG thermal equivalent circuit is shown in Fig. 1. In accordance with the diagram, body 1 (stator winding) is characterized by heat capacity C_1 and is connected with the third body 3 (stator steel) by thermal conductivity Λ_{13}. Losses ΔP_1 are allocated in body 1. Analogously, body 2 (rotor) is characterized by heat capacity C_2, is connected with body 3 by thermal conductivity Λ_{23}. Losses ΔP_2 are allocated in body 2. In its turn, body 3 is characterized by heat capacity C_3 and is connected with the environment by thermal conductivity Λ_3. Losses ΔP_3 are allocated in body 3.

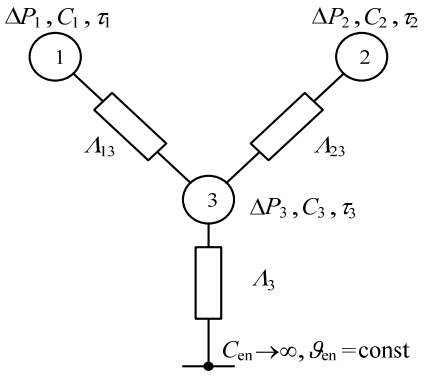

Fig. 1. Thermal diagram of an induction motor as a system of three bodies: 1 – stator winding; 2 – rotor; 3 – stator steel

The following designations are adopted in Fig. 1: τ_1, τ_2, τ_3 – excess of the temperature of the stator winding, rotor and IM steel, respectively; ϑ_{en} – ambient temperature; C_{en} – environment heat capacity.

According to [1, 2], the heat balance equations for IM each body are presented in the form:

$$\begin{cases} \Delta P_1 = C_1 \dfrac{\mathrm{d}\tau_1}{\mathrm{d}t} + \Lambda_{13}(\tau_1 - \tau_3); \\ \Delta P_2 = C_2 \dfrac{\mathrm{d}\tau_2}{\mathrm{d}t} + \Lambda_{23}(\tau_2 - \tau_3); \\ \Delta P_3 = C_3 \dfrac{\mathrm{d}\tau_3}{\mathrm{d}t} + \Lambda_{13}(\tau_3 - \tau_1) + \\ \quad + \Lambda_{23}(\tau_3 - \tau_2) + \Lambda_3 \tau_3, \end{cases} \quad (1)$$

where the stator winding active power losses at the winding temperature θ_1:

$$\Delta P_1 = 3R_s I_s^2, \quad (2)$$

where I_s – active value of the stator current; R_s – resistive impedance of the stator winding; rotor winding active power losses at the rotor temperature θ_2:

$$\Delta P_2 = 3R_r I_r^2, \quad (3)$$

where I_r – active value of the rotor current; R_r – resistive impedance of the rotor winding.

The stator steel losses are caused by the hysteresis and eddy-currents in the stator core [7, 9].

According to the conventional method, the steel losses are determined by expression:

$$\Delta P_3 = \Delta P_{st} = \Delta P_{st.r} \left(\frac{U_1}{U_{1r}} \right)^2, \quad (4)$$

where $\Delta P_{st.r}$ – active power steel losses at rated voltage; U_1 – voltage current value; U_{1r} – rated phase voltage.

During the analysis of steel magnetization reversal processes a dependence for the calculation of steel losses under the condition of magnetic system saturation was found:

$$\Delta P_3 = \Delta P_{st}(I_\mu) = \frac{\xi}{\left(\dfrac{\mathrm{d}E(I_\mu)}{\mathrm{d}I_\mu} \right)} (E(I_\mu))^2, \quad (5)$$

where $E(I_\mu)$ – electromotive force active value dependence on IM magnetization current active value I_μ; ξ – coefficient depending on the material parameters.

Expression (5) demonstrates that at the non-saturation section of the magnetization curve the electromotive force changes by the linear law, i.e. $\mathrm{d}E(I_\mu)/\mathrm{d}I_\mu \to$ const. In this case the equation takes the form analogous to Steinmetz equation [10]. When IM operates in the saturation mode, the velocity of electromotive force intensification decreases, i.e. $\mathrm{d}E(I_\mu)/\mathrm{d}I_\mu \to 0$. In this case there occurs a sharp growth of steel losses caused by lagging.

IM 4A90L4U3 was used in the analysis to research the thermal processes. The IM parameters are given in Table 1. The thermal condition parameters are given in Table 2.

Table 1

Parameters of 4A90L4U3 induction motor

Parameter	Value
Rated power, kW	2.2
Rated voltage, V	220
Stator rated current, A	5
Efficiency	0.8
Rated slid	0.051
Stator resistive impedance, Ohm	4.15
Stator inductive reactance, Ohm	3.218
Rotor reduced resistive impedance, Ohm	2.629
Rotor reduced inductive reactance, Ohm	5.697
Magnetization circuit inductive reactance, Ohm	92.03

Table 2

Thermal condition parameters of 4A90L4U3 induction motor

Thermal conductivities, W/°C	
Λ_{13}	10.5707
Λ_{23}	2.7648
Λ_3	13.9969
Thermal capacities, J/°C	
stator winding C_1	726.1
rotor C_2	3260
stator steel C_3	9623
Stator rated temperature θ_{1r}, K	403

As a result of using the conventional method and the method for losses determination in a highly-saturated mode the IG rotor winding temperature excess curves were obtained (Fig. 2).

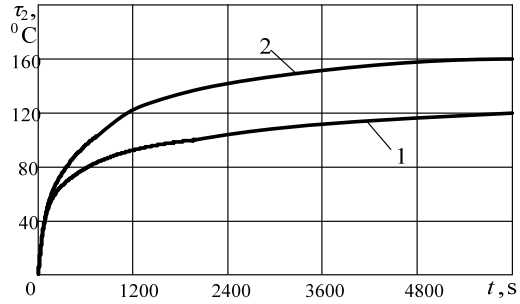

Fig. 2. Rotor temperature excess curve at different methods of steel losses calculation:
1 – with the use of the conventional method (based on expression (4)); 2 – based on expression (5)

The analysis of the presented dependences revealed that IG unit heating rates essentially differ at different methods of steel losses calculation. So, the windings temperature at the conventional method of steel losses account is considerably lower than with the use of the method for steel losses determination in a highly-saturated mode.

A thermal imager was used for verification of the adequacy of the thermal model. The thermogram of IG operation at self-excitation is presented in Fig. 3. It is seen in the figure that IG rotor windings heats up to the temperature of 148.7 °C. The results of comparison of the experiment and modeling (Fig. 2) revealed that the calculated excess of temperature with the use of expression (5) is 158 °C. It suggests the conclusion that the proposed approach is adequate. The analysis of the obtained results revealed that the stator end windings are the most heated IG parts.

Fig. 3. A thermogram of the induction generator

Conclusions.

Steel losses influence on the IG thermal characteristics at high saturation of the magnetic system has been researched in the paper. It enables determination of temperature excess at particular units of the generator.

The developed heat model makes it possible to calculate maximal current temperatures in different parts of the motor with sufficient accuracy. The mathematical model allows determination of temperature at IG units that are inaccessible for direct measurement. The proposed heat model can be used at IG monitoring with the aim of forecasting their resource.

REFERENCES

1. Qiu Y., Zhang W., Cao M., Feng Y., Infield D. An Electro-Thermal Analysis of a Variable-Speed Doubly-Fed Induction Generator in a Wind Turbine, *Energies*, 2015, vol.8, no.5, pp. 3386-3402. **doi: 10.3390/en8053386.**

2. Hodgins N., Mueller M.A, Tease W.K., Staton D. Thermal model of an induction generator in oscillating water column wave energy converter. *5th IET International Conference on Power Electronics, Machines and Drives (PEMD 2010), 2010.* **doi: 10.1049/cp.2010.0020.**

3. Zagirnyak M., Romashykhina Zh., Kalinov A. Diagnostic signs of induction motor broken rotor bars in electromotive force signal. *17th International Conference Computational Problems of Electrical Engineering (CPEE), 2016.* **doi: 10.1109/CPEE.2016.7738722.**

4. Rodkin D.I., Romashihin Y.V. Rationale for settlement circuit for induction motors. *Tekhnichna Elektrodynamika*, 2012, no.2, pp. 89-90. (Rus).

5. Zagirnyak M., Rodkin D., Romashykhin Iu., Rudenko N., Chenchevoi V. Identification of nonlinearities of induction motor equivalent circuits with the use of the instantaneous power method, *17th International Conference Computational Problems of Electrical Engineering (CPEE), 2016.* **doi: 10.1109/CPEE.2016.7738721.**

6. Rygal R., Moses A.J., Derebasi N., Schneider J., Schoppa A., Influence of cutting stress on magnetic field and flux density distribution in non-oriented electrical steels, *Journal of Magnetism and Magnetic Materials*, 2000, vol.215-216, pp. 687-689. **doi: 10.1016/S0304-8853(00)00259-6.**

7. Zidarič B., Zagirnyak M., Lenasi K., Miljavec D. Hysteresis losses in soft magnetic composite materials. *COMPEL - The international journal for computation and mathematics in electrical and electronic engineering*, 2006, vol.25, no.1, pp. 157-168. **doi: 10.1108/03321640610634416.**

8. Reinert J., Brockmeyer A., De Doncker R.W. Calculation of losses in ferro- and ferrimagnetic materials based on the modified Steinmetz equation. *Conference Record of the 1999 IEEE Industry Applications Conference. Thirty-Forth IAS Annual Meeting (Cat. No.99CH36370).* **doi: 10.1109/IAS.1999.806023.**

9. Maga D., Zagirnyak M., Miljavec D. Additional losses in permanent magnet brushless machines. *Proceedings of 14th International Power Electronics and Motion Control Conference EPE-PEMC 2010*, 2010. **doi: 10.1109/EPEPEMC.2010.5606520.**

10. Steinmetz C. On the law of hysteresis. *Proceedings of the IEEE*, 1984, vol.72, iss.2, pp. 197-221. **doi: 10.1109/PROC.1984.12842.**

Received 05.06.2017

Vladimir Chenchevoi[1], *Candidate of Technical Science,*
Iurii Romashykhin[1], *Candidate of Technical Science,*
Zhanna Romashykhina[1], *Candidate of Technical Science,*
Atef S. Al-Mashakbeh[2], *Candidate of Technical Science,*
[1] Kremenchuk Mykhailo Ostrohradskyi National University,
20, Pershotravneva Str., Kremenchuk, Poltava region, 39600, Ukraine,
phone +38 098 2723441,
e-mail: vladchen.86@gmail.com, romashykhin.iurii@gmail.com, romashykhina.zhanna@gmail.com
[2] Tafila Technical University,
Et Tafila New Hauway Str., 179, Tafila, Et Tafila, 66110, Jordan,
phone 00962772075700, e-mail: dr.atef_almashakbeh@yahoo.com

How to cite this article:
Chenchevoi V., Romashykhin Iu., Romashykhina Zh., Al-Mashakbeh Atef S. Analysis of the special features of the thermal process in an induction generator at high saturation of the magnetic system. *Electrical engineering & electromechanics*, 2017, no.3, pp. 16-18. **doi: 10.20998/2074-272X.2017.3.02.**

UDC 621.313.333 **doi: 10.20998/2074-272X.2017.3.03**

K.M. Vasyliv

A MATHEMATICAL MODEL OF THERMAL POWER PLANTS SMOKE EXHAUSTERS INDUCTION MOTORS SYSTEM OPERATION MODES

Purpose. Development of a model-software complex (MSC) for computer analysis of modes of the system of induction motors (IM) of smoke exhausters of thermal power plant (TPP), the basic elements of which are mathematical models and corresponding software written in the programming language FORTRAN. Methodology. Mathematical model serves as a system of differential equations of electrical and mechanical condition. The equation of electric state is written in phase coordinates based on Kirchhoff's laws, and mechanical condition described by the d'Alembert equation. Mathematical model focuses on explicit numerical integration methods. Scientific novelty. The equation of state of electrical connections takes into account the mutual electromagnetic circuits for transformer of own needs (TON) and induction motors and interdependence (in all possible combinations) between: TON (from which motors powered) and each of the two IM and blood pressure between themselves. The complex allows to simulate electromagnetic and electromechanical processes in transitional and steady, symmetric and asymmetric modes including modes of self-induction motors. Results. Complex is used for computer analysis of electromagnetic and electromechanical processes and established the basic laws of motion modes of starting, stopping and self-start of IM of smoke exhausters of the TPP unit. Practical value. The complex is suitable for computer analysis of modes of other similar units of own needs of thermal power plants. References 9, figures 12.

Key words: **mathematic model, numerical methods, thermal power plant, induction motors.**

Разработана математическая модель электротехнического комплекса: «Электрическая сеть – трансформатор – два асинхронных двигателя» в фазных координатах, ориентированную на явные методы численного интегрирования системы дифференциальных уравнений. На базе математической модели создан программный комплекс и произведено исследование электромагнитных и электромеханических процессов и установлено основные закономерности их протекания в режимах пуска, останова и самозапуска асинхронных двигателей дымососов энергоблока тепловой электрической станции. Библ. 9, рис. 12.

Ключевые слова: **математическая модель, численные методы, тепловая электростанция, асинхронные двигатели.**

Problem definition. Powerful thermal power plants (TPP) are used as one base structures of modern power system of Ukraine. At least a half of electricity generated in Ukraine is accounted for the power station. It should be noted that thermal power plants generate huge electricity percent in other advanced industrially developed countries and Europe, and the world.

The reliability and efficiency of thermal power plants in general, scrap, and their power blocks, in particular, essentially depends on the stability and reliability of operation, and the resulting performance of large-keel bones electricity consumers, including powerful industries, transport systems and other consumers.

Reliability of large thermal power plants is determined by reliable operation of turbogenerators that generate electrical energy directly and therefore considered the most important units of power blocks of TPP. Turbogenerators operation, in its turn, is determined by units such important units as steam turbines and boilers, which belong to the group of key ones.

Modern TPP units are highly advanced and automated. This means that the operation of the basic units of TPP provides large number number of other units that belong to auxiliary. These include mechanisms for transportation and fuel supply (if the TPP is working on coal), a number of different pumps (nutritious condensate, circulation) and blowing devices and smoke exhausters and so on. All these auxiliary units called units of own needs (ON), which divided into important and non-important. Refusal to operation of important ON units leads to a violation of basic technological cycle of production of electrical energy and even disable of main units: turbogenerators, steam turbines, boilers, and refusal of non-important has no such a critical influence.

In modern thermal power plants almost all their needs mechanisms of ON driven by short-circuit induction motors (IM) power of which reaches several MW. Induction motors are used to drive and smoke exhausters, whose operation is critical for the unit. After the rejection in the other two smoke exhausters leads to lower unit productivity by 30-40 % and the rejection of two smoke exhausters – emergency stop to the boiler and consequently disable the unit.

ON units in its purpose serves as a «hand» that provides the service personnel unit in the set mode (start and stop the unit, increasing and decreasing issuing power to the grid, and so on). Virtually supports the following modes of power control of electric motors (EM) own power needs. Therefore, to correct and efficient operation of the TPP issue analysis modes of electric motors of own needs is crucial. In this context, critical analysis is correct mode start-up and running-out of electric motors, increase and decrease the frequency of rotation to adjust the performance of the mechanisms set in motion these motors, as well as the self and switch to back-and-purpose and urgent supply.

Analysis of the results of scientific publications and case studies. The issue analysis modes of electric motors mechanisms of own needs of power plants is given quite a large number of scientific papers. Preferably, these works are based on the classical theory of electrical machines and aimed at studying the characteristics and regularities of electromagnetic and electromechanical processes that occur in systems of

electric motors ON main types of power plants (thermal and nuclear). In terms of the practice of power units of power plants is urgent analysis of electromagnetic and electromechanical processes of electric own needs without exception in all modes of operation: starting, nominal mode and learning processes and self freewheel. These questions serve as the subject of analysis modes of their electric needs sources [1, 3-5, 7, 9]. For example, in [1] describes the overall structure, basic mechanisms, motors, electrical circuits OP thermal power plants. Considered electric modes of their own needs, the control circuit relay protection and automation of electric motors and network elements 6.3 and 0.4 kV. The question of improving the reliability of the electric power station and ON prospects of controlled electric AC. The analysis of the characteristics of damage ON and the ways to prevent them [3] the general characteristics of units own needs of power plants (PP), the processes of starting and running-out of electric motors own needs. Self-described impact on technological operation unit is described. The above general requirements for electrical circuits and ON are the most common ones. A simplified calculation of self electric motors own needs. In [4] the system of own needs of different types of plants, their characteristics are mechanisms as well as the analysis of the mechanisms of self motors own needs. The question of choice of transformers, DC installations and electrical circuits personal needs.

Fundamental analysis of modes of asynchronous and synchronous motors is made in [7]. Here are some key features of loading, considerable attention is highlighted issues of electric heating. The problems of asymmetric modes of the motors and jacks are considered. Sufficiently and thoroughly describes the self-starter and electric motors. The problem of self motor conditions and results of experimental studies of these regimes is considered. The question of single and group run out of electric AC motors. All these questions are important for practical operation of electric motors needs its own power station.

Relevance of the research. The presence of scientific works which made analysis modes of electric motors mechanisms of own needs of power plants and research results are reliable definitely enhance the efficiency of their operation. However, a material described in the literature reviewed obvious that its use in the practice of specific operating units of own needs power plants needed substantial revision of it. Because these sources are contained in the material presented in the general conceptual form, which makes it difficult to use on specific situations with different motor types for different purposes and capacities, and features of power circuits.

In this context, it is evident that today not enough attention highlighted the issues of development of means of analyzing modes of electric motors of own needs the PP, which would be suitable for direct use in their practice use. Clearly, more reliable results concerning modes of electric motors ON can be based on the solution of differential equations that describe processes in dynamic mode (start-up, run-down, self, and so on) with modern computer systems. In addition, analysis of the situation in question operation of power plants indicates that, on the one hand, the practice of service personnel mostly uses only normative materials and documents, and therefore cannot always get into the essence of regularities of electromagnetic and electromechanical processes EM specific units in their various modes of the particular circumstances and, on the other hand, to physical experiment in terms of the analysis of modes of electric motors of ON in terms of the energy operation of power block not only difficult but often impossible.

The above gives reason to believe that the development of tools to analyze modes of electric motors own needs TPP, which serve as mathematical models and corresponding software systems is an actual scientific and practical problems.

The goals of investigations. Improving the reliability and efficiency of thermal power plants is only possible through the maximum utilization of knowledge in the context regularities of flow of electromagnetic and electromechanical processes that occur primarily in the turbo generators and electric motors in the systems mechanisms to their needs during their operation in normal and emergency modes of to the specific terms and condition these motors (connection schemes and the specific situation of the system ON power in the relationship of its elements IL themselves). The research results obtained in the literature (including listed here) allow only general and predominantly qualitative estimate modes EM. Combining advanced theories of mathematical modeling in the field of electricity and electrical engineers with the capabilities of modern information technology will make it possible to develop a mathematical model of a high level of adequacy, based on which, in turn, create a corresponding set of programs with which you can quickly perform calculations necessary operating modes and operational decisions concerning the positive effects on the motor.

Thus, the **goal of the paper** is to develop a mathematical model of the two short-induction motors smoke exhausters unit of thermal power stations that are powered by the transformer's own needs, and appropriate software designed for the rapid analysis of motor operating modes using modern computer technology.

Presentation of main material. In the real world of individual thermal power boiler smoke one driven by two short-circuited electric motor. To achieve adequacy of mathematical modeling of motor of smoke exhausters sufficient for practical purposes it is necessary to model processes not only the motors themselves, but also in the transformer of own needs (TON) unit, which feed motors. This will allow better display motor operating conditions and will enable modeling processes that occur in motors during the loss and recovery of working power TON and associated with this mode of self induction motors.

Based on these considerations, with the object of study made electrical complex circuit diagram is shown in Fig. 1.

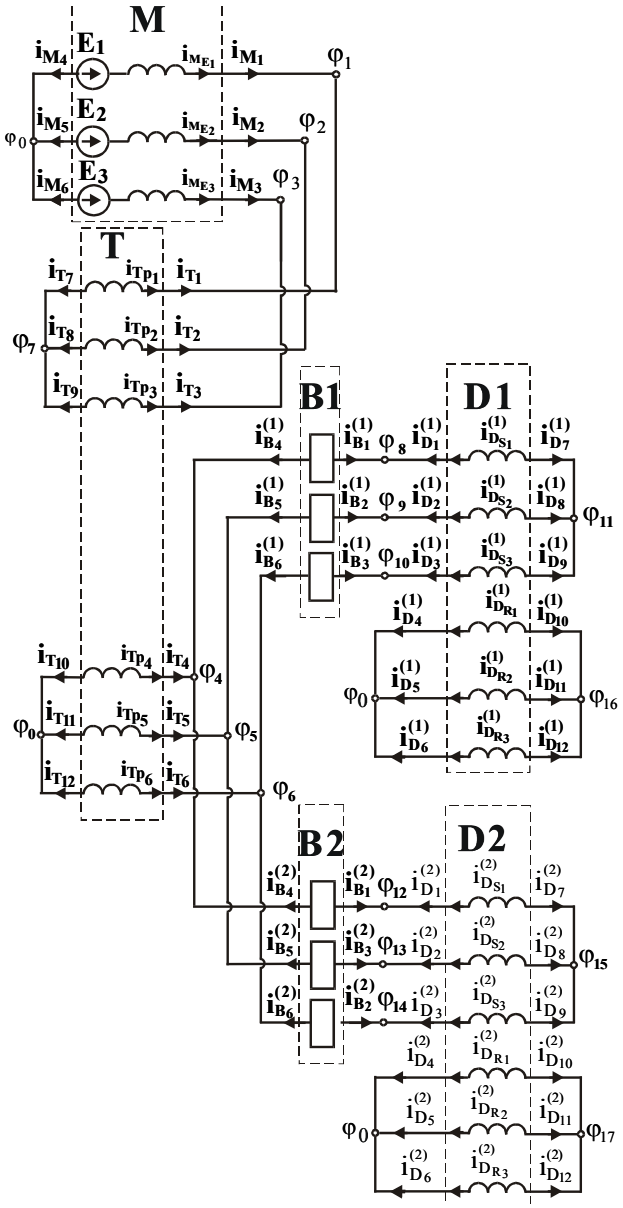

Fig. 1. Electrical circuit diagram of the complex «electric network – transformer – two induction motors»

This Figure shows that smoke exhausters electric motors powered by a transformer secondary winding their needs through switches, and the primary winding of the transformer is powered from the mains, which are presented turbine. In Fig. 1 *M* letter marked three-phase electric network; TON letter marked *T*; texts *B*1, *B*2 – switches that connect through the stator winding induction motor to the secondary winding TON and inscriptions *D*1, *D*2 – two induction motors of the smoke exhausters. The letters indicated potentials *φ* independent nodes schemes, the letter «*i*» – current phase of structural element branches, and the letter *E* – electromotive force network. In the lower index numbers marked numbers of independent units, the numbers of branches structural phase circuit elements and external room-branch structural elements. The letter *M*, *T* indicated in subscript currents belonging to external branches and network transformer, and inscriptions M_E and T_P – belonging to the internal network and current transformer. The letters *S*, *R* indicated in subscript currents belonging to the stator and rotor induction motor and the letter *D* – external branches to the current induction motors.

Mathematical models of electrotechnical complex (ETC) «three-phase electric network – transformer – two induction motors» (EN – T – IM) develop on the basis of the theory of mathematical modeling of electric machines, valve systems [6] and a number of other developments outlined in [2, 8] . Thus, the mathematical model of the ETC «EN – T – IM» is a system of differential equations for the state electrical circuit in Fig. 1 and differential equations mechanical condition for induction motors and smoke exhausters. The first set of equations describing electromagnetic processes of the entire circuit in Fig. 1, and the second – electromechanical processes that occur in asynchronous motors. The system of equations written in state electric phase coordinates and focuses on explicit numerical integration methods. Each of the structural elements (electrical network, transformer and switch, asynchronous motors) are in the form of equations multipoles recorded the second law of Kirchhoff. Consider the mathematical models of structural elements.

Mathematical model of the first induction motor is designed according to [2, 6, 8]. Electromagnetic and electromechanical processes describe the electrical system of differential equations balance and mechanical balance differential equation respectively. The first group form equations based on Kirchhoff's laws, and describe the mechanical balance d'Alembert equation.

So, will be the first electric induction motor vector equations describe the external branches which is as follows [6]:

$$p i_D^{(1)} + \Gamma_D^{(1)} \cdot \varphi_D^{(1)} + C_D^{(1)} = 0, \qquad (1)$$

where $p=d/dt$ is the differential operator in time t;

$i_D^{(1)} = (i_{D1}^{(1)}, i_{D2}^{(1)}, i_{D3}^{(1)}, i_{D4}^{(1)}, i_{D5}^{(1)}, i_{D6}^{(1)}, i_{D7}^{(1)}, i_{D8}^{(1)}, i_{D9}^{(1)}, i_{D10}^{(1)}, i_{D11}^{(1)}, i_{D12}^{(1)})$

is the vector of external branches currents;

$\varphi_D^{(1)} = (\varphi_{D_1}^{(1)}, \varphi_{D_2}^{(1)}, \varphi_{D_3}^{(1)}, \varphi_{D_4}^{(1)}, \varphi_{D_5}^{(1)}, \varphi_{D_6}^{(1)}, \varphi_{D_7}^{(1)}, \varphi_{D_8}^{(1)}, \varphi_{D_9}^{(1)}, \varphi_{D_{10}}^{(1)}, \varphi_{D_{11}}^{(1)}, \varphi_{D_{12}}^{(1)})$

is the vector of external nodes potentials;

$$\Gamma_D^{(1)} = \begin{bmatrix} (L_D^{(1)})^{-1} & -(L_D^{(1)})^{-1} \\ -(L_D^{(1)})^{-1} & (L_D^{(1)})^{-1} \end{bmatrix}; C_D^{(1)} = \begin{bmatrix} (L_D^{(1)})^{-1} \\ -(L_D^{(1)})^{-1} \end{bmatrix} \times E_D^{(1)} \qquad (2)$$

are the matrix of coefficients and the vector of free members.

Components of the matrix of coefficients have the following structure:

$$L_D^{(1)} = \begin{bmatrix} L_{S,S}^{(1)} & L_{S,R}^{(1)} \\ L_{R,S}^{(1)} & L_{R,R}^{(1)} \end{bmatrix}, \qquad (3)$$

where $L_{S,S}^{(1)}$ is the matrix of own inductances of stator circuits; $L_{S,R}^{(1)}$, $L_{R,S}^{(1)}$ are the matrices of mutual inductances between stator and rotor circuits and between rotor and stator circuits, respectively; $L_{R,R}^{(1)}$ – is the matrix of own inductances of rotor circuits.

Components of the vector of free members have the following structure in (2) $E_D^{(1)} = L_{DS,R}^{'(1)} \cdot i_{DR}^{(1)} + R_{DS}^{(1)} \cdot i_{DS}^{(1)}$, where $L_{DS,R}^{'(1)}$ is the derivative of the matrix $L_{DS,R}^{(1)}$ by the rotation angle of the motor $\gamma_D^{(1)}$;

$R_{DS}^{(1)} = diag(R_{DS_1}^{(1)}, R_{DS_2}^{(1)}, R_{DS_3}^{(1)})$ is the diagonal matrix of the stator phase active resistances;
$i_{DS}^{(1)} = (i_{DS_1}^{(1)}, i_{DS_2}^{(1)}, i_{DS_3}^{(1)}) = (i_{D1}^{(1)}, i_{D2}^{(1)}, i_{D3}^{(1)})$;
$i_{DR}^{(1)} = (i_{DR_1}^{(1)}, i_{DR_2}^{(1)}, i_{DR_3}^{(1)}) = (i_{D4}^{(1)}, i_{D5}^{(1)}, i_{D6}^{(1)})$ are the vectors of phase currents of the stator and rotor, respectively.

Mechanical processes that occur in induction motor differential describe the equation of mechanical equilibrium. For the first induction motor this equation is as follows:

$$(J_D^{(1)} + J_H^{(1)}) \cdot p\omega_D^{(1)} - (M_D^{(1)} - M_H^{(1)}) = 0, \quad (4)$$

where $J_D^{(1)}$, $J_H^{(1)}$ are the moment of inertia of the motor rotor and rotating parts of its mechanical load, respectively; $p\omega_D^{(1)}$ is the derivative of the rotor rotation speed by time; $M_D^{(1)}$ is the motor electromagnetic torque; $M_H^{(1)}$ is the mechanical load torque on the motor shaft.

Mechanical load torque is determined by the formula:

$$M_H^{(1)} = M_{H0}^{(1)} + K_{H1}^{(1)} \cdot (\omega_H^{(1)})^{K_{H2}^{(1)}}, \quad (5)$$

where $M_{H0}^{(1)}$ is the static mechanical load torque; $K_{H1}^{(1)}$ is the ratio factor; $K_{H2}^{(1)}$ is the exponent of the rotation speed $\omega_H^{(1)}$.

The structure of the formula (5) allows the selection of numerical values of its individual elements as input to make choices required mechanical characteristics of motor load among a number of possible.

Electrical circuit breakers envision separate systems of three-phase branches Fig. 1. The mathematical models of switches each of the phases present electrical branch consisting of series-connected active resistance and inductance values for which the on state of the switch are made small (e.g., corresponding to real value) and for open-loop-large, i.e. those that correspond disconnected circle in which no current. The transition from open-loop switch to a running state performed immediately (jump) and transition from a running state to off – a smooth increase in resistance and inductance phase branch circuit breaker during certain specified time (corresponding real-time switching) for objectified law as a function of time. It provides lines of second law of increasing resistance and inductance phase branch circuit breaker. This approach will help to reduce the current switch to a certain value, which is at the start off of the switch to zero.

So, electrical state of the first switch is described by the vector equation of external branches in the form:

$$p\,i_B^{(1)} + \Gamma_B^{(1)} \cdot \varphi_B^{(1)} + C_D^{(1)} = 0, \quad (6)$$

where $i_B^{(1)} = (i_{B1}^{(1)}, i_{B2}^{(1)}, i_{B3}^{(1)}, i_{B4}^{(1)}, i_{B5}^{(1)}, i_{B6}^{(1)})$ is the vector of external branches currents;
$\varphi_B^{(1)} = (\varphi_{B1}^{(1)}, \varphi_{B2}^{(1)}, \varphi_{B3}^{(1)}, \varphi_{B4}^{(1)}, \varphi_{B5}^{(1)}, \varphi_{B6}^{(1)})$ is the vector of external branches potentials;

$$\Gamma_B^{(1)} = \begin{bmatrix} (L_B^{(1)})^{-1} & -(L_B^{(1)})^{-1} \\ -(L_B^{(1)})^{-1} & (L_B^{(1)})^{-1} \end{bmatrix}; C_B^{(1)} = \begin{bmatrix} (L_B^{(1)})^{-1} \\ -(L_B^{(1)})^{-1} \end{bmatrix} \times E_B^{(1)} \quad (7)$$

are the matrix of coefficients and the vector of free members in which $L_B^{(1)} = diag(L_{B1}^{(1)}, L_{B2}^{(1)}, L_{B3}^{(1)})$ is the diagonal matrix of inductances, $E_B^{(1)} = colon(R_{B1}^{(1)} \cdot i_{B1}^{(1)}, R_{B2}^{(1)} \cdot i_{B2}^{(1)}, R_{B3}^{(1)} \cdot i_{B3}^{(1)})$ is the column vector of voltage drop on switch phase supports.

The mathematical model of the transformer of own needs is represented in the correspondence with [6, 8] by the differential equation of external branches in the form:

$$p\,i_T + \Gamma_T \cdot \varphi_T + C_T = 0, \quad (8)$$

where $i_T = (i_{T_1}, i_{T_2}, i_{T_3}, i_{T_4}, i_{T_5}, i_{T_6}, i_{T_7}, i_{T_8}, i_{T_9}, i_{T_{10}}, i_{T_{11}}, i_{T_{12}})$ is the vector of external branches currents;
$\varphi_T = (\varphi_{T_1}, \varphi_{T_2}, \varphi_{T_3}, \varphi_{T_4}, \varphi_{T_5}, \varphi_{T_6}, \varphi_{T_7}, \varphi_{T_8}, \varphi_{T_9}, \varphi_{T_{10}}, \varphi_{T_{11}}, \varphi i_{T_{12}})$ is the vector of external nodes potentials;

$$\Gamma_T = \begin{bmatrix} (L_T)^{-1} & -(L_T)^{-1} \\ -(L_T)^{-1} & (L_T)^{-1} \end{bmatrix}; C_T = \begin{bmatrix} (L_T)^{-1} \\ -(L_T)^{-1} \end{bmatrix} \times E_T \quad (9)$$

is the matrix of coefficients and the vector of free members in which L_T is the matrix of inductances with dimension of 6×6;

$$E_T = (R_{Tp_1} \cdot i_{Tp_1}, R_{Tp_2} \cdot i_{Tp_2}, R_{Tp_3} \cdot i_{Tp_3}, R_{Tp_4} \cdot i_{Tp_4}, R_{Tp_5} \cdot i_{Tp_5}, R_{Tp_6} \cdot i_{Tp_6})$$

is the column vector of voltage drop on transformer phase branches supports.

Electrical networks present system of three-phase branches, each of which consists of series-connected active resistance, inductance and electric motive power AC. Phase electromotive forces shifted by 120 degrees. Equation of external branches of a three-phase electrical network is presented as follows:

$$p\,i_M + \Gamma_M \cdot \varphi_M + C_M = 0, \quad (10)$$

where $i_M = (i_{M1}, i_{M2}, i_{M3}, i_{M4}, i_{M5}, i_{M6})$ is the vector of external branches currents;
$\varphi_M = (\varphi_{M_1}, \varphi_{M_2}, \varphi_{M_3}, \varphi_{M_4}, \varphi_{M_5}, \varphi_{M_6})$ is the vector of external nodes potentials;

$$\Gamma_M = \begin{bmatrix} (L_M)^{-1} & -(L_M)^{-1} \\ -(L_M)^{-1} & (L_M)^{-1} \end{bmatrix}; C_M = \begin{bmatrix} (L_M)^{-1} \\ -(L_M)^{-1} \end{bmatrix} \times E_M \quad (11)$$

is the matrix of coefficients and the vector of free members in which
$L_M = diag(L_{M_1}, L_{M_2}, L_{M_3})$ is the diagonal matrix of inductances;
$E_M = (R_{M_1} \cdot i_{M_1} - e_{M_1}, R_{M_2} \cdot i_{M_2} - e_{M_2}, R_{M_3} \cdot i_{M_3} - e_{M_3})$
is the column vector of free members, and
$e_{M_j} = E_m \sin(\omega \cdot t - (j-1) \cdot \rho)$ $(j = 1, 2, 3)$, where E_m is the amplitude of the network electromotive force; $\rho = 2 \cdot \pi/3$.

Mathematical models of the second induction motor and the second switch models are identical to the first motor and the first switch respectively.

The complete system of equations of electrical state is written in electric potential basis of independent nodes circuit in Fig. 1 and according to [6] is as follows:

$$A \cdot \varphi + B = 0, \quad (12)$$

Where *A*, *B* are the matrix of coefficients and the vector

of free members; $\varphi = (\varphi_1, \varphi_2, \ldots, \varphi_{17})$ is the vector of independent nodes potentials in the circuit of Fig. 1.

Matrix coefficients and vector of the system of equations (12) formed from the matrix coefficients vector of (2) (7) (9) (10) and matrix of incidention structural elements of the circuit in Fig. 1 according to [6] by the formulas:

$$\begin{aligned} A &= \Pi_M \cdot \Gamma_M \cdot \Pi_M^t + \Pi_T \cdot \Gamma_T \cdot \Pi_T^t + \\ &+ \Pi_B^{(1)} \cdot \Gamma_B^{(1)} \cdot \Pi_B^{t(1)} + \Pi_B^{(2)} \cdot \Gamma_B^{(2)} \cdot \Pi_B^{t(2)} + \\ &+ \Pi_D^{(1)} \cdot \Gamma_D^{(1)} \cdot \Pi_D^{t(1)} + \Pi_D^{(2)} \cdot \Gamma_D^{(2)} \cdot \Pi_D^{t(2)}; \\ B &= \Pi_M \cdot C_M + \Pi_T \cdot C_T + \\ &+ \Pi_B^{(1)} \cdot C_B^{(1)} + \Pi_B^{(2)} \cdot C_B^{(2)} + \Pi_D^{(1)} \cdot C_D^{(1)} + \Pi_D^{(2)} \cdot C_D^{(2)}, \end{aligned} \tag{13}$$

where

$$\begin{aligned} &\Gamma_M, \Gamma_T, \Gamma_B^{(1)}, \Gamma_B^{(2)}, \Gamma_D^{(1)}, \Gamma_D^{(2)}; \\ &C_M, C_T, C_B^{(1)}, C_B^{(2)}, C_D^{(1)}, C_D^{(2)} \end{aligned} \tag{14}$$

are the matrices of coefficients and vectors of free members of the electrical network, transformer, switches and induction motors;

$$\Pi_M, \Pi_T, \Pi_B^{(1)}, \Pi_B^{(2)}, \Pi_D^{(1)}, \Pi_D^{(2)} \tag{15}$$

are the matrices of incidention of the electrical network,transformer, switches and induction motors describing topology of the electrical circuit of Fig. 1, and

$$\Pi_M^{\mathrm{t}}, \Pi_T^{\mathrm{t}}, \Pi_B^{t(1)}, \Pi_B^{t(2)}, \Pi_D^{t(1)}, \Pi_D^{t(2)}$$

are the matrices transpose regarding the incidention matrices (15).

Algorithm for calculating electromagnetic and electromechanical processes. The main inputs serve Catalog parameters: transformer own needs, smoke exhausters induction motors and electrical network and initial conditions systematized in integrated vector variables has the following structure:

$$\begin{aligned} V &= (V_M, V_T, V_B^{(1)}, V_B^{(2)}, V_D^{(1)}, V_D^{(2)}, t) = \\ &= (i_{M_{E_1}}, i_{M_{E_2}}, i_{M_{E_3}}, i_{Tp_1}, i_{Tp_2}, i_{Tp_3}, i_{Tp_4}, i_{Tp_5}, i_{Tp_6}, \\ &\quad i_{B1}^{(1)}, i_{B2}^{(1)}, i_{B3}^{(1)}, i_{B1}^{(2)}, i_{B2}^{(2)}, i_{B3}^{(2)}, \\ &\quad i_{DS_1}^{(1)}, i_{DS_2}^{(1)}, i_{DS_3}^{(1)}, i_{DR_1}^{(1)}, i_{DR_2}^{(1)}, i_{DR_3}^{(1)}, \gamma_D^{(1)}, \omega_D^{(1)}, \\ &\quad i_{DS_1}^{(2)}, i_{DS_2}^{(2)}, i_{DS_3}^{(2)}, i_{DR_1}^{(2)}, i_{DR_2}^{(2)}, i_{DR_3}^{(2)}, \gamma_D^{(2)}, \omega_D^{(2)}, t). \end{aligned} \tag{16}$$

Main stages of the processes calculation algorithm are:

- based on the initial conditions vector V (16) and catalog data, forming the matrix coefficients and vector of structural elements and through them the coefficient matrix A and the vector of the electric system of equations in the state (12), which solved regarding vector φ;
- to reverse course under the vector φ, define the vector pV integration, which is the original integrated vector variable V (16) in time t ($pV=dV/dt$);
- by one explicit numerical integration methods, based on the vector pV integration and integration step Δt, defining new value vector V;
- described the procedure continues to exit the current integration time t out of the final.

Based on the above-described mathematical models and algorithms developed software system programming language FORTRAN, which allows using computers to calculate electromagnetic and electromechanical processes in electrotechnical complex systems, smoke exhausters TPP.

Below is a generalized analysis of modes of asynchronous motors smoke exhausters thermal power on the basis of the results obtained by mathematical modeling.

In practice, the operation modes of asynchronous motors of smoke exhausters defined mode of operation of thermal power. Depending on the amount of power delivery to the grid must reconcile the boiler unit of power, and hence smoke exhausters work. This means that motors should provide a balanced performance smoke exhausters, defined modes including their motors periodically unlocking. Accordingly, a practical interest is in motors of smoke exhauster mode, which provides switching and unlocking individual motors that provide information on starting mode and free wheel mode. In addition, it is important to model treatment short voltage loss at transformer captive switching to backup power motors and further self-start.

Thus, the simulation of electromagnetic and electromechanical processes to fulfill this mode of induction motors smoke exhausters: at the beginning (at time t_1=0 s) performed simultaneous launch of both IM. At time t_2=5 s stops supply voltage to the transformer in ON cont interval Δt=0.2 s. At time t_3=7 s denies first motor, and at time t_4=20 s it on again. At time t_5=26 s off both induction motors. This mode will allow smoke exhausters motor cover almost all the important stages of their work, including the group ran and simultaneously assess the possibilities offered by mathematical models and corresponding software system.

Perform calculation of electromagnetic and electromechanical processes motors of smoke exhausters of the 11-th unit of the Burshtyn TPP. The power of these motors of 1500 kW and 850 kW respectively and the number of poles is 8 and 10.

Input data catalog data serve as induction motors, transformers and electricity needs of their network and initial conditions, which serves as the integrated vector variables (16). In addition to the input data includes information complementary nature that defines modes of the software complex (integration step, the final integration time, and so on).

Simulation results serve as calculated according to the time of instantaneous values of potential independent units, transformer phase currents, phase currents of the stator and rotor rotation speed motors and electromagnetic motor torque and mechanical resistance points smoke exhausters.

Fig. 2 shows calculated depending on the instantaneous values of phase currents of the stator of the first motor. Waveform phase stator currents reflect the entire operating cycle of the motor (intervals of work and stop) and the nature of the starting transients. Fig. 3 shows a calculated depending on the instantaneous values of phase currents of the first rotor motor, which in addition to the stator currents complementary information

about the peculiarities of electromagnetic processes first induction motor in quality and proportion. Curves rotor currents are so important that it happens in the rotor electromagnetic energy conversion.

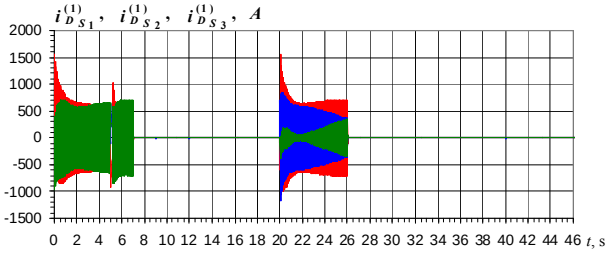

Fig. 2. $i_{D_{S_1}}^{(1)}$, $i_{D_{S_2}}^{(1)}$, $i_{D_{S_3}}^{(1)}$ – phase currents of the stator winding D1

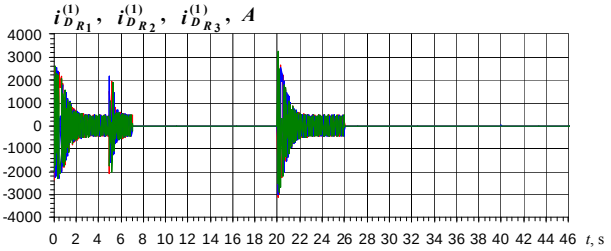

Fig. 3. $i_{D_{R_1}}^{(1)}$, $i_{D_{R_2}}^{(1)}$, $i_{D_{R_3}}^{(1)}$ – phase currents of the rotor winding D1

Fig. 4 and 5 respectively depict calculated depending on the instantaneous values of phase currents stator and rotor of the second motor. The curves of the currents clearly reflect the mutual influence of asynchronous motors on each other. And this influence is manifested through the change of variables one motor current depending on the second (when the power on). From Fig. 4 and 5 it can be seen that the current second motor when the first big off.

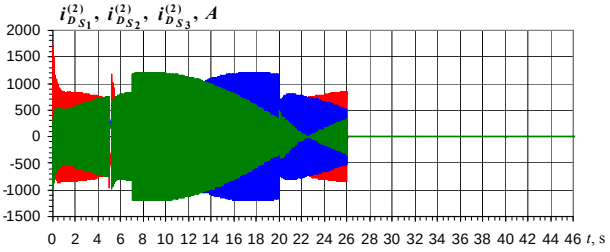

Fig. 4. $i_{D_{S_1}}^{(2)}$, $i_{D_{S_2}}^{(2)}$, $i_{D_{S_3}}^{(2)}$ – phase currents of the stator winding D2

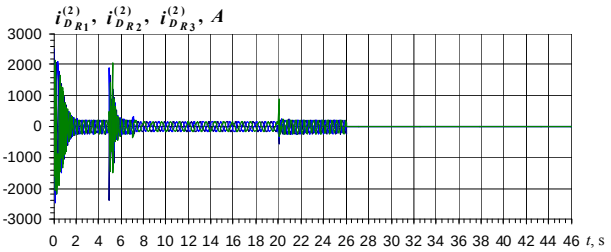

Fig. 5. $i_{D_{R_1}}^{(2)}$, $i_{D_{R_2}}^{(2)}$, $i_{D_{R_3}}^{(2)}$ – phase currents of the rotor winding D2

Shown in Fig. 2-5 depending characterize current patterns of electromagnetic processes. But to assess the operation ability of motors of smoke exhausters must have accurate information about the regularities of electromechanical processes. Such information serve as calculated depending on the electromagnetic motor torque and mechanical resistance smoke exhausters points, which for the first and second motors respectively shown in Fig. 6, 7.

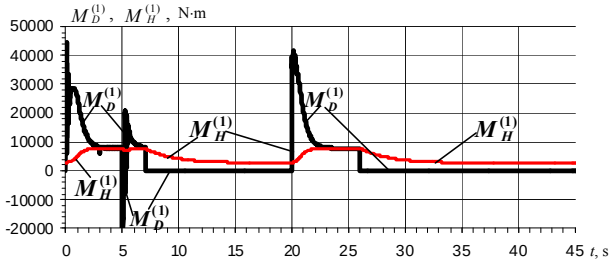

Fig. 6. $M_D^{(1)}$, $M_H^{(1)}$ – electromagnetic torque of the first motor and mechanical moment of resistance of its smoke exhauster

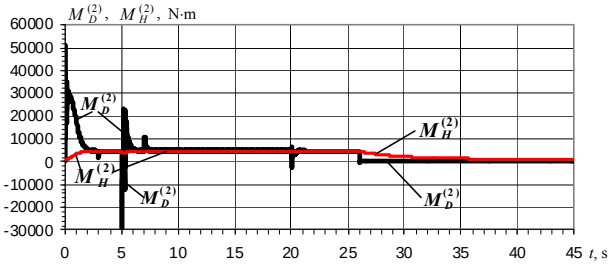

Fig. 7. $M_D^{(2)}$, $M_H^{(2)}$ – electromagnetic torque of the second motor and mechanical moment of resistance of its smoke exhauster

From these Figures shows that the nature of the curve reflects electromagnetic moments regularities of electromagnetic processes asynchronous motors. At the initial stage of starting points transient electromagnetic motors are alternating in nature. This is a large (close to unity) the value of slip induction motors. As mentioned electromagnetic gain momentum out of the point zone of the sign changing and become more sustainable value and a steady constant.

To obtain correct results of asynchronous motors regarding important to have not only the functional dependence of the electromagnetic motor torque, but the curves point mechanisms are driven by motors. Mechanical resistance points and blowing smoke exhausters mechanisms for changing fan characteristic that is proportional to the square of speed. The value of static mechanical moment for these units is very small relative to the mechanical moment in nominal mode and is friction torque. Defaults mechanical moment curves smoke exhausters fans get the point balancing points in electromagnetic motors electrical resistance with mechanical fan moments that clearly illustrate the curves in Fig. 6, 7.

Performance smoke exhausters determined by the frequency of their rotation. Therefore, in terms of motor operating practices smoke exhausters units of thermal power plants is an important law change rotor speed induction motors.

Rotor speed induction motors frequency determined by the supply voltage and the number of pole pairs. But, on the other hand, the rotor speed IM affects value since the mechanical load. Therefore, the motor speed is

determined by the resulting smoke exhausters influence of these two factors. Fig. 8 shows the calculated depending on the time rotor speed (in radians per second) of two induction motors $\omega_D^{(1)} = \omega_D^{(1)}(t)$ – the first and $\omega_D^{(2)} = \omega_D^{(2)}(t)$ – the second.

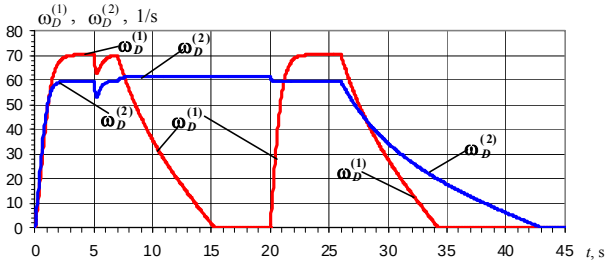

Fig. 8. $\omega_D^{(1)}$, $\omega_D^{(2)}$ – mechanical rotation speed of the induction motors rotors

The nature of the curves in Fig. 8 gives a fairly complete and integrated picture of the substantive operation of units smoke exhausters in general, as well as during motor starting mode and during their run-down modes, in particular. After all, they reflect the performance of the smoke exhausters not only in these modes, but the mutual influence their work and display their work during power loss TON. Mutual influence is manifested in increasing motor rotational speed of the second motor on the period of time when the first motor off (time from t = 7 s to t = 20 s, see curves in Fig. 9). Nature of Fig. 9 allows to determine the run-time motor that depends on the mass moment of inertia wing characteristics and mechanical load.

Smoke units are responsible to their own needs, because electric motors smoke exhausters included in the list of those subject to self. Therefore, for practical operation is important to have accurate information about the regularities of electromagnetic and electromechanical processes during self-run. As noted above, in our experiment provides self-fulfillment after the break power equal to 0.2 s. In this situation it is important to have functional versus time rpm and outlines current motors. The nature of motor speed curves during self motors are illustrated in Fig. 8, which is easy to determine the depth of the failure to coordinate interval voltage loss and recovery time nominal motor speed after the twice supply voltage.

For further information regarding the self if you can analyze patterns of electromagnetic processes based on the analysis of functional dependencies instantaneous values of phase currents of the stator and rotor induction motors. Fig. 9, 10 show the calculated depending on the instantaneous values of phase currents of the first stator and rotor induction motor. From Fig. 9 shows that during the period of time pressure loss phase currents is aperiodic nature with a tendency to decrease their values, and after recovery voltage characteristic is availability aperiodic components that are smaller, than when starting the motor from rest. But seats rotor currents in the range of loss with sinusoidal voltage shape and their amplitude tends to decrease.

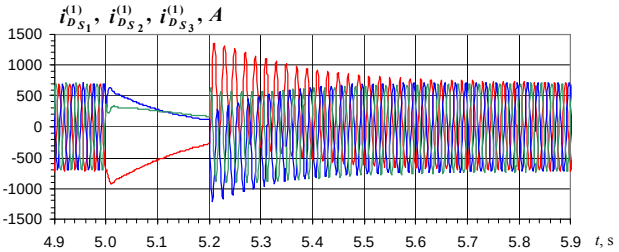

Fig. 9. $i_{D_{S_1}}^{(1)}$, $i_{D_{S_2}}^{(1)}$, $i_{D_{S_3}}^{(1)}$ – phase currents of the stator winding D1

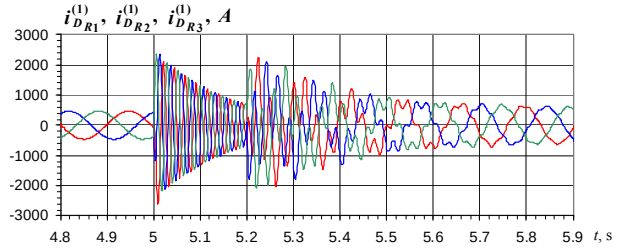

Fig. 10. $i_{D_{R_1}}^{(1)}$, $i_{D_{R_2}}^{(1)}$, $i_{D_{R_3}}^{(1)}$ – phase currents of the rotor winding D1

Fig. 11 and 12 shows the calculated depending on the instantaneous values of phase currents second stator and rotor induction motor.

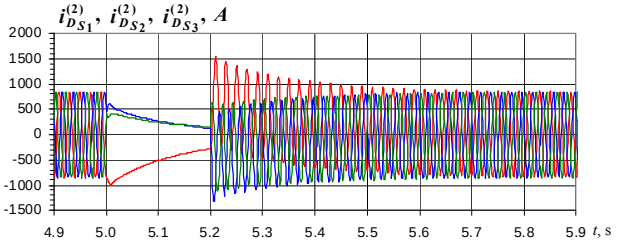

Fig. 11. $i_{D_{S_1}}^{(2)}$, $i_{D_{S_2}}^{(2)}$, $i_{D_{S_3}}^{(2)}$ – phase currents of the stator winding D2

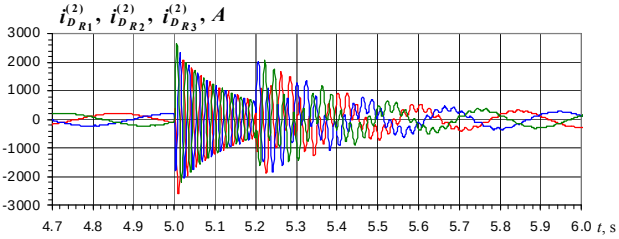

Fig. 12. $i_{D_{R_1}}^{(2)}$, $i_{D_{R_2}}^{(2)}$, $i_{D_{R_3}}^{(2)}$ – phase currents of the rotor winding D2

Such experiments had not observed, and therefore, in my opinion, they are the subject of scientific innovation. Results of mathematical experiments allow self-assess conditions for the possibility of its success, which is practical means-city.

Pattern of change of phase currents second motor are similar to the first, and thus analyze them separately is not necessary.

Conclusions.

1. Analysis of scientific literature shows that the present study modes of motor smoke exhausters TPP performed only in the context of general assemblies of own needs based on the main provisions of the classical theory of electrical machines without the use of differential equations to describe the dynamic modes of the motors, which significantly reduces opportunities reliable results. Therefore, development of special means

of investigation modes of motors of smoke exhausters TPP as mathematical models as a system of differential equations electrical and mechanical condition of the motor smoke exhausters TPP and the corresponding software system is an actual scientific and practical problem.

2. The mathematical model of induction motors smoke exhausters that addresses the key factors influencing the course of electromagnetic and electromechanical processes, communications circuits nonlinearity electromagnetic motors, motors and mutual influence transformer's own needs, the impact of the loss and recovery of supply voltage, and mutual the impact of the motor and mechanism driven by a motor.

3. On the basis of a mathematical model developed software system that enables the TPP in operation to carry out research almost essential modes of the system of induction motors smoke exhausters. Mathematical model and software system lets you simulate electromagnetic and electromechanical processes in symmetric and asymmetric, steady-state and dynamic modes.

4. Using the developed software system performed research of electromagnetic and electromechanical processes asynchronous motors smoke exhausters TPP major modes. In particular, studies starting mode, after the loss of self-renewal and voltage, and received qualitative and quantitative parameters freewheel motors.

REFERENCES

1. Abbasov E.M., Golodnov Iu.M., Zil'berman V.A., Murzakov A.G. *Sobstvennye nuzhdy teplovykh elektrostantsii* [Own needs of thermal power plants]. Moscow, Energoatomizdat Publ., 1991. 272 p. (Rus).

2. Vasyliv K.M. *Metody i modeli analizu protsesiv avtonomnykh system elektrozhyvlennya na bazi asynkhronizovanoho heneratora z bezkontaktnym kaskadnym modul'ovanym zbudzhuvachem*. Diss. dokt. techn. nauk [Methods and models for analyzing the processes of autonomous power supply systems based on an asynchronous generator with a noncontact cascade modulated exciter. Doc. tech. sci. diss.]. Kyiv, 2010. 398 p. (Ukr).

3. Kurbangaliev U.K. *Samozapusk dvigatelei sobstvennykh nuzhd elektrostantsii* [Self-starting engines for power plants own needs]. Moscow, Energoizdat Publ., 1982. 56 p. (Rus).

4. Lahutin V.M., Teptya V.V., Vyshnevs'kyy S.Ya. *Vlasni potreby elektrychnykh stantsiy* [Own needs of power plants]. Vinnytsya, VNTU Publ., 2008. 102 p. (Ukr).

5. Neklepaev B.N. *Elektricheskaia chast' elektrostantsii i podstantsii* [Electric part of power plants and substations]. Moscow, Energoatomizdat Publ., 1986. 640 p. (Rus).

6. Plakhtyna E.G. *Matematicheskoe modelirovanie elektromashinno-ventil'nykh sistem* [Mathematical modeling of electro-machine-valve systems]. Lviv, Vishcha shkola Publ., 1986. 164 p. (Rus).

7. Syromiatnikov I.A. *Rezhimy raboty asinkhronnykh i sinkhronnykh dvigatelei* [Modes of operation of asynchronous and synchronous motors]. Moscow, Energoatomizdat Publ., 1984. 240 p. (Rus).

8. Fil'ts R.V. *Matematicheskie osnovy teorii elektromekhanicheskikh preobrazovatelei* [Mathematical foundations of the theory of electromechanical transducers]. Kyiv, Naukova dumka Publ., 1979. 208 p. (Rus).

9. Vasil'eva A.A. *Elektricheskaia chast' stantsii i podstantsii* [Electrical part of stations and substations]. Moscow, Energoatomizdat Publ., 1990. 576 p. (Rus).

Received 30.05.2017

K.M. Vasyliv, Doctor of Technical Science, Professor,
Lviv Polytechnic National University,
28a, S. Bandera Str., Lviv, 79013, Ukraine,
phone +38 032 2226403,
e-mail: karl.vasyliv @gmail.com

How to cite this article:
Vasyliv K.M. A mathematical model of thermal power plants smoke exhausters induction motors system operation modes. *Electrical engineering & electromechanics*, 2017, no.3, pp. 19-26. **doi: 10.20998/2074-272X.2017.3.03.**

UDC 621.315.2 **doi: 10.20998/2074-272X.2017.3.04**

O.O. Tkachenko

DETERMINATION OF ANALYTICAL CALCULATION ERROR OF MAGNETIC FIELD OF HIGH-VOLTAGE CABLE LINES WITH TWO-POINT BONDED CABLE SHIELDS CAUSED BY NON-UNIFORM CURRENT DISTRIBUTION IN THE SHIELDS

This paper deals with the determination of analytical calculation error of magnetic field of high-voltage cable lines in two-point bonded cable shields caused by non-uniformity of the current distribution in the shields. The relative error is determined by comparing numerical calculation of magnetic field obtained in the COMSOL Multiphysics software with the analytical one. It is shown that the maximum value of relative error does not exceed 8 %. The obtained error values are verified by testing the numerical calculation and confirmed by results of experiment. In paper proves the correctness of the analytical calculation of magnetic field of cable lines at the points of its normalization, which is carried out without taking into account the non-uniform current distribution in the cable shields. References 13, tables 2, figures 4.
Key words: **cable line, cable shield, bonded shields, magnetic field, calculation error.**

В работе определена относительная погрешность аналитического расчета индукции магнитного поля трехфазной кабельной линии, обусловленная неравномерностью плотности тока в экранах одножильных кабелей. Погрешность получена путем сравнения численного расчета в программной среде COMSOL Multiphysics с аналитическим методом расчета. Показано, что максимальное значение погрешности не превышает 8 %. Полученные значения погрешности верифицированы путем тестирования численного расчета и подтверждены результатами эксперимента. Обоснована корректность аналитического расчета магнитного поля кабельных линий в точках его нормирования при двухстороннем замыкании экранов кабелей, выполняемого без учета неравномерности плотности тока в экранах кабелей. Библ. 13, рис. 4, табл. 2.
Ключевые слова: **кабельная линия, экран кабеля, двухстороннее заземление, магнитное поле, погрешность расчета.**

Introduction. The problem of calculating the RMS value of the flux density of the magnetic field (MF) of high-voltage cable lines consisting of single-core cables [1, 2] arises when they are designed and is necessary to limit the MF along the cable lines to the maximum permissible level. In Ukraine, this level is regulated by normative documents [3, 4] and for residential development is 10 μT over the cable lines, at an altitude of 0.5 m from the surface of the earth, and 0.5 μT in nearby residential areas.

A certain complexity is the calculation of the flux density of the MF of cable lines with two-point bonded cable shields [4], when longitudinal currents are induced in them [5, 6]. The known engineering methods for calculating MF of cable lines [1, 4, 5], for such cases, are based on numerical methods. When using these techniques, the results of the calculation are presented in the form of tables with a limited number of discrete values of the calculated quantities, which causes difficulties in their practical application in the design of the cable lines.

In [7], an analytical technique is proposed for calculating the MF of cable lines with the two-point bonded cable shields, free from the above disadvantages, and allowing calculation at any cable line parameters. However, this technique does not take into account the influence of the proximity effect on the MF of cable line [8, 9], which related to non-uniformity of the densities of the longitudinal currents in the cable shields, the description of which is analytically difficult. In this connection, the problem arises of determining the error in the analytical calculation of the MF of cable lines.

The goal of this paper is the determination of the relative error of the analytical calculation of the magnetic flux density of three-phase high-voltage cable line at the points of its normalization caused by non-uniform current distribution in the cable shields.

Investigation technique. The required relative error ε of the analytical calculation of the flux density of the MF of cable line is defined as

$$\varepsilon = \left|1 - \frac{B}{B_{num}}\right| \cdot 100\% , \qquad (1)$$

where B is analytical value of the magnetic flux density, without taking into account the non-uniform current distribution in the cable shields; B_{num} is the exact RMS value of the magnetic flux density, which it is determined with taking into account the non-uniformity current distribution.

To determine B_{num}, a numerical calculation is used that has a verified relative error, which is substantially less than the error permissible in engineering calculations.

Calculation of the magnetic flux density is carried out for real high-voltage cable line [1, 4] at the point of normalization P for trefoil and flat arrangement (Fig. 1). The value of h varies from 0.5 m to 2 m by step 0.5 m, taking into account [3, 4]. In this case, the distance between the cables axes d varies from 0.1 m to 0.3 m by step 0.1 m. The diameter of the cable shields D is 55 mm and 70 mm, the cross-section of shields S is 100 mm^2, 200 mm^2 and 300 mm^2.

Numerical calculation of B_{num}. To calculate B_{num}, the software package *COMSOL Multiphysics* [10] is used,

the relative error of which is verified in [5] when solving a similar problem and does not exceed 1 %. The computational model, in contrast to [5], is performed in accordance with [11] and allows one to find the flux distribution of the MF of a three-phase cable line with allowance for the non-uniform current distribution in shields with a smaller error.

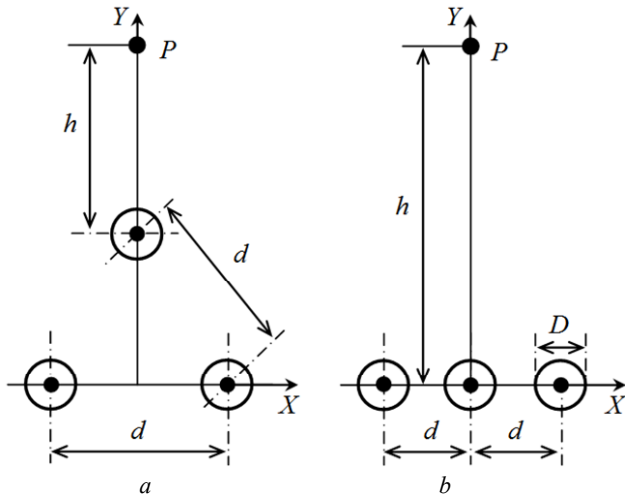

Fig. 1

The following assumptions are made in the calculation:

1) Cables are infinitely long and laid parallel to each other;

2) The cable line operates in the steady-state mode, the RMS values of currents in the cores have a frequency of 50 Hz, are equal in magnitude and their phases are shifted from each other by 120°.

In this case, the MF of the cable line is a plane-parallel, which allows us to solve the problem in a two-dimensional formulation (Fig. 2).

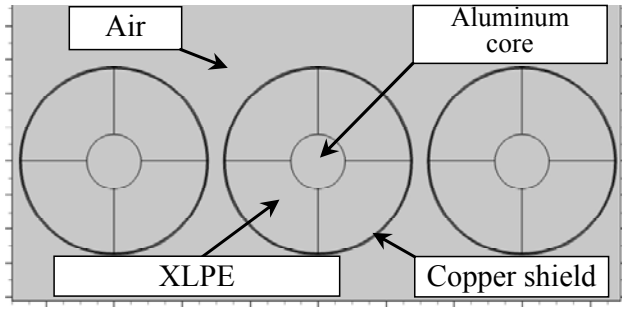

Fig. 2

The theoretical basis for describing the accepted design model of MF is the equation of the law of the total current in the quasi-stationary approximation [8, 12]. Taking into account the connection between the vector potential and the magnetic field strength and taking into account that the vector potential has only one non-zero component, this equation takes the form:

$$\frac{\partial^2 \dot{A}_z}{\partial x^2}+\frac{\partial^2 \dot{A}_z}{\partial y^2}-j\mu_0\omega\sigma\dot{A}_z=0,$$

where $\dot{A}_z$ is the complex amplitude of the component of the vector potential of the electromagnetic field along the Z axis directed parallel to the cable line; j is the imaginary unit; $\mu_0=4\pi\cdot10^{-7}$ H/m is the magnetic constant; $\omega=2\pi\cdot50$ s^{-1} is the cyclic current frequency; σ is the conductivity of the medium for which the equation is written ($\sigma_{Al}=3.8\cdot10^7$ S/m, $\sigma_{Cu}=5.0\cdot10^7$ S/m, $\sigma_{air}=0$ S/m).

The numerical simulation is carried out using the *«Magnetic Fields»* interface, which is included in the *«AC/DC Module»* [10] of the software package. When constructing a two-dimensional model in the Cartesian coordinate system, the option *«Space Dimension»* was set to *«2D»*.

The calculation area is a circle with a diameter L=6 m. Inside it there are the cable line and airspace. To reduce the size of the calculated area on the periphery of the circle, the layer *«Infinite element domains»* of thickness $L/3$ is located.

The calculation model of each of the three cables consists of an aluminum core and a copper shield (Fig. 2). Since the electrical conductivities of the external medium and cross-linked polyethylene (XLPE) are negligible compared to the conductivity of the shield, their effect on the current density distribution in the shields is not taken into account.

The current in each cable core is set using the *«Single-Turn Coil»* function in the *«Magnetic Fields»* menu. For the option *«Coil excitation»*, the variant *«Current»* is selected, for which:

$$\dot{I}_k^c=I_0e^{j\phi_k},$$

where I_0 is the current amplitude in cores; $\phi_k=\{-2\pi/3,\,0,\,2\pi/3\}$ is the current phase in the cable core; $k=\overline{1,3}$ is the cable number.

The boundary conditions are following:

$$\begin{cases}\dot{A}_z^i=\dot{A}_z,\\ \dfrac{\partial\dot{A}_z^i}{\partial n}=\dfrac{\partial\dot{A}_z}{\partial n},\end{cases}$$

where n is the unit vector of the normal to the boundary; the superscript i indicates the conductive medium.

In the area of the shields, the mesh of the *«Mapped»* type is used (Fig. 3,*b*). Along the thickness, the shield is divided into 20 elements, and along the perimeter – into 200. In the other regions, the mesh of the *«Free Triangular»* type is used (Fig. 3,*a*). The mesh density is *«Extremely fine»*, the minimum element size is 1/40 of the diameter of the cable core.

The result of the calculation is the distribution of $\dot{A}_z$. Taking into account that the complex amplitudes of the magnetic flux density are equal to $\dot{B}_x=\partial\dot{A}_z/\partial y$ and $\dot{B}_y=-\partial\dot{A}_z/\partial x$, the expression for the RMS value of the magnetic flux density of the cable line takes the form:

$$B_{num}=\frac{1}{\sqrt{2}}\sqrt{\left|\frac{\partial\dot{A}_z}{\partial y}\right|^2+\left|\frac{\partial\dot{A}_z}{\partial x}\right|^2}.$$

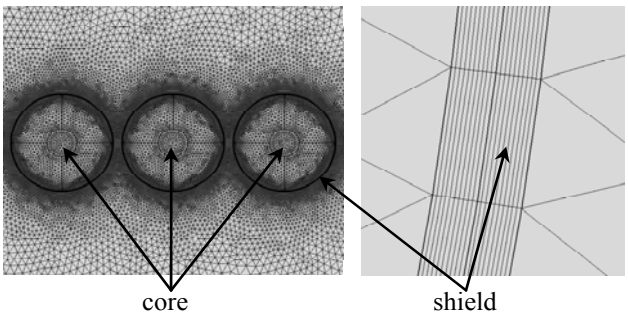

a *b*

Fig. 3

It is worth noting that the proposed calculation model is applicable for an arbitrary method of cables arrangement.

The verification of the numerical calculation was performed by comparison with the solutions obtained by doubling the size of the calculated area and using a finest grid. In this case, the error of calculation does not exceed 0.5 %. The results of the calculation also coincide with the experimental data [5].

Analytical calculation of *B*. The analytical method for calculating the MF of cable line is proposed in [7]. When obtaining the calculated ratios, the same assumptions were used in it as for the numerical calculation considered above, but the distribution of the current density in the shields of each cable was assumed to be uniform.

As the calculated one we use the following relation obtained from [7] by transition from the complex amplitude of the magnetic flux density to its RMS value:

$$B=\frac{1}{\sqrt{2}}\sqrt{\left|\frac{\mu_0}{2\pi}\sum_{k=1}^{3}\left(\dot I_k^c+\dot I_k^{sh}\right)\left(\frac{-(y-y_k)}{(x-x_k)^2+(y-y_k)^2}\right)\right|^2+\left|\frac{\mu_0}{2\pi}\sum_{k=1}^{3}\left(\dot I_k^c+\dot I_k^{sh}\right)\left(\frac{x-x_k}{(x-x_k)^2+(y-y_k)^2}\right)\right|^2}, \quad (2)$$

where $\dot I_k^c$ and $\dot I_k^{sh}$ are the complex amplitudes of currents in the core and shield of the k-th cable, respectively; (x, y) are the coordinates of the point P, in which MF is calculated (see Fig. 1); (x_k, y_k) are the coordinates of the k-th cable axis; $k=\overline{1,3}$ is the cable number.

The values of the currents in (2) are determined as follows. For the case of cable lines in the flat arrangement (Fig. 1,*b*), the currents in the cores form a system of direct sequence, and the currents in the shields are determined by the following relationships [7, 13]:

$$\dot I_1^{sh}=-\dot I_1^c\cdot\frac{Q\cdot\ln 2\Delta\cdot\ln\frac{\Delta^3}{2}+\sqrt{3}\ln 2-j\ln 4\Delta^3}{Q\cdot\ln 2\Delta\cdot\ln\frac{\Delta^3}{2}-\frac{3}{Q}-2j\ln 2\Delta^3},$$

$$\dot I_2^{sh}=-\dot I_2^c\cdot\frac{jQ\ln\frac{\Delta^3}{2}}{3+jQ\ln\frac{\Delta^3}{2}}, \quad (3)$$

$$\dot I_3^{sh}=-\dot I_3^c\cdot\frac{Q\cdot\ln 2\Delta\cdot\ln\frac{\Delta^3}{2}-\sqrt{3}\ln 2-j\ln 4\Delta^3}{Q\cdot\ln 2\Delta\cdot\ln\frac{\Delta^3}{2}-\frac{3}{Q}-2j\ln 2\Delta^3},$$

where $Q=\frac{\mu_0\omega}{2\pi R}$ and $\Delta=\frac{d}{r}$ are the dimensionless parameters of the cable line; R is the cable length unit resistance, Ω/m; d is the inter-phase distance (distance between axes of neighbor cables), m; r is the shield radius, m.

In the case of trefoil arrangement of the cable line (Fig. 1,*a*), the calculation dependence for currents in shields has a more compact form [7, 13]:

$$\dot I_k^{sh}=-\dot I_k^c\cdot\frac{jQ\ln\Delta}{1+jQ\ln\Delta}. \quad (4)$$

Consequently, B is analytically calculated using expression (2) with (3) or (4), for cables with a trefoil or flat arrangement, respectively.

The analysis of analytical calculation error. Fig. 4 shows the results of the calculation of the RMS values of B (analytical calculation) and B_{num} (numerical calculation) using the proposed methods for the 1000A current. The calculation of the magnetic flux density is performed as a function of the distance h to the observation point P (see Fig. 1) for the case of maximum non-uniformity of the current distribution in cable shields. At the same time, the shield diameter is maximal D=70 mm [4], the shield cross section is S =300 mm^2 and the cables are laid close d=0.1 m. As can be seen on Fig. 4, the scatter of the results of the analytical and numerical calculations is negligible.

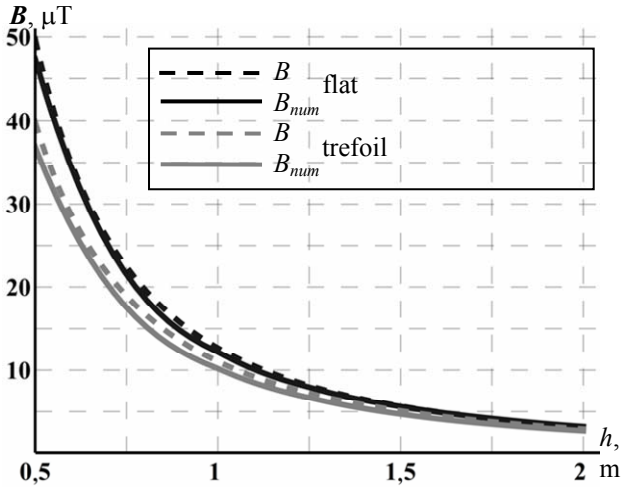

Fig. 4

To quantify the error of the analytical calculation, Table 1, 2 show the results of calculating the value of ε (1) for real high-voltage cable lines [4].

Table 1

Values of ε, % for cable line of trefoil arrangement

h, m	d, m	Shield diameter D, mm					
		55			70		
		Shield section S, mm^2					
		100	200	300	100	200	300
0.5	0.1	**1.0**	**2.7**	**4.3**	**1.6**	**4.8**	**7.9**
	0.2	**0.2**	**0.4**	**0.6**	**0.4**	**1.0**	**1.5**
	0.3	**0.1**	**0.1**	**0.1**	**0.2**	**0.3**	**0.5**
1.0	0.1	**1.0**	**2.8**	**4.3**	**1.6**	**4.8**	**7.9**
	0.2	**0.2**	**0.4**	**0.6**	**0.4**	**1.0**	**1.5**
	0.3	**0.1**	**0.1**	**0.1**	**0.2**	**0.3**	**0.5**
1.5	0.1	**1.0**	**2.7**	**4.3**	**1.6**	**4.8**	**7.9**
	0.2	**0.2**	**0.4**	**0.6**	**0.4**	**1.0**	**1.5**
	0.3	**0.1**	**0.1**	**0.1**	**0.2**	**0.3**	**0.5**
2.0	0.1	**1.0**	**2.7**	**4.3**	**1.6**	**4.8**	**7.9**
	0.2	**0.2**	**0.4**	**0.6**	**0.4**	**1.0**	**1.5**
	0.3	**0.1**	**0.1**	**0.1**	**0.2**	**0.3**	**0.5**

Table 2

Values of ε, % for cable line of flat arrangement

h, m	d, m	Shield diameter D, mm					
		55			70		
		Shield section S, mm^2					
		100	200	300	100	200	300
0.5	0.1	**1.5**	**2.5**	**3.0**	**2.0**	**3.8**	**4.8**
	0.2	**1.1**	**1.5**	**1.6**	**1.2**	**1.8**	**2.1**
	0.3	**1.1**	**1.2**	**1.3**	**1.1**	**1.4**	**1.6**
1.0	0.1	**0.6**	**1.3**	**1.5**	**1.1**	**2.6**	**3.2**
	0.2	**0.9**	**1.2**	**1.3**	**1.0**	**1.5**	**1.7**
	0.3	**1.0**	**1.1**	**1.2**	**1.0**	**1.4**	**1.5**
1.5	0.1	**0.8**	**0.7**	**0.9**	**0.2**	**0.7**	**0.8**
	0.2	**0.5**	**0.6**	**0.6**	**0.6**	**0.9**	**1.0**
	0.3	**0.8**	**0.9**	**0.9**	**0.8**	**1.1**	**1.2**
2.0	0.1	**2.1**	**2.6**	**3.2**	**2.0**	**1.8**	**2.3**
	0.2	**0.1**	**0.1**	**0.1**	**0.1**	**0.2**	**0.2**
	0.3	**0.5**	**0.6**	**0.6**	**0.6**	**0.8**	**0.8**

As follows from Table 1, 2, the maximum error of the analytical calculation of MF is 7.9 % for cable line of trefoil and 4.8 % of flat arrangement, and occurs at the minimum value of d(0.1 m), maximum values of D(70 mm) and S(300 mm^2). This case corresponds to dense cable routing, which is often unacceptable, since it can cause a limitation of the current carrying capacity of the cable. With increasing d to 0.2 m, the value of ε does not exceed 2.5 %.

The obtained results of the calculation with a spread of not more than 5 % agree with the results of the experimental investigations of the MF of cable line carried out in [5].

Thus, the relative error ε of the analytical calculation of the MF of cable line does not exceed 8 %, which confirms the correctness of the assumption made in it about the uniformity of the current distribution in each of the cable shields in the engineering calculation of the MF of cable line.

Conclusions.

1. The maximum value of the error of the analytical calculation of magnetic field does not exceed 7.9 % for cable line of trefoil and 4.8 % of flat arrangement, and occurs with the maximum diameter and cross section of the cable shields (70 mm and 300 mm^2), and the minimum distance between the cable cores axes (0.1 m).

2. The obtained error values are verified by testing the numerical calculation performed in the *COMSOL Multiphysics* software (the error of less than 0.5 %), and comparing the results with the experiment.

3. The presented analysis confirms the correctness of the analytical calculation of the flux density of magnetic field of cable lines at the points of its normalization, which is carried out without taking into account the non-uniformity of current distribution in the cable shields.

REFERENCES

1. SOU-N EE 20.179:2008. *Rozrakhunok elektrychnoho i mahnitnoho poliv linii elektroperedavannia. Metodyka* [Calculation of the electric and magnetic fields of power line. Method]. Kyiv, Minenergovugillya of Ukraine Publ., 2016, 34 p. (Ukr).

2. Rozov V.Yu., Reutskiy S.Yu., Piliugina O.Yu. The method of calculation of the magnetic field of three-phase power lines. *Tekhnichna Elektrodynamika*, 2014, no.5, pp. 11-13. (Rus).

3. *Pravila ulashtuvannya electroustanovok* [Electrical installation regulations]. 5th ed. Kharkiv, Minenergovugillya of Ukraine, 2014. 793 p. (Ukr).

4. SOU-N MEV 40.1-37471933-49:2011.2. *Proektuvannia kabelnykh linii napruhoiu do 330 kV. Nastanova* [Design of cable lines with voltage up to 330 kV. Guidance]. Kyiv, Minenergovugillya of Ukraine Publ., 2017, 139 p. (Ukr).

5. Rozov V.Yu., Kvytsynskyi A.A., Dobrodeyev P.N., Grinchenko V.S., Erisov A.V. and Tkachenko O.O. Study of the magnetic field of three phase lines of single core power cables with two-end bonding of their shields. *Electrical engineering & electromechanics*, 2015, no.4, pp. 56-61. (Rus). **doi: 10.20998/2074-272X.2015.4.11.**

6. *Kovrigin L.A.* The longitudinal currents in the screens of the single-core cables. *Kabel-news*, 2009, no.3, pp. 56-58. (Rus).

7. Rozov V.Yu., Tkachenko O.O., Erisov A.V. and Grinchenko V.S. Analytical calculation of magnetic field of three-phase cable lines with two-point bonded shields. *Tekhnichna Elektrodynamika*, 2017, no.2, pp. 13-18 (Rus).

8. Demirchyan K., Neiman L., Korovkin N. and Chechurin V. *Teoreticheskie osnovy elektrotekhniki: V 3 t.*[Theoretical Basis of Electrical Engineering: in 3 vols.]. Saint Petersburg: Piter, vol.3, 2003, 377 p. (Rus).

9. Podoltsev A., Kucheryavaya I. *Multifizicheskoe modelirovanie v elektrotehnike. Monografiya* [Multi-physical modeling in electrical engineering. Monograph]. Kyiv: Inst. of Electrodynamics of NAS of Ukraine, 2015, 305 p. (Rus).
10. https://www.comsol.com/models/acdc-module
11. Grinchenko V.S., Tkachenko O.O. and Chunikhin K.V. Calculation of shield currents in three-phase cable lines with a trefoil arrangement of phases. *Anotatsiï dopovidei 24 Mizhn. nauk.-prakt. konf. «Informatsiini tekhnologiï: nauka, tekhnika, tekhnologiia, osvita, zdorov'ia»* [Abstracts of 24th Int. Sci.-Pract. Conf. «Information technology: science, engineering, technology, education and health»]. Kharkiv, Ukraine, 2016, 18-20 May, 324 p. (Rus).
12. del-Pino-López J.C., Cruz-Romero P., Serrano-Iribarnegaray L. and Martínez-Román J. Magnetic field shielding optimization in underground power cable duct banks. *Electric Power Systems Research*, 2014, vol. 114, pp. 21-27. **doi: 10.1016/j.epsr.2014.04.001.**
13. Grinchenko V.S., Tkachenko O.O. and Grinchenko N.V. Improving calculation accuracy of currents in cable shields at double-sided grounding of three-phase cable line. *Electrical engineering & electromechanics*, 2017, no.2, pp. 39-42. **doi: 10.20998/2074-272X.2017.2.06.**

Received 31.03.2017

O.O. Tkachenko, Postgraduate Student,
State Institution «Institute of Technical Problems of Magnetism of the NAS of Ukraine»,
19, Industrialna Str., Kharkiv, 61106, Ukraine,
phone +380 572 992162,
e-mail: oleksandr.tk7@gmail.com

How to cite this article:
Tkachenko O.O. Determination of analytical calculation error of magnetic field of high-voltage cable lines with two-point bonded cable shields caused by non-uniform current distribution in the shields. *Electrical engineering & electromechanics*, 2017, no.3, pp. 27-31. **doi: 10.20998/2074-272X.2017.3.04.**

UDC 621.3.022:537.311.8:621.3.015.52 **doi: 10.20998/2074-272X.2017.3.05**

M.I. Baranov, S.V. Rudakov

AN APPROXIMATE CALCULATION OF ENERGY DISSIPATION AND ELECTRIC EROSION OF ELECTRODES IN THE HIGH-VOLTAGE HIGH-CURRENT AIR SWITCH OF ATMOSPHERIC PRESSURE

Purpose. *To obtain new calculation correlations, determining approximate energy dissipation and electric erosion of massive basic metallic electrodes in the high-voltage high-current air switchboard (HVCAS) of atmospheric pressure, in-use in the bit chain of the high-voltage electrophysics setting (HVES) with the powerful capacity store of energy (CSE).* ***Methodology.*** *Electrophysics bases of technique of high-voltage and large impulsive currents (LIC), scientific and technical bases of development and planning of high-voltage heavy-current impulsive electro-devices, including HVES and powerful CSE, and also methods of measuring in their bit chains of LIC of the microsecond temporal range.* ***Results.*** *On the basis of new engineering approach the results of calculation estimation of excretions energy and electric erosion of massive basic metallic electrodes are resulted in probed HVCAS. New correlations are obtained for the approximate calculation of thermal energy, selected in an impulsive air spark and on the workings surfaces of anode and cathode of HVCAS. It is entered and a new electrophysics concept, touching equivalent active resistance of impulsive air spark, is mathematically certain. New formulas are obtained for the approximate calculation of most depth of single round crater of destruction on the workings surfaces of basic metallic electrodes of HVCAS, and also mass of metal, thrown out magnetic pressure from this crater of destruction on the electrodes of switch for one electric discharge through them powerful CSE HVES. It is shown that the radius of the indicated single crater of destruction is approximately equal to the maximal radius of plasma channel of a spark discharge between a cathode and anode of HVCAS. The executed high-current experiments in the bit chain of HVES with powerful CSE validated row of the got and in-use calculation correlations for the estimation of energy dissipation and electric erosion of metallic electrodes in examined HVCAS.* ***Originality.*** *New engineering approach is developed for the approximate calculation and estimation of energy dissipation and electric erosion of basic metallic electrodes in HVCAS. A formula is firstly got for approximate calculation unchanging in the process of swaying or aperiodic discharge of CSE HVES on the electric loading of active resistance of impulsive air spark between the electrodes of probed HVCAS.* ***Practical value.*** *Drawing on the got results in a high-voltage impulsive technique provides operative implementation of calculation of balance of electric energy in the high-current circuit of HVES with powerful CSE and point electric load, and also prognostication of the technical state of workings surfaces of massive basic metallic electrodes of HVCAS.* References 21, figures 3.

Key words: **high-voltage high-current air switch, dissipated thermal energy in air spark and on the electrodes of switch, electric erosion of metallic electrodes of switch, depth of single crater of destruction on the electrodes of switch, thrown out mass of metal from the single crater of destruction of electrodes of switch.**

Приведены результаты применения нового инженерного подхода к расчету тепловой энергии, выделяющейся в плазменном канале искрового разряда и на массивных металлических электродах высоковольтного сильноточного воздушного коммутатора (ВСВК) атмосферного давления, используемого в составе высоковольтной электрофизической установки (ВЭФУ) с мощным емкостным накопителем энергии (ЕНЭ). Полученные соотношения для определения указанной энергии позволяют выполнять расчетную оценку баланса электрической энергии в разрядной цепи ВЭФУ с ЕНЭ с учетом ее тепловых потерь в ВСВК. Показано, что на основе разработанного подхода может быть выполнен расчет электрической эрозии основных металлических электродов ВСВК. Получены новые расчетные выражения для нахождения глубины одиночного кратера разрушения на металлических электродах ВСВК и массы металла, выбрасываемой искрой из электродов исследуемого коммутатора за один разряд ЕНЭ установки. Библ. 21, рис. 3.

Ключевые слова: **высоковольтный сильноточный воздушный коммутатор, выделяемая тепловая энергия в воздушной искре и на электродах коммутатора, электрическая эрозия металлических электродов коммутатора, глубина одиночного кратера разрушения на электродах коммутатора, выбрасываемая масса металла из одиночного кратера разрушения электродов коммутатора.**

Introduction. It is known that the commutation of the accumulated electric energy in a high-capacity capacitive energy storage (CES) device of a high-voltage electrophysical setting (HVES) is performed by means of a special electrical engineering device termed arrester by domestic terminology, and by foreign terminology by a switch [1, 2]. In the future, let us dwell

on the latest technical term, which has become most widely used in modern high-voltage pulse technology (HVPT). Vacuum, various gases and their mixtures, liquids and solids can be used as working dielectric media of the considered HVES discharge circuit switches with powerful CSE [1-4]. A wide application in the field of modern HVPT because of its comparative cheapness and simplicity in manufacturing has received high-voltage high-current air switches (HVCAS) of atmospheric pressure at a constant voltage up to ±125 kV and commutated pulse currents up to ±1 MA amplitude [1, 5-7]. As a rule, the main electrodes of HVCAS are made of medium and refractory metals (for example, steel and molybdenum) or metal compositions (for example, «tungsten-copper» compositions) [1, 3-7]. One of the drawbacks of these HVCAS is the increased electroerosive wear of the working surfaces of their main metal electrodes, caused by the intense exposure of the high-power heat flux of the plasma channel of the spark discharge in the areas of its binding at the electrodes of such switches. In this connection, for HVCAS, the actual tasks are those related to the calculation estimation in such high-current heat loss in switches in the plasma spark channel and on the main electrodes of the HVCAS, as well as the electrical erosion of the working surfaces of their main metal electrodes.

The goal of the paper is obtaining new calculation relationships that determine in an approximate form the energy dissipation and electrical erosion of massive metal main electrodes in the HVCAS used in the discharge circuits of a number of HVES with the CSE.

1. Research objective definition. Let us consider the HVES discharge circuit with a powerful CSE and an actively inductive load, switching large impulse current (LIC) in which the HVCAS performs with massive uniform base metal electrodes of a hemispherical shape-the cathode and the anode (Fig. 1). We suppose that these electrodes of HVCAS located in atmospheric air under normal conditions (air pressure is $1.013 \cdot 10^5$ Pa and its temperature is equal to θ_0=0 °C [8]) at the distance l_k from each other form a two-electrode system (TES). Let the radius R_e of the working surfaces of the cathode and the anode of the considered HVCAS exceeds the penetration depths in their conductive materials of the electromagnetic and thermal fields created by a cylindrical channel of a spark discharge of radius $r_c<R_e$ in the areas of its binding on the working surfaces of the electrodes of the investigated HVCAS.

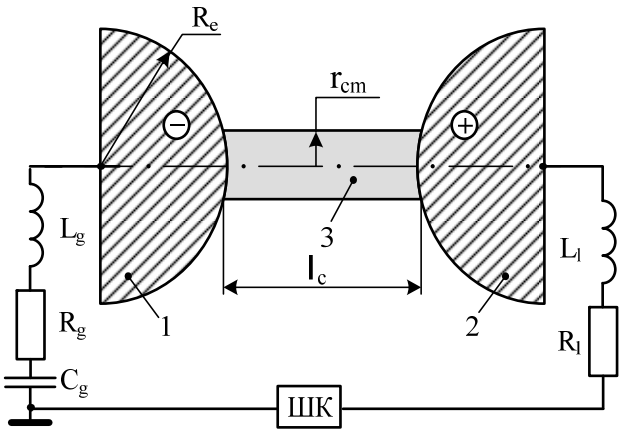

Fig. 1. The principal electrical circuit of the HVES discharge circuit with a powerful CSE and a high-voltage high-current two-electrode air switch (1, 2 – massive metal cathode and anode of HVCAS of hemispherical shape with an outer radius R_e; 3 – plasma high-current channel of an air spark discharge with length l_c and maximum radius r_{cm}; R_g, L_g, C_g – the own electrical parameters of the HVES with CSE; R_l, L_l – the own electrical parameters of the active-inductive load; ШК – the measuring coaxial ШК-300 shunt designed to measure a microsecond pulse current with an amplitude of I_m up to ±300 kA with its action integral J_a up to $2.5 \cdot 10^6$ J/Ω [9, 10])

In this connection we assume that the working surfaces of these electrodes of the HVCAS of the high-current spark in the zones of fastening of the high-current spark in the first approximation will be close to flat. We assume that in the TES of the switchboard, the length l_c of the plasma spark channel is equal to the minimum length l_k of the interelectrode gap in the HVCAS. We assume that the heat flux density $g_e(t)$ and the density δ_d (t) of the discharge current $i_d(t)$ of the HVES with CSE in the cylindrical spark discharge channel for the investigated HVCAS are practically uniformly distributed over its transverse circular cross section with a time-varying in t radius r_c. One of the confirmations to this can be the fact that in a high-current plasma channel of a gas discharge thermodynamic electron and ion temperatures are characterized by a practically uniform distribution in its current radius r_c [11]. We use the assumption that the holes (craters) of failure appearing in the areas of binding of the plasma channel of the spark discharge on the working surfaces of the anode and the cathode of the HVCAS have a geometric shape close to the shape of the spherical segment [12, 13]. It is required, within the proposed engineering approach, to obtain new relationships for the approximate calculation of the energy release and electrical erosion of massive metal electrodes in the HVCAS of the HVES discharge circuit with powerful CSE, and also to perform in a high-voltage laboratory using a powerful capacitor-type generator that generates, on the *RL*-load, a microsecond range, experimental verification of the performance of some of these relationships.

2. Approximate calculation of the energy dissipation in the HVCAS of the discharge circuit of the HVES with CSE. First, let us dwell on the estimated evaluation of the thermal energy W_c, which is dissipated directly in the plasma channel of the air spark discharge, which arises between the metal electrodes of the HVCAS. Proceeding from the known positions of electro- and thermophysics, the expression for W_c can be represented in the following form:

$$W_c = R_c J_a, \quad (1)$$

where $J_a = \int_0^\infty i_d^2(t)dt$ is the action integral of the pulsed current $i_d(t)$ in the discharge circuit of the HVES with CSE; R_c is the equivalent active resistance of the plasma channel of the air spark in the switch.

Next, let us determine the calculation in (1) of the action integral J_a of the current flowing in the HVES discharge circuit with CSE through the investigated HVCAS. In the case of a change in the current $i_d(t)$ according to the law of an exponentially damped sinusoid, which has the analytical form $i_d(t)=k_{ds}I_{ms}\exp(-\delta t)\sin(\omega t)$, the following calculation relation can be used for the action integral J_a of the discharge current in the HVES circuit with a powerful CSE:

$$J_a = 0.25k_{ds}^2 I_{ms}^2 \delta^{-1}\left[(\delta/\omega)^2+1\right]^{-1}, \quad (2)$$

where I_{ms} is the first amplitude of the discharge circuit $i_d(t)$ changing with angular frequency ω and the attenuation coefficient δ in the high-current circuit of the HVES with CSE;

$k_{ds}=\left[\exp(-\delta\omega^{-1}arcctg\,\delta\omega^{-1})\sin(arcctg\,\delta\omega^{-1})\right]^{-1}$ is the normalizing coefficient for a current varying in time t according to the law of a damped sinusoid [14].

In the case of a change in the discharge current, $i_d(t)$ by aperiodic law having the analytical form $i_d(t)=k_{da}I_{ma}[exp(-\alpha_1 t)-exp(-\alpha_2 t)]$, the calculated ratio for the action integral J_a in the HVES discharge circuit with CSE will have the following view:

$$J_a = 0.5k_{da}^2 I_{ma}^2\left[\alpha_1^{-1}+\alpha_2^{-1}-4(\alpha_1+\alpha_2)^{-1}\right], \quad (3)$$

where I_{ma} is the amplitude of the unipolar pulse current $i_d(t)$ with coefficients of the temporal shape α_1 and α_2; $k_{da}=\left[(\alpha_1/\alpha_2)^{\alpha_1/(\alpha_2-\alpha_1)}-(\alpha_1/\alpha_2)^{\alpha_2/(\alpha_2-\alpha_1)}\right]^{-1}$ is the normalizing coefficient for the impulse current of the HVES, which varies aperiodically with time t [14].

In the practical application of (3), it should be borne in mind that $\alpha_1\approx 0.76/\tau_p$ and $\alpha_2\approx 2.37/\tau_f$, [14], where τ_f, τ_p are, respectively, the front of the aperiodic discharge current pulse $i_d(t)$ between levels (0.1-0.9) I_{ma} and the duration of the aperiodic current pulse in the discharge circuit under study at a level of $0.5\cdot I_{ma}$. It is useful to find the ratio of the form $\tau_f\approx t_{ma}/1.6\approx 0.625ln(\alpha_2/\alpha_1)/(\alpha_2-\alpha_1)$ [14] when finding the amplitude-time parameters (ATP) of the aperiodic pulse of the discharge current $i_d(t)$ of the HVES with CSE, where t_{ma} is the time corresponding to the I_{ma} amplitude of the unipolar current in the high-current circuit of the HVES with CSE.

With regard to the concept of the equivalent active resistance R_c of the plasma channel of a spark used in (1), we mean by it a constant resistance averaged over time t, at which, when passing through the circuit of the HVES with CSE of the impulse discharge current $i_d(t)$, the same thermal energy, as well as on a real variable in time t resistance of the spark discharge channel in the TES of the considered HVCAS. When determining the active resistance $R_c(t)$ of the plasma channel of a spark discharge in the general form of the variable in time t in the investigated switch, we use the following classical relation [14]:

$$R_c(t) = l_c/[\pi r_c^2(t)\gamma_c], \quad (4)$$

where $r_c(t)$ is the radius of the plasma channel of spark discharge varying with time t, with constant length l_c between the metal electrodes of the HVCAS; γ_c is the averaged conductivity of low-temperature plasma in the channel of the switch spark.

The radius $r_c(t)$ of a single plasma spark channel in any design of the HVCAS varies, as is known, during the course of the impulse current $i_d(t)$ in the HVES discharge circuit with CSE in the range from zero to its maximum value r_{cm} [1, 9-12]. Initially, on the increasing part of the discharge current $i_d(t)$, this change occurs from zero to r_{cm}, and then on the falling part of this impulse current in the HVCAS circuit with CSE – from r_{cm} to zero. Therefore, according to (4), the time variation curve t of the value of the active resistance $R_c(t)$ of the plasma spark channel in the HVCAS can be approximated by a symmetric U-shaped curve characterized by its two maximum values at times t corresponding to zero current values $i_d(t)$ and equality $r_c=0$, and its one minimum value at time t, when the current $i_d(t)$ reaches its amplitude value and $r_c=r_{cm}$. Then, taking into account the corresponding change in (4) in time t of the radial function of the form $f(r_c)=r_c^2$ on the interval [0; r_{cm}] and finding the average value for the equivalent and constant in time t of the active resistance R_c of a single plasma spark-gap channel in the investigated HVCAS, we obtain the following calculated expression:

$$R_c = l_c/(\pi\gamma_c r_{cm}^{-1}\int_0^{r_{cm}} r_c^2 dr_c) = 3l_c/(\pi r_{cm}^2\gamma_c). \quad (5)$$

From (5), the proposed approach in the definition of R_c implies the calculated ratio for the equivalent radius r_{ce} of the plasma channel of a high-current spark in the HVCAS, equal to $r_{ce}\approx 0.577\cdot r_{cm}$. The magnitude of the maximum radius r_{cm} (m) of the plasma channel of a spark discharge in an atmospheric pressure HVCAS is found from the well-known Braginskiy formula [1, 15]:

$$r_{cm} = 0.093(I_m)^{1/3}(t_m)^{1/2}, \quad (6)$$

where I_m, t_m are, respectively, the amplitude (A) of the pulse current $i_d(t)$ in the HVES discharge circuit with powerful CSE and the time (s) corresponding to this current amplitude.

From (5) and (6), the generalized expression for the equivalent active resistance R_c (Ω) of a single high-current plasma high-current spark discharge channel in the HVCAS placed in the HVES with CSE discharge circuit assumes the following final form:

$$R_c = 110.41 \cdot l_c /(\gamma_c I_m^{2/3} t_m). \quad (7)$$

When selecting (7) for the numerical values of γ_c values will be based on its own computational and experimental data obtained earlier for plasma spark discharge air passage in the high-current circuit of HVES with powerful CSE [15]. According to the results of the studies presented in [15], for high-voltage atmospheric air switches at operating DC voltage up to ±35 kV and pulse currents of microsecond duration in the discharge circuit of HVCAS capacitor bank with a low resistance *RL*-load at their amplitude up to ±250 kA, characteristic for a pulse components artificial lightning current [16], the averaged conductivity value *γc* low-temperature plasma in a cylindrical channel HVCAS spark in the first approximation, taking into account (5) and (6) numerically from 4000 to 5000 $(\Omega \cdot m)^{-1}$. It should be noted that these values γ_c differ significantly from the corresponding values of the estimated temperature plasma conductivity of high spark air (about $20 \cdot 10^3$ $(\Omega \cdot m)^{-1}$) is given in [1] and the characteristic of the highly ionized plasma. Let us note that, at an electron temperature in the high-current spark discharge channel of the order of 10^4 K, which is characteristic of the channel of an air high-current spark in the investigated HVCAS [17], even in a dense plasma of the underwater spark discharge channel initiated by an electric explosion of a thin copper wire, the numerical values for its specific electric conductivity γ_c channel depending on the pressure level is not more than a few thousand $(\Omega \cdot m)^{-1}$ [18].

Next, we estimate the value of thermal energy W_e, which is released on two massive metal electrodes of the considered HVCAS, schematically shown in Fig. 1. The determining effect on W_e will be the power density $g_c(t)$ of the heat flux in the plasma spark channel between the cathode and the anode of the HVCAS. In the estimation of $g_c(t)$ in the proposed approach, a relationship of the form [17] can be used:

$$g_c(t) = \delta_d(t) \cdot U_{ac}, \quad (8)$$

where U_{ac} is the electrode voltage drop in the considered HVCAS, equal to the difference of electrical potentials at the interface between the «spark-metal» media.

It is known that the value of U_{ac} in the investigated HVCAS with the main electrodes made of such traditional conductor materials as steel, copper, brass and beryllium bronze varies in a very narrow quantitative range, ranging from 5 to 10 V [19]. Thus, for steel grade Ст.3, the near-electrode voltage drop U_{ac} is numerically about 6.1 V, for copper – 8.6 V, and for brass – 8.0 V [19]. Taking into account the assumed assumptions and (8) for the thermal energy W_e dissipated on the working surfaces of the metal electrodes of the TES we can write the calculated expression:

$$W_e = 2\pi \int_0^\infty g_c(t) r_c^2(t) dt = 2\pi U_{ac} \int_0^\infty \delta_d(t) r_c^2(t) dt = 2U_{ac} q_c, \quad (9)$$

where $q_c = \int_0^\infty i_d(t) dt$ – the module of the electric charge flowing through the plasma channel of the spark discharge in the high-current circuit of the HVES with powerful CSE and the metal electrodes of the investigated HVCAS.

It is seen from (9) that for the calculated determination of the thermal energy W_e we need to first know the amount of electricity q_c that has flowed through the electrodes of the HVCAS. Moreover, the desired value of W_e is directly proportional to the electric charge q_c. When changing the impulse current $i_d(t)$ in the discharge chain of HVES with SNE according to the law of an exponentially damped sinusoid, the following relation can be used to calculate the charge q_c:

$$q_c = k_{ds} I_{ms} \omega^{-1} \left[(\delta / \omega)^2 + 1 \right]^{-1}. \quad (10)$$

At changing the impulse current $i_d(t)$ with respect to the aperiodic time dependence for q_c, we have:

$$q_c = k_{da} I_{ma} (\alpha_2 - \alpha_1)(\alpha_1 \alpha_2)^{-1}. \quad (11)$$

One of the checks on the correctness of the calculation results for (10) and (11) for q_c is the data obtained from the expression $q_c = C_g U_{gc}$, where C_g and U_{gc} are the electrical capacitance and charging voltage of the high-voltage capacitors of CSE, respectively.

Thus, by determining the value of the heat energy W_c dissipated in the spark channel by (1) – (3) and (7) and calculating the thermal energy by the heat energy W_e scattered at the cathode and the anode of the TES by (9) – (11), from the expression $W_k = W_c + W_e$ can find the total energy release in the high-current air circuit of the HVES discharge circuit with CSE.

3. Approximate calculation of the electrical erosion of electrodes in the HVCAS of the discharge circuit of the HVES with CSE. In the framework of this study, let us dwell on the estimated estimation of the electric erosion of the working surface of the metal electrode-anode HVCAS caused by a stream of free electrons accelerating in the longitudinal electric field of

the channel, bombarding the indicated surface of the anode of the switch under consideration. In this case, for the thermal energy W_a, which is dissipated in the circular zone of the binding of the spark discharge channel with a radius r_{cm} on the working surface of the anode of the HVCAS, one can, on the basis of (9), write the following relationship:

$$W_a = U_{ac} q_c . \quad (12)$$

On the other hand, for the sought value of the thermal energy W_a, based on the positions of thermal physics, the following calculated formula will hold true:

$$W_a = M_e \left[C_e (\theta_m - \theta_0) + C_m \right], \quad (13)$$

where $M_e = d_e \cdot V_e$ is the mass of intensely heated by the pulsed discharge current $i_d(t)$ in the circular binding zone on the surface of the electrode electrode-anode of the HVCAS of the spark channel to the melting point θ_m of its material having the density d_e and volume V_e; C_e, C_m are, respectively, the specific heat and specific heat of fusion of the anode material of the considered HVCAS.

The value of the volume V_e of the melt and ejected outward by the magnetic pressure of the liquid metal of the switch, for one exposure of the spark channel to it, taking into account the assumed assumption about the geometric form of the crater of destruction on its working surface in the form of a ball segment, can be described by the following relation:

$$V_e = 0.5 \pi r_{cm}^2 h_e , \quad (14)$$

where h_e is the depth of the rupture crater with an outer radius r_{cm} on the working surface of the HVCAS anode during the time of exposure to a spark from one high-current discharge of the HVES capacitor bank.

From (12) – (14), taking into account (6), the calculated expression for the maximum depth h_e (m) of a single erosion crater of destruction on the electrode-anode of the switch under consideration takes the following form:

$$h_e = 73.61 U_{ac} q_c d_e^{-1} \left[C_e (\theta_m - \theta_0) + C_m \right]^{-1} (I_m^{2/3} t_m)^{-1}. \quad (15)$$

For the reduce the mass M_e (kg) of metal emitted outward by a high-current spark from the anode electrode for one spark discharge in the HVES circuit with CSE and the working air gap of the HVCAS in question, we obtain the following calculated ratio:

$$M_e = U_{ac} q_c \left[C_e (\theta_m - \theta_0) + C_m \right]^{-1} . \quad (16)$$

It follows from (16) that the calculated loss of the metal mass M_e from the electrode-anode of the investigated switch for one discharge of powerful CSE in the HVES circuit is directly proportional to the charge q_c that has flowed through the main electrodes of the HVCAS. Note that such dependence for M_e was previously established experimentally for commutation in the HVES discharge circuit with CSE of large pulsed exponentially decaying sinusoidal currents of microsecond duration for copper, molybdenum and titanium electrodes of the HVCAS [20]. In the first approximation, for the loss of the M_{eN} mass due to the anode electrode of the switch for N spark discharges of the powerful CSE of the electrophysical unit through the HVCAS, one can use the calculated ratio of the form: $M_{eN} \approx N \cdot M_e$. In addition, we point out that when calculating the electrical erosion of the metal electrode-cathode of the HVCAS, the calculated expressions (15) and (16) can be used.

4. Experimental verification of the results of calculating the electrical erosion of steel electrodes in the HVCAS discharge circuit of the HVES with ENE. This test was performed in the HVES discharge circuit with a powerful single-module CSE for a rated voltage of ±50 kV with nominal power capacity of its capacitor bank $W_{g0} \approx 416$ kJ (111 pieces of parallel-connected high-voltage capacitors of the type ИК-50-3) forming on the concentrated RL-load ($R_l \approx 10$ mΩ, $L_l \approx 0.3$ μH) LIC of microsecond duration [9, 14]. We will point out that the experimental HVES had the following electric parameters (up to the prefabricated steel buses of the CSE collector without taking into account the influence of the switch) [9, 14]: capacitance C_g=333 μF; inductance L_g = 2.05 μH; active resistance R_g = 57 mΩ. To switch the energy used by the HVES to the CSE a cascade-type HVCAS was used for a rated voltage of ±50 kV, containing two main massive hemispherical electrodes of radius $R_e \approx 61.5$ mm and one controlling a massive spherical electrode 30 mm in diameter made of steel of grade Ст.3 (Fig. 2) [7, 9].

Fig. 2. Enlarged view of a three-electrode system of the cascade type HVCAS with two hemispherical massive main electrodes and one control electrode of a spherical steel Ст.3 marks on the rated voltage ±50 kV and a pulse microsecond current amplitude I_m up to ±300 kA (type after a single exposure at its electrodes in steel HVES discharge circuit with powerful pulse CSE damped sinusoidal current frequency $\omega/2\pi$=4.9 kHz and amplitude of the first I_{ms}=–202 kA; J_a=2,12·10^6 J/Ω; experimental channel radius value sparks $r_{cm} \approx 31$ mm length channel spark $l_c \approx 13.5$ mm)

At the charging voltage of high-voltage impulse capacitors of this CSE is equal to U_{gc}=±29.7 kV and the energy stored in them is W_g=147 kJ, the working air gap between the control electrode of the HVCAS and its

potential main electrode is l_{c1}≈9 mm, and from the non-potential side The main electrode of the switch, the working air gap was l_{c2}≈4.5 mm. In this connection, in the experimental HVCAS, the length of the high-current spark was approximately $l_c=l_{c1}+l_{c2}$≈13.5 mm. After a high voltage igniting microsecond voltage pulse of amplitude of ±100 kV (its polarity corresponded to the charge polarity of the CSE capacitors) was applied to the control electrode of the HVCAS from a special generator [7, 9], an electrical breakdown of an air gap of length l_{c2} occurred, which resulted in the breakdown of an air gap of length l_{c1} and trip mentioned switch as a whole. As a result of triggering HVCAS between its steel electrodes a high-current air spark appeared, which destroys the working surfaces of the anode, cathode and control electrode of the switch. In Fig. 2 the results of such electrothermal action on these steel electrodes of the high-current plasma channel of an air spark discharge occurring in the HVCAS of the experimental HVES (U_{gc} =–29.7 kV) are shown, in the case of LIC flowing through them, whose oscillogram is shown in Fig. 3.

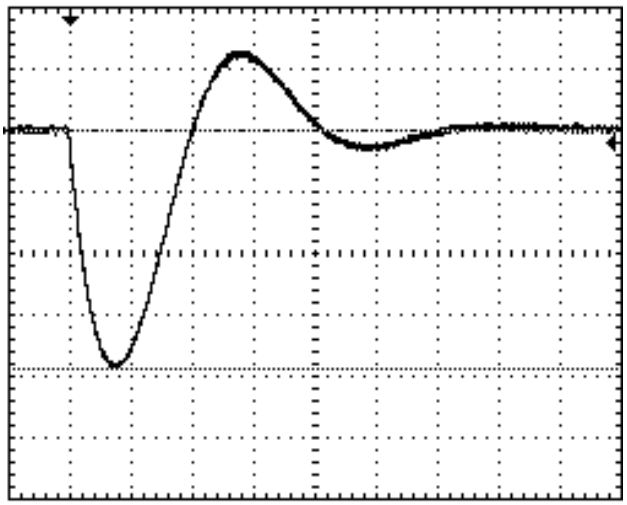

Fig. 3. . Oscillogram of a pulsed damped sinusoidal current $i_d(t)$ in the HVES discharge circuit with powerful CSE and a low-resistance concentrated *RL*-load, a switched cascaded HVCAS with two massive basic hemispherical electrodes and one control spherical electrode of Ст.3 grade for a nominal voltage of ±50 kV and pulsed microsecond current of amplitude I_m up to ±300 kA (U_{gc}=−29.7 kV; W_g=147 kJ; I_{ms}=−202 kA; δ=13.00·10^3 s^{-1}; ω=30.79·10^3 s^{-1}; k_{ds}=1.783; t_{ms}=36 μs; t_0=500 μs; J_a=2.12·10^6 J/Ω; q_c=9.93 C; vertical scale – 52.1 kA/division; horizontal scale – 50 μs/division).

Measurement of the ATP of the pulsed damped sinusoidal current $i_d(t)$ in the discharge circuit of the experimental HVES with powerful CSE was carried out using a measuring coaxial shunt of the ШК-300 type, certified by the state metrological service, with an intrinsic active resistance of about R_s≈0.2 mΩ and a conversion factor of about K_s≈10,42·10^3 A/V [10, 14], and the digital storage oscilloscope Tektronix TDS 1012. According to the diagram in Fig. 3 the oscillogram of the damped sinusoidal LIC $i_d(t)$ with the first half-wave of negative polarity in the discharge circuit of the HVES of its ATP at the total duration of the current pulse t_0=500 μs was approximately equal in absolute value: I_{ms}=202 кА; δ=13.00·10^3 s^{-1}; ω=30.79·10^3 s^{-1}; k_{ds}=1.783; t_{ms}=36 μs.

To the above-mentioned ATP discharge current $i_d(t)$ in the circuit of the experimental HVES with CSE according to (6) corresponds to the calculated maximum radius r_{cm} of the plasma channel of the air spark in the investigated switch, equal to about 32.7 mm. From the experimental data presented in Fig. 2, it follows that the maximum radius r_{cm} of the circular crater hole on the working surfaces of the main steel electrodes in the HVCAS of the applied experimental HVES with the CSE is approximately 31 mm. It can be seen that the calculated and experimental results for the radius r_{cm} of the binding zone of the plasma channel of the high-current spark on the working steel surfaces of the anode and the cathode of the said HVCAS differ within 5 %. In this connection, we can say that the experimental data obtained by us confirm the operability of the calculated Braginskiy formula for the plasma channel of an air spark used in [1, 15] for practical application in the LIC region of microsecond time range.

The results of a survey of the working hemispherical surfaces of the steel anode and the cathode of the HVCAS, shown in Fig. 2, indicate that in the case under consideration the geometrical shape of single circular craters of destruction with a radius of r_{cm}≈31 mm in the areas of attachment of a high-current air spark to them was close to the shape of the spherical segment, and their experimental depth he did not exceed 7 μm. In accordance with (10) and (15) with given initial data (I_{ms}=202 kA; δ=13.00·10^3 s^{-1}; ω=30.79·10^3 s^{-1}; k_{ds}=1.783; t_{ms}=36 μs; U_{ac}=6.1 V; d_e=7870 kg/m^3; C_e=460 J/(kg·^{o}C); C_m=84·10^3 J/kg; θ_0=0 ^{o}C; θ_m=1500 ^{o}C [8, 10]) we find that in our case the calculated maximum depth h_e for erosion craters of failure at their design radius r_{cm}≈32.7 mm on the working surfaces of the massive main steel electrodes of HVCAS when flowing through the switchboard in a single pulse discharge of a powerful CSE (U_{gc} =–29.7 kV; W_g=147 kJ) in the high-current circuit of the experimental WEFU electric charge q_c=9.93 C will be approximately 5.9 μm. As we can see, the discrepancy between the calculated and experimental values for h_e with respect to the HVCAS used is no more than 16%. We will point out that in this case the calculated loss of the metal mass M_e from the working surface of the steel electrode-anode in accordance with (16) is approximately 78.2 mg. Then, for the specific electric erosion of M_e/q_c of the steel electrode-anode of the considered HVCAS, we obtain a numerical value equal to about 78.7·10^{-4} g/C. To compare this specific electroerosion wear M_e/q_c of the massive steel main

electrodes of the investigated HVCAS with known similar electrophysical data, we note that in high-current high-voltage gas-discharge switches for nominal voltage of ±50 kV type РГУ1-50-100 with the main electrodes from the metal composition «tungsten-copper», designed for commutation of damped sinusoidal microsecond LIC with duration $t_0 \leq 100$ μs and an amplitude of I_{ms} up to 100 kA, a specific electroerosive wear of their composite anode and a cathode But is almost two orders of magnitude smaller numerical value and is approximately $4.4 \cdot 10^{-5}$ g/C [21].

Conclusions.

1. In accordance with the proposed new engineering approach to approximate calculated energy estimates and electrical erosion in large metal electrodes in the HVCAS of atmospheric pressure, performing switching in a discharge circuit of the HVES with powerful CSE, only necessary data on the electrical and thermal characteristics of the anode metal and its cathode TES averaged conductivity γ_c of low-temperature plasma in a channel of the air spark discharge between the electrodes of the HVCAS ATP of pulsed discharge current $i_d(t)$ in high-current circuit of the HVES with CSE.

2. It has been established that when calculating the thermal energy W_c that is dissipated in the air spark of the investigated HVCAS, a new electrophysical concept concerning the equivalent active resistance R_c of a pulsed air spark that is constant during the whole process of oscillating or aperiodic discharge of the CSE of the HVES on the electric load can be used. The original calculation formula (7) is obtained to find the approximate numerical value of R_c from the known data for γ_c, the length l_c of the air spark channel, and the ATP of pulsed sinusoidal (aperiodic) discharge current of the CSE in the high-current HVES circuit on the *RL*-load.

3. The performed high-current experiments in the HVES discharge circuit with powerful CSE confirmed the reliability of certain obtained and used formulas calculation relations (in particular, formulas (6), (10), (15) and (16)) for approximate estimation of energy dissipation and electric erosion of massive metal electrodes of TES in the investigated HVCAS of atmospheric pressure.

REFERENCES

1. Dashuk P.N., Zayents S.L., Komel'kov V.S., Kuchinskiy G.S., Nikolaevskaya N.N., Shkuropat P.I., Shneerson G.A. *Tehnika bol'shih impul'snyh tokov i magnitnyh polej* [Technique large pulsed currents and magnetic fields]. Moscow, Atomizdat Publ., 1970. 472 p. (Rus).

2. Bostic W., Nardi V., Zucker O. *Nakoplenie i kommutacija energii bol'shih plotnostej* [Accumulation and commutation of energy of high densities]. Moscow, Mir Publ., 1979. 474 p. (Rus).

3. Baranov M.I. Application of new gas-discharge and solid-state semiconductor switchboards in high-current circuits of powerful high-voltage electrophysical installations. *Electrical engineering & electromechanics*, 2009, no.1, pp. 55-58. (Rus). **doi: 10.20998/2074-272X.2009.1.11.**

4. Baranov M.I. Application of new vacuum switchboards in high-current circuits of powerful high-voltage electrophysical installations and emergency protection circuits of power electrical equipment. *Electrical engineering & electromechanics*, 2009, no.3, pp. 5-10. (Rus). **doi: 10.20998/2074-272X.2009.3.01.**

5. Boyko N.I., Evdoshenko L.S., Zarochentsev A.I., Ivanov V.M., Tour A.N. High-Voltage Spark Gaps for Technological Purposes. *Instruments and Experimental Technique*, 2001, vol.44, no.2, pp. 204-212. **doi: 10.1023/a:1017515003483.**

6. Baranov M.I., Bocharov V.A., Zyabko Yu.P., Melnikov P.N. High-voltage strong current spark switches for high-voltage impulse and current generators. *Tekhnichna elektrodynamika*, 2003, no.3, pp. 41-47. (Rus).

7. Baranov M.I., Koliushko G.M., Kravchenko V.I., Nedzel'skii O.S., Nosenko M.A. High-voltage high-current air-filled spark gaps of an artificial-lightning-current generator. *Instruments and Experimental Techniques*, 2008, vol.51, no.6, pp. 833-837. **doi: 10.1134/s0020441208060109.**

8. Kuhling H. *Spravochnik po fizike. Per. s nem*. [Dictonary on Physics. Translated from German]. Moscow, Mir Publ., 1982. 520 p. (Rus).

9. Baranov M.I., Koliushko G.M., Kravchenko V.I., Nedzel'skii O.S., Dnyshchenko V.N. A Current Generator of the Artificial Lightning for Full-Scale Tests of Engineering Objects. *Instruments and Experimental Technique*, 2008, vol.51, no.3, pp. 401-405. **doi: 10.1134/s0020441208030123**.

10. Baranov M.I., Kniaziev V.V., Rudakov S.V. Calculation and experimental estimation of results of electro-thermal action of rationed by the international standard IEC 62305-1-2010 impulse current of short blow of artificial lightning on the thin-walled coverage from stainless steel. *Electrical engineering & electromechanics*, 2017, no.1, pp. 31-38. (Rus). **doi: 10.20998/2074-272X.2017.1.06.**

11. Raiser Yu.P. *Fizika gazovogo razrjada* [Physics of gas discharge]. Moscow, Nauka Publ., 1987. 592 p. (Rus).

12. Namitokov K.K. *Elektroerozionnye javlenija* [Electroerosion phenomena]. Moscow, Energia Publ., 1978. 456 p. (Rus).

13. Butkevich G.V., Belkin G.S., Vedeshenkov N.A., Zhavoronkov M.A. *Elektricheskaja erozija sil'notochnyh kontaktov i elektrodov* [Electrical erosion of high current contacts and electrodes]. Moscow, Energia Publ., 1978. 256 p. (Rus).

14. Baranov M.I. *Izbrannye voprosy elektrofiziki. Tom 3: Teorija i praktika elektrofizicheskih zadach* [Selected topics of Electrophysics. Vol. 3: Theory and practice of electrophysics tasks]. Kharkiv, Tochka Publ., 2014. 400 p. (Rus).

15. Lozanskiy E.D., Firsov O.B. *Teorija iskry* [Theory of spark]. Moscow, Atomizdat Publ., 1975. 272 p. (Rus).

16. SAE ARP 5412: 2013. Aircraft Lightning Environment and Ralated Test Waveforms. SAE Aerospace. USA, 2013. − pp. 1-56.

17. Baranov M.I. An approximate calculation of the maximum temperature of the plasma in high-current high-voltage spark discharge channel switch air atmospheric pressure. *Tekhnichna Elektrodynamika*, 2010, no.5, pp. 18-21. (Rus).

18. Gulyi G.A. *Nauchnye osnovy razriadno-impul'snykh tekhnologii* [Scientific basis of the discharge-pulse technology]. Kiev, Naukova Dumka Publ., 1990. 208 p. (Rus).

19. Abramov N.R., Kuzhekin I.P., Larionov V.P. Characteristics of penetration of the walls of metal objects when exposed to lightning. *Electricity*, 1986, no.11, pp. 22-27. (Rus).
20. Belkin G.S., Kiselev V.Ya. Influence of electrode material on erosion at strong currents. *Technical Physics*, 1967, vol.37, no.5, pp. 977-979. (Rus).
21. Ermilov I.V. Development of a complex of high-voltage high-current equipment of a new generation for magnetic-pulse processing of materials. *Trudy mezhdunarodnoi nauchno-tekhnicheskoi konferentsii MIOM-2007* [Proceedings of the International Scientific and Technical Conference MPPM-2007]. Russian Federation, Samara, SGAU, 18-19 September, 2007, pp. 88-98. (Rus).

M.I. Baranov[1], *Doctor of Technical Science, Chief Researcher,*
S.V. Rudakov[2], *Candidate of Technical Science, Associate Professor,*
[1] Scientific-&-Research Planning-&-Design Institute «Molniya», National Technical University «Kharkiv Polytechnic Institute», 47, Shevchenko Str., Kharkiv, 61013, Ukraine,
phone +38 057 7076841,
e-mail: eft@kpi.kharkov.ua
[2] National University of Civil Protection of Ukraine,
94, Chernyshevska Str., Kharkiv, 61023, Ukraine,
phone +38 057 7073438,
e-mail: serg_73@i.ua

Received 27.03.2017

How to cite this article:
Baranov M.I., Rudakov S.V. An approximate calculation of energy dissipation and electric erosion of electrodes in the high-voltage high-current air switch of atmospheric pressure. *Electrical engineering & electromechanics*, 2017, no.3, pp. 32-39. **doi: 10.20998/2074-272X.2017.3.05.**

UDC 621.317.39 **doi: 10.20998/2074-272X.2017.3.06**

A.A. Korobko

MULTIFREQUENCY ALGORITHMS FOR DETERMINING THE MOISTURE CONTENT OF LIQUID EMULSIONS BY THE METHOD OF RESONANCE DIELCOMETRY

Purpose. *The main attention is paid to the development and investigation of multifrequency algorithms for the realization of the method of resonance dielcometric measurement of the humidity of emulsions of the type «nonpolar liquid dielectric-water». Multifrequency algorithms take into account the problem of «uncertainty of varieties» and increase the sensitivity of the dielcometric method.* ***Methodology.*** *Multifrequency algorithms are proposed to solve the problem of «uncertainty of varieties» and improve the metrological characteristics of the resonance dielcometric method. The essence of the algorithms is to use a mathematical model of the emulsion and to determine the permittivity of the dehydrated liquid and the emulsion. The task of developing algorithms is to determine and take into account the influence of the parasitic electrical capacitance of the measuring oscillator and the measuring transducer. The essence of the method consists in alternately determining the resonance frequency of the oscillatory circuit with various configurations, which allows to take into account errors from parasitic parameters. The problem of «uncertainty of varieties» is formulated and solved. The metrological characteristics of the resonance dielcometric method are determined using algorithms.* ***Results.*** *Frequency domains of application of mathematical model of an emulsion are defined. An algorithm in a general form with four frequencies suitable for practical implementation in dielcometric resonance measurements is developed. Partial algorithms with three and two frequencies are developed. The systematic values of simulation errors in the emulsion in the microwave range are determined. Generalized metrological characteristics are obtained. The ways of increasing the sensitivity of the dielcometric method are determined. The problem of «uncertainty of varieties» was solved. Experimental data on determination of humidity for the developed algorithms are obtained. The value of the volumetric moisture in the transformer oil was measured.* ***Originality.*** *New multifrequency algorithms for determining the moisture content by the resonance dielcometric method have been proposed, investigated and practically realized. A generalized metrological characteristic for an algorithm with four frequencies is obtained. Metrological characteristics of algorithms for three and two frequencies are obtained. The problem of «uncertainty of varieties» was solved. Recommendations for increasing the sensitivity of dielcometric resonance moisture meters are developed and implemented.* ***Practical value.*** *The results of this work allow to solve the problem of «variability of varieties», increase sensitivity and accurately determine the moisture content in most nonpolar liquid dielectrics to a value of 10^{-5}. This is applicable in a large field of electrical engineering, machine building, oil refining and the chemical industry.* References 10, tables 3, figures 2.

Key words: **moisture, method of resonance dielcometry, varietal uncertainty, mathematical model of emulsion, multifrequency algorithm, generalized metrological characteristics.**

Предложены многочастотные алгоритмы определения влагосодержания эмульсии типа: «неполярный жидкий диэлектрик – вода» методом резонансной диэлькометрии. Использована математическая модель эмульсии с представлением воды в виде идеально проводящих сфер. Определены частотные области применимости модели в ВЧ и СВЧ диапазонах. В СВЧ диапазоне определены величины систематических погрешностей модели. Для решения проблемы «сортовой неопределенности» и улучшения метрологических характеристик резонансного диэлькометрического метода разработан четырехчастотный алгоритм, являющийся обобщенным видом трех- и двухчастотных алгоритмов. Определена обобщенная метрологическая характеристика четырехчастотного алгоритма и его предельные характеристики. Получены метрологические характеристики для трех- и двухчастотных алгоритмов. Проведен анализ погрешностей и корректности теоретических исследований путем сравнения их результатов с экспериментальными данными для ВЧ и СВЧ диапазонов. Библ. 10, табл.3, рис.2.

Ключевые слова: **влагосодержание, резонансная диэлькометрия, сортовая неопределенность, математическая модель эмульсии, многочастотный алгоритм, метрологическая характеристика.**

Introduction. The problem of determining the moisture content of technical fluids is relevant for practical applications in various areas of industry. In this case, the lower values of the measured values of the volumetric moisture content W in emulsions of the «nonpolar liquid dielectric-water» type can be from 10 cm^3/m^3 for transformer oil up to 100 cm^3/m^3 for aviation kerosene. The measurement of such small values of moisture content is a complex technical task and requires the development of methods and technical means for measuring moisture content with the appropriate characteristics.

Using dielcometry for the calculated determination of the volume moisture content W of emulsions is based on the dependence of the dielectric constant ε_{eml} of a homogeneous emulsion of the «liquid nonpolar dielectric-water» type on the moisture content and permittivity ε_{nld} of an anhydrous nonpolar liquid dielectric. Moreover, this dependence can be obtained both experimentally (by the method of preliminary calibration of moisture meters using «reference» emulsions) and analytically, in the form of a functional connection, the values of the volume moisture content W and the dielectric permittivities ε_{eml}

and ε_{nld}. This functional relationship is determined on the basis of various mathematical models of the emulsion. In both cases, the reliability of the results obtained is significantly influenced by the so-called «varietal uncertainty». This is the dependence of the moisture content on the magnitude of the permittivity and, consequently, on the grade of the liquid being investigated.

In this paper, theoretical and practical aspects of ways to improve metrological characteristics, both the dieelcometric method itself and technical means for measuring the moisture content of nonpolar liquids, are simultaneously considered, while solving the problem of «varietal uncertainty».

Analysis of the current state of the problem. To determine low levels of volumetric moisture content, a high sensitivity of the method is necessary. The maximum sensitivity is characterized by resonance dielcometric methods. The essence of these methods is to determine the dielectric constant of a liquid by measuring the resonance frequency of an oscillating circuit, which includes a capacitive type measuring transducer (MT) filled with the test liquid. They use a wide range of frequencies of electromagnetic oscillations from sound to HF and microwave ranges [1].

In order to clarify the technical level of modern resonant high-frequency and microwave dielcometric moisture meters for liquid nonpolar dielectrics, an analysis of the characteristics of modern standard moisture meters on the market was carried out (Table 1).

The moisture meters considered differ substantially in their technical level, which can be characterized by the magnitude of the absolute error in measuring the moisture content at the lower range.

Table 1

Characteristics of typical modern HF and microwave moisture meters

No.	Moisture meter type (measurement range W, cm^3/m^3)	Absolute measurement error, cm^3/m^3
1	EASZ-1 ($0 – 10^4$)	$\pm$100
2	УВДН-1ПМ1 ($100 – 6\cdot10^4$)	$\pm$100
3	EASZ-1BS&W ($0 – 10^4$)	$\pm$100
4	FIZEPR – SW 100.30 (1000 – 3000)	$\pm$200
5	ЭУДВН-1л ($200 – 2\cdot10^4$)	$\pm$200
6	УДВН-1эп ($100 – 2\cdot10^4$)	$\pm$250
7	Universal IV CM ($0 – 10^4$)	$\pm$300
8	OW–301 ($0 – 10^4$)	$\pm$500
9	МВН – 1 ($0 – 3\cdot10^4$)	$\pm$500
10	PHASE DYNAMICS – L ($0 – 2\cdot10^4$)	$\pm$500

As can be seen from Table 1, the dielcometric hygrometers corresponding to the best samples (No. 1 – 3 of Table 1) do not allow a correct measurement of the volume moisture content less than 100 cm^3/ m^3. It should be noted that in all the moisture meters examined, the problem of «varietal uncertainty» is not solved, since it is necessary to pre-calibrate them.

The existing algorithms for solving the problem of «varietal uncertainty» of dielcometric moisture meters are considered in [1-5]. These include the following algorithms.

A. Algorithm with the introduction of dielectric cylinders into the working space.

B. Algorithms: with the separation of flows of the investigated emulsion; with the addition of a predetermined water flow rate; with additives of water and controlled medium.

C. Algorithm with the use of least squares methods.

D. Algorithm with the use of polynomials Lagrange.

E. Algorithms of additive and multiplicative types.

F. Additive algorithm with the introduction of a metal plate into the interelectrode space of a capacitive-type capacitor.

The analysis showed that these algorithms are not applicable for increasing the sensitivity of dielcometric moisture meters to values of the volumetric moisture content of the order of 10 cm^3/m^3 (10^{-5} in dimensionless quantities) for the following reasons: parasitic parameters of the capacitive-type capacitor type (and edge effects for algorithm *F*) ; The relative error in measuring the dielectric constant (algorithm *A*), the flow and volume of liquids (algorithms *B-E*), and the geometric dimensions (algorithm *F*) of no more than 10^{-6} in the laboratory is an extremely difficult practical task.

On the basis of the foregoing, the way of realization of the dielcometric resonance method with increased sensitivity and simultaneous solution of the problem of «varietal uncertainty» is determined. This is the use of algorithms with a controlled change in the state of the emulsion for the resonance dielcometric method, taking into account the effect on the metrological characteristics of the parasitic parameters and the edge effects of the capacitive-type MT.

The goal of the work is the development, investigation and justification of multifrequency algorithms for determining the moisture content of emulsions of the «nonpolar dielectric-water» type by the method of resonance dielcometry with improved metrological characteristics and solving the problem of «varietal uncertainty».

Proceeding from this goal, the tasks of the work are: determining the areas of applicability of the physical model of the emulsion in the frequency domain; Development of multifrequency algorithms for solving the problem of «varietal uncertainty»; determination of the main metrological characteristics of the proposed

algorithms, taking into account the influence of parasitic parameters of MT and measuring generator (MG); experimental verification of the correctness of the proposed test algorithms.

Selection of the emulsion model and determination of its applicability areas. As a mathematical model of the emulsion, a model was chosen [7], in which individual water droplets were replaced by ideally conducting spheres of small diameter, which are much larger than their diameter and uniformly distributed throughout the volume. By definition, the volume moisture content is the ratio of the volume of water in the emulsion V_{wat} to the total emulsion volume V_{eml}:

$$W = V_{wat} / V_{eml} \ . \qquad (1)$$

The mathematical model of the emulsion determines the functional relationship between the values of the volumetric moisture content W and the permittivity ε_{eml} and ε_{nld} [7]:

$$\varepsilon_{eml} = \varepsilon_{nld}(1+3W) \ . \qquad (2)$$

In [7] the frequency domain of the correctness of this model for the HF frequency band was determined, which extends to 2 MHz. In this frequency range, water behaves like an ideal conductor with a permittivity equal to infinity.

On the other hand, the electrophysical properties of water are such that in the frequency range from about 100 MHz to 1 GHz ε_{wat} varies insignificantly (from 78.2 to 78.0). In this range, water behaves like a perfect dielectric (the magnitude of the dielectric loss tangent does not exceed 0.005) [8]. Taking into account that $\varepsilon_{wat} >> \varepsilon_{eml}$, we can extend this mathematical model of the emulsion to the frequency range 100 MHz – 1 GHz. As a result, a systematic error arises due to the properties of the most simplified mathematical model at these frequencies. Ideally conducting spheres simulating real water droplets in the emulsion (ε_{wat} = 81) are replaced in the mathematical model of emulsion by spheres of similar dimensions from an ideal dielectric ($\varepsilon_{wat} = \infty$).

An idealized calculation scheme for determining the systematic error of a mathematical model due to the effect of a change in ε_{wat} for a generalized capacitive MT scheme is shown in Fig. 1.

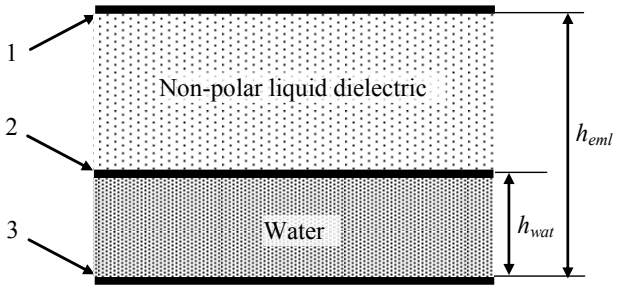

Fig. 1. Idealized calculation scheme of the MT for determining the systematic errors of the emulsion model:
1, 3 – MT electrodes; 2 – flat interface;
h_{eml} and h_{wat} – Thicknesses of emulsion and water layers
($W = h_{wat} / h_{eml}$)

Water droplets with total volume V_{wat} are replaced by a linear layer of constant thickness h_{wat} on the surface of the lower electrode of the MT.

Determination of the value of the systematic error for the 100 MHz – 1 GHz range is reduced to a comparison of capacitance values of a flat capacitor formed by plates 1, 3 of MT for values $\varepsilon_{wat} = \infty$ и ε_{wat} = 81 of the medium between interface 2 and the lower plate. Taking into account the expression (1) and the fact that the capacitance of the MT between the plates 1 and 3 is determined by the capacity of two series-connected capacitors (with electrodes 1 – 2 and electrodes 2 – 3), the effective dielectric permittivity ε' of the layered medium is generally:

$$\varepsilon' = \frac{1}{\frac{1}{\varepsilon_{wat.}} + \frac{1-W}{\varepsilon_{nld}}} \ . \qquad (3)$$

In Table 2 shows the calculated values of ε' for ε_{wat} = ∞ и ε_{wat} = 81 for different values of the volumetric moisture content, as well as the values of the systematic errors of the mathematical model in the frequency range 100 MHz – 1 GHz, which are defined as $(\varepsilon'_{\infty} - \varepsilon'_{81})/ \varepsilon'_{\infty}$ (ε'_{∞} ND ε'_{81} are the equivalent dielectric permittivities of a layered medium for $\varepsilon_{wat} = \infty$, ε_{wat} = 81 and ε_{nld} = 2).

Table 2

Systematic errors of the mathematical model of the emulsion for the frequency range 100 МГц – 1 ГГц

W, %	10^{-1}	10^{-2}	10^{-3}	10^{-4}	10^{-5}
ε'_{∞}	2.22	2.02	2.002	2.0002	2.00002
ε'_{81}	2.162	1.97	1.953	1.9519	1.9518
$\frac{\varepsilon'_{\infty} - \varepsilon'_{81}}{\varepsilon'\infty}$	0.0261	0.0248	0.0245	0.0241	0.0241

Taking into account the linearity of the relation (2), replacing ε_{wat} = 81 by $\varepsilon_{wat} = \infty$ for a moisture content of $10^{-5} \le W \le 0.1$ leads to the appearance of a systematic relative error in determining the ε_{eml} of the given mathematical model of the emulsion no more than 2.61 % for the frequency range from 100 MHz to 1 GHz, which meets the requirements of practical application.

The general algorithm for solving the problem of «varietal uncertainty». To solve the problem of «varietal uncertainty» and take into account the influence of parasitic capacitances MT and MG, a number of multifrequency algorithms are proposed, the generalized form of which is the four-frequency algorithm. Fig. 2 shows a generalized equivalent circuit for the replacement of the resonant moisture meter, which characterizes capacitive MT of both concentrated and distributed type.

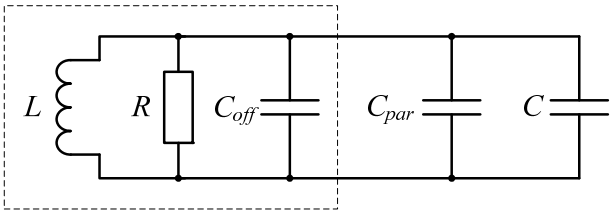

Fig. 2. Generalized equivalent circuit of the replacement of a resonant moisture meter with a capacitive-type MT: L – inductive element of the MG; C_{off} – parasitic capacitance of the generator; C_{par} – «blind» (constructive) capacitance of the MT; C – working capacity of the measuring transducer; R – loss resistance

Four-frequency algorithm requires the following four stages.

1. Determination of the resonance frequency F_{off} of the oscillatory circuit with the MT OFF.

2. Determination of the frequency of the resonance F_{air} of the oscillatory circuit with the connected MT filled with air.

3. Determination of the frequency of the resonance of the F_{nld} of the oscillatory circuit with connected MT filled with an anhydrous liquid nonpolar dielectric.

4. Determination of the resonance frequency F_{eml} of the oscillating circuit with the connected MT filled with the emulsion under investigation.

Four values of the resonant frequencies of the oscillatory circuit make it possible to determine four unknown quantities. Depending on how the measuring transducer is filled, the value C takes the following different values. For the case of MT filling with air, this value is equal to the working capacitance of the MT in air $C = C_{air}$; for the case of MT filling with a dehydrated liquid nonpolar dielectric $C = \varepsilon_{nld} \cdot C_{air}$; for the case of filling the API with the emulsion investigated $C = \varepsilon_{eml} \cdot C_{air}$.

The value of the «blind» capacitance C_{par} is constant and is determined by the constructive method of fastening the potential electrode MT. In general, the value of C_{par} is the fraction m from the working capacity of the measuring transducer C_{air}:

$$C_{par} = m \cdot C_{air}\ ;\ (m \geq 0). \qquad (4)$$

For simplicity, we will assume that the value m is given, and the reduced RLC oscillatory circuit is a lossless loop ($R = \infty$).

The practical implementation of this multifrequency algorithm for determining the values of ε_{nld} and ε_{eml} consists in the sequential determination of the resonant frequencies the F_{off}, F_{air}, F_{nld}, F_{eml}. of the circuits. Here, the frequency F_{off} is the resonance frequency of the circuit L, C_{off} with the MT OFF:

$$F_{off} = \frac{1}{2\pi\sqrt{LC_{off}}}. \qquad (5)$$

The next step is to determine the resonance frequency F_{air} of the circuit at the MT filled with air:

$$F_{air} = \frac{1}{2\pi\sqrt{LC_{off} + LC_{air}(1+m)}}. \qquad (6)$$

When the MT is filled with a dehydrated liquid nonpolar dielectric, the resonance frequency F_{nld} is:

$$F_{nld} = \frac{1}{2\pi\sqrt{LC_{off} + LC_{air}m + LC_{air}\varepsilon_{nld}}}. \qquad (7)$$

And, finally, when the MT is filled with the emulsion investigated, the resonance frequency F_{eml} is:

$$F_{eml} = \frac{1}{2\pi\sqrt{LC_{off} + LC_{air}m + LC_{air}\varepsilon_{eml}}}. \qquad (8)$$

The solution of the system of equations defined by expressions (5) – (8) with respect to unknown quantities ε_{nld} и ε_{eml} allows to determine the unknown moisture content W through the values of the resonance frequencies F_{off}, F_{air}, F_{nld}, F_{eml} and the constructive coefficient of the measuring transducer m:

$$W = \frac{A}{3B}, \qquad (9)$$

where $A = F^2_{air} \cdot F^2_{nld} \cdot (F^2_{off} - F^2_{eml}) - F^2_{air} \cdot F^2_{eml} \cdot (F^2_{off} - F^2_{nld})$; $B = F^2_{air} \cdot F^2_{eml} \cdot (F^2_{off} - F^2_{nld}) - F^2_{nld} \cdot F^2_{eml} \cdot (F^2_{off} - F^2_{air}) \cdot m / (m+1)$.

Expression (9) is the main generalized metrological characteristic of the four-frequency algorithm for determining moisture content by the method of resonance dielcometry to determine the moisture content of the emulsion as a function of the quantities F_{off}, F_{air}, F_{nld}, F_{eml} и m.

In the general case, the error in determining the moisture content includes both systematic and random errors. The systematic errors caused by the inaccuracy of the mathematical model of the emulsion were determined earlier.

Based on the analysis of expression (9), the value of the random error in determining the moisture content $\Delta W/W$ as a function of the absolute errors (ΔF_{off}, ΔF_{air}, ΔF_{nld}, ΔF_{eml}; Δm) of determination of values F_{off}, F_{air}, F_{nld}, F_{eml} and m has the following form (in this case the processes of determining F_{off}, F_{air}, F_{nld}, F_{eml} and m are independent):

$$\frac{\Delta W}{W} = \frac{\sqrt{\sum_{n=1}^{5} Y_n^2}}{W(F_{off}, F_{air}, F_{nld}, F_{eml}, m)}, \qquad (10)$$

where

$$Y_1^2 = \left(\frac{\partial W}{\partial F_{off}}\right)^2 \Delta F^2_{off}\ ;\ Y_2^2 = \left(\frac{\partial W}{\partial F_{air}}\right)^2 \Delta F^2_{air}$$

$$Y_3^2 = \left(\frac{\partial W}{\partial F_{nld}}\right)^2 \Delta F^2_{nld}\ ;\ Y_4^2 = \left(\frac{\partial W}{\partial F_{eml}}\right)^2 \Delta F^2_{eml}\ ;$$

$$Y_5^2 = \left(\frac{\partial W}{\partial m}\right)^2 \Delta m^2 \quad .$$

The values of the absolute errors ΔF_{off}, ΔF_{air}, ΔF_{nld}, ΔF_{eml} and Δm include both systematic and random errors in their determination.

The three-frequency algorithm. For m = 0, the «blind» capacitance of the MT is not taken into account in expression (9). Then expression (9) is essentially simplified and goes over to a form analogous to the expression obtained earlier for W in [8]:

$$W = \frac{1}{3} \cdot \frac{\frac{1}{F_{eml}^2} - \frac{1}{F_{nld}^2}}{\frac{1}{F_{nld}^2} - \frac{1}{F_{off}^2}} . \qquad (11)$$

Expression (11) is a metrological characteristic of the three-frequency algorithm for determining moisture content by the method of resonance dielcometry.

For the specific design of the capacitive MT [9], the values of the volumetric moisture content W were determined from the exact formula (9) ($W_{(9)}$) and the approximate formula (11) ($W_{(11)}$) and were $W_{(9)}$ = 0.0215 и $W_{(11)}$ = 0.0209, respectively.

The difference between $W_{(9)}$ and $W_{(11)}$ determines the magnitude of the absolute systematic error in determining the moisture content without taking into account the «blind» capacity, and the quantity ($W_{(9)}$ и $W_{(11)}$) / $W_{(9)}$ characterizes the systematic relative error. This relative systematic error for m = 0.0664 and for the MT frequency range up to 2 MHz is: ($W_{(9)}$ − $W_{(10)}$) / $W_{(9)}$ = 0.027 [9].

Analysis of the limiting characteristics of four- and three-frequency algorithms. For a specific moisture meter with MT of lumped type [9], in which four- and three-frequency algorithms are implemented, an analysis was made of the accuracy of determining the moisture content in an emulsion of the «transformer oil-water» type at F_{off} = 1145290.4 Hz; ΔF_{off} = 2 Hz; F_{air} = 946516.0 Hz; ΔF_{air} = 1.5 Hz; F_{nld} = 827303.9 Hz; ΔF_{nld} = 0.9 Hz; F_{eml} = 821291.0 Hz; ΔF_{eml} = 3.4 Hz; m = 0.0664; Δm = 0.0038. The analysis was made for the four-frequency algorithm, as the most accurate one.

The values of m and Δm were determined by calculation, proceeding from the geometrical dimensions of the MT and the dielectric characteristics of the fluoroplastic-4: a structural insulating element that fixes the potential electrode of the MT and determines the value of the «blind» capacitance of the MT [9].

The calculated value of the relative error in determining the moisture content obtained from expressions (5) – (10) was: $\Delta W/W$ = 0.011. This value defines the restriction on the lower limit of the measured moisture content to moisture meters with a concentrated type of MT for four- and three-frequency algorithms (in the HF range up to 2 MHz) of the order of 600 cm^3 /m^3 [9].

Two-frequency algorithm. The analysis of expressions (9, 10) and the circuit in Fig. 2 showed that an increase in sensitivity is facilitated by a decrease in the effect of capacitance C_{off} on the resonance frequency of the MT. The minimum influence of the parasitic capacitance of the generator will be at C_{off} = 0. In this case, m = 0, Δm = 0, F_{off} = ∞, and expression (11) is transformed to the form:

$$W = \frac{1}{3} \cdot \frac{\frac{1}{F_{eml}^2} - \frac{1}{F_{nld}^2}}{\frac{1}{F_{nld}^2}} = \frac{1}{3} \cdot \frac{F_{nld}^2 - F_{eml}^2}{F_{eml}^2} . \qquad (12)$$

For small values of the relation

$$(F^2_{nld} - F^2_{eml}) / F^2_{eml} < 0.1$$

the expression (12) is simplified and has the following form, up to terms of the second order:

$$W \approx \frac{2}{3} \cdot \frac{F_{nld} - F_{eml}}{F_{eml}} . \qquad (13)$$

Expressions (12) and (13) are a metrological characteristic of the two-frequency algorithm for determining moisture content by the method of resonance dielcometry.

Technical aspects of practical realizability of the two-frequency algorithm. Let's analyze the technical possibilities of creating a MT with the values m = 0 and C_{off} = 0. The most radical way to ensure m = 0 is to replace the structural dielectric material that supports the potential electrode of the capacitive MT with a «metallic» insulator, for example, the implementation of the MT in the form of a short-circuited quarter-wave line. In this case, the central (potential) electrode of this line is tightly connected to the outer electrode, and the liquid under investigation is in the space between these electrodes [10]. An MT of this type is a system with distributed parameters and allows the mode m = 0 to be realized. As shown in [6, 10], the transition to the microwave frequency range makes it possible to substantially increase the sensitivity of the resonance dielcometric method. The main problem in this case is the large geometric length of the MT when operating in the frequency range 100 MHz – 1 GHz, as well as the small difference between the first and subsequent resonant frequencies of distributed type MT.

The distributed type IP with the measuring element in the form of a stepped inhomogeneous coaxial resonator (SICR), proposed and investigated in [10], is free from the indicated shortcomings and allowed to realize its operation in the microwave frequency range (100-200 MHz) with its minimum dimensions.

In order to realize the case C_{off} = 0, a characteristic of a SICR-based MT was used, consisting in an essentially larger value of its quality factor with respect to capacitive foci of a concentrated type. This makes it possible to realize the C_{off} = 0 mode due to the very small coupling factor of the measuring oscillator with the PI via

an inductive loop connection, which is geometrically located near the grounded end of the internal (potential) electrode of the SICR. At the same time, a minimal influence of the coupling loop on the electric field in the SICR is ensured, since the electric field in this place of the SICR is extremely small, and the introduced capacitance of the IG in the working capacitance of the SICR is substantially reduced and its influence can be neglected. Thus, a two-frequency algorithm for resonance dielcometry (m = 0, C_{off} = 0) is realized in moisture content meters of the SICR type. This algorithm is the theoretical limit of resonance dielcometry, when two unknown quantities (ε_{eml} and ε_{nld}) and moisture content, as a function of these quantities, are determined by two values of the measured frequencies.

Results of experimental investigations. For experimental verification of the results of theoretical studies, the moisture content of the prepared test emulsions of the «transformer oil-water» type was determined by two specific moisture meters: with lumped type MT [9] and a distributed type MT in the form of SICR [10]. Experimental studies of the first moisture meter were carried out to test the generalized four-frequency algorithm, and the purpose of the second moisture meter was to test the two-frequency algorithm. The results are shown in Table. 3.

Table 3

The results of the experimental determination of the volume moisture content of the test emulsions

MT type	Moisture content, cm^3/m^3		Absolute discrepancy, cm^3/m^3	Relative discrepancy, %
	Prepared test emulsion	Measured value		
Concentrated MT, HF range (1 MHz)	5000 ± 20	4800±54	±200	±4.0
Distributed IP CSCR, microwave range (0.1 GHz)	100±5.1	98.3±0.6	±1.7	±1.8
	10±1	9.51±0.5	±0.49	±5.2

For a moisture meter with concentrated type of MT, the values of the volumetric moisture content were determined in accordance with the expression (9), and for a moisture meter with distributed type of MT – in accordance with the expression (12), absolute errors were determined using expression (10) for both moisture meters.

The correctness of the results of theoretical studies characterizes the magnitude of the absolute and relative discrepancies between the measured values of the volumetric moisture content and the moisture content of the prepared test emulsions. In this case, the magnitude of the absolute divergence was determined as the difference between the moisture content of the prepared test emulsion and its calculated value, and the magnitude of the relative divergence as the ratio of the absolute error to the moisture content of the prepared test emulsion.

Analysis of the data given in Table 3 shows the following.

1. The values of the relative discrepancies do not exceed 4 % and 5.2 % (for the concentrated and distributed types of MT, respectively), which indicates a good coincidence of the calculated results with the moisture content of the test emulsions and the correctness of the results of the theoretical studies.

2. The magnitude of the absolute divergence for a moisture analyzer with concentrated type of MT (200 cm^3/m^3) practically confirms the results of estimating the lower limit of the measured volumetric moisture content (600 cm^3/m^3).

3. A moisture meter with distributed type MT in the form of SICR makes it possible to measure the moisture content of emulsions based on nonpolar liquid dielectrics with lower limit of 10 cm^3/m^3 without preliminary calibration operations.

4. Metrological characteristics of a moisture meter with distributed type of MT in the form of SICR exceed the analogous characteristics of the known dielcometric moisture meters presented in Table 1.

Conclusions.

The proposed and practically realized multifrequency algorithms for determining the volumetric moisture content of liquid emulsions by the method of resonance dielcometry, taking into account parasitic parameters of MT and MG, solved the problem of «varietal uncertainty» of the liquids under investigation, significantly improving the metrological characteristics of the dielcometric method, and measuring the volume moisture content of liquid nonpolar dielectrics up to 10^{-5}.

The correctness of the results of theoretical investigations is confirmed experimentally with a maximum value of the relative discrepancy of not more than 5.2 %.

A promising direction for the further development of the proposed multifrequency algorithms in order to improve the metrological characteristics can be the consideration of their systematic errors.

REFERENCES

1. Golub E.Yu. *Metody i sredstva povyshenija tochnosti diel'kometricheskih vlagomerov. Diss. cand. techn. nauk* [Methods and means of increasing the accuracy of dielectric metric moisture meters. Cand. tech. sci. diss.]. Kharkov, 2016. 199 p. (Rus).

2. Zabolotnyy A.V. Technical realization of additive tests in a capacitive primary converter of the diesel-electric moisture meter of petroleum products. *Measuring and Computing Devices in Technological Processes*, 2013, no.3, pp. 49-53. (Rus).

3. Marcel L. Mounge. *Method and apparatus for measuring and calculating bulk water in crude oil.* Patent USA, no.4916940, 1990.
4. Zabolotnyy O.V. *Sposib vymiryuvannya volohosti materialiv* [The method of measuring moisture content]. Patent UA, no.201201992, 2014. (Ukr).
5. Platon G., Ramm C., Lohr K. *Capacitive moisture sensor*. Patent USA, no.7129713, 2006.
6. Suslin M. A. *Mikrovolnovyy kontrol' aviatsionnykh GSM s ispol'zovaniyem radiotekhnicheskikh metodov rascheta tsepey s raspredelennymi parametrami* [Microwave monitoring of aviation fuel and lubricants using radio engineering methods for computing circuits with distributed parameters]. Moscow, Mashinostroenie Publ., 2006. 120 p. (Rus).
7. Rudakov V.V., Korobko A.I., Korobko A.A. Electrophysical model of behavior emulsion mineral oil – water engineering type. *Bulletin of NTU «KhPI»*, 2009, no.39, pp. 158-161. (Rus).
8. Hippel A.R. *Dielektriki i ikh primeneniye* [Dielectrics and their application]. Moscow, Gosenergoizdat Publ., 1953. 336 p. (Rus).
9. Rudakov V.V., Korobko A.A. Increasing the sensitivity of the moisture content measurements in transformer oil dielcometric method in resonant mode. *Bulletin of NTU «KhPI»*, 2014, no.50(1092), pp. 143-149. (Rus).
10. Rudakov V.V., Korobko A.A. A high sensitive microwave measuring device of the moisture content in the non-polar dielectric liquids based on an inhomogeneous step coaxial resonator. *Electrical engineering & electromechanics,* 2016, no.5, pp. 51-56. (Rus). **doi: 10.20998/2074-272X.2016.5.08.**

Received 13.04.2017

A.A. Korobko, Postgraduate Student,
National Technical University «Kharkiv Polytechnic Institute»,
2, Kyrpychova Str., Kharkiv, 61002, Ukraine,
phone +38 093 65 080 88,
e-mail: andarleks@gmail.com

How to cite this article:
Korobko A.A. Multifrequency algorithms for determining the moisture content of liquid emulsions by the method of resonance dielcometry. *Electrical engineering & electromechanics*, 2017, no.3, pp. 40-46. **doi: 10.20998/2074-272X.2017.3.06.**

UDC 621.31.048.015 **doi: 10.20998/2074-272X.2017.3.07**

A.Yu. Chernukhin

INFLUENCE OF CORONARY DISCHARGE PARAMETERS ON THE EFFICIENCY OF LIGHTNING PROTECTION SYSTEM ELEMENTS

Purpose. ***Investigation of the formation of space charge in the region of the apex of lighting rod, under the action of the electric field of a thunderstorm cloud, to evaluate the efficiency of elements of lighting protection systems. Methodology. We have applied the mathematical simulation of electromagnetic field distribution on the top of metal rod by different forms. As a mathematical apparatus, we use the finite element method. We considered two forms of the rod section: round and square. The round (cylindrical) rod has a sharp apex. The square rod has a flat top. The experimental study investigates the features of corona discharge formation. A high-voltage test equipment is created an electric field. Experiments carried out using a configuration consisting a potential plate and vertical rod electrode on grounded plate. The electric field strength varied from 1 kVm^{-1} to 100 kVm^{-1}. This range corresponds to the thunderstorm condition. Results. We have obtained a correlation between the corona current and the strength of the electric field for various shapes of the rod top. The results of experimental studies confirmed the correctness of the conclusions of theoretical estimates. We show that the time parameters of streamer current pulses vary by no more than 30%, but a streamer charge increase to three time with increasing electric field strength. We proposed and applied a method for measuring the velocity of motion of a streamer in the discharge gap. As a result, it is established that the streamer speed is nonlinear in time. For a discharge gap of 1.2 m, the speed varies from $1.8 \cdot 10^4$ m/s to $1.1 \cdot 10^6$ m/s. Originality. For the first time, we have carried out a complex of studies of corona discharge parameters from lightning protector rod to apply for the certification procedure of ESE terminals. Practical value. Based on the set of obtained results, it is obviously that the standard NF C 17-102:2011 will not be introduced as a national standard of Ukraine before full introduction of scientifically justified data will be include into the requirements of the standard.*** References 10, tables 4, figures 9.

Key words: **rod lightning terminal, pulse corona, electric field intensity of thunderstorm cloud, corona current, streamer speed.**

Приведены результаты теоретических и экспериментальных исследований процессов формирования объемного заряда в области вершины стержневого молниеприемника. Рассмотрены особенности формирования стримерной короны на стержневых молниеприемниках с различными конфигурациями вершины в электрическом поле грозового облака. Установлены зависимости силы тока короны от напряженности электрического поля и высоты для каждого варианта стержня. Показано, что при этом временные параметры импульсов тока стримера меняются не более чем на 30%, а заряд стримера, и как следствие, сила тока короны увеличиваются по мере роста напряженности электрического поля. Предложено метод измерения скорости продвижения стримера. Метод основан на одновременном измерении напряжения и тока на разрядном промежутке. Результаты предлагается учесть при сертификации молниеприемников. Библ. 10, табл. 4, рис. 9.

Ключевые слова: **стержневой молниеприемник, импульсная корона, напряженность электрического поля грозового облака, ток короны, скорость стримера.**

Introduction. The basis of lightning protection systems for buildings and structures from direct lightning strikes are metal structures in the form of rod, cable and grid lightning receivers. The requirements for the device of such systems are regulated by the Standards IEC 62305-1: 2010 and IEC 62305-3: 2010. In contrast to the systems mentioned above, which can be conditionally called «passive», attempts have been made in the world over the last decade to create active devices that provide a significant increase in the size of the protection zone, compared to the protection zone of the classical Franklin lightning detector (hereinafter referred to as the passive rod lightning detector – PRL). Such devices include the so-called «Early streamer emission terminals (ESE)», which, according to the developers, provide a faster, compared with the PRL, the creation of a counter streamer that facilitates the interception of lightning. The declared radius of protection ESE of lightning receivers is directly proportional to the lead time [1]. The basis of such an approach is the fact of experimenting repeatedly formed by the formation of counter leaders from metal objects, both grounded and not having contact with the ground. However, not all the features and conditions for the formation of the counter leader have been sufficiently studied. In particular, the probability of meetings of the channel of the descending lightning with the ascending leaders is of a probabilistic nature. In addition, the speed of advancement of the oncoming ascending leader depends on the potential of the head of the lightning channel, which also has a random value.

The market also offers various options for devices called dissipaters, which reduce the likelihood of lightning striking the object by creating a volume of air around the top of the object, saturated with charged particles. This effect provides a reduction in the electric field strength above the top of the object, as a result of which the counter leader appears at high values of the electric field strength formed by the lightning channel, which leads to a decrease in the probability of the object being struck by lightning.

At the Scientific-&-Research Planning-&-Design Institute Molniya» of the National Technical University «Kharkiv Polytechnic Institute» (NIPKI «Molniya» NTU

«KhPI») over the past 10 years, more than 20 types of different ESE lightning detector and dissipater samples of almost all companies presented on the world market. In 2007, comparative tests of the ESE terminal of ERICO Company (USA) were conducted at the laboratories of the Technical University of Valencia (Spain) and NTU «KhPI» (Ukraine). The results of the tests showed that the provisions of the first edition (1995) of the Standard of France [1] are not sufficient for a reliable estimate of the size of the protective zone of ESE lightning detectors. During the discussion of the results it was proved [2] that it is necessary to introduce additional requirements for the variance of lead time and to establish the parameters of the reference PRL. In the new edition (2011) of the Standard [1], these recommendations are taken into account.

A significant part of the scientific community, united in the framework of the International Conference of the International Conference Lightning Protection (ICLP), categorically denies the scientific validity of the provisions of the standard [1]. The main aspects that do not have the proper experimental confirmation are:

– estimation of the radius of the ESE lightning protection zone is carried out by multiplying the advance time (defined as the arithmetic mean value of 100 digits) by the speed of advancement of the oncoming leader from the lightning detector, which is set equal to 10^6 m·s^{-1}. The experimental velocities obtained with the help of high-speed video cameras lie in the range (10^4 – 10^6) m·s^{-1};

– the lack of a documented experimentally confirmed larger protection radius compared to the PRL. Repeated joint tests on simulations did not confirm this fact.

Another part of the community, which is mainly composed of manufacturers and distributors of the devices under consideration, is integrated within the International Lightning Protection Association (ILPA), which conducts its own scientific symposia.

The arising contradiction has not only a scientific aspect, but it causes important problems of practical application of new devices. The erroneous determination of the size of the protection zone causes a decrease in the probability of interception of lightning by the lightning protection system, which can have negative consequences. Nevertheless, to date, the Standard [1] has been implemented in a number of countries, including France, Spain, Kazakhstan, Latvia, which have actually legalized the use of ESE lightning detectors in view of the design protection zone. Persistent attempts are being made to introduce the Standard [3] in Ukraine. The current circumstances prompted NIPKI «Molniya» NTU «KhPI» and the Technical Committee of Ukraine on standardization in the field of electromagnetic compatibility (TC 22) to initiate research in order to understand the physics of the accompanying phenomena.

The basis of the principle of operation of both types of new devices is the processes of corona discharge from metal rods and needles. Therefore, the scientific justification of the real protective properties of such devices requires a detailed study of the physics of corona discharge in conditions of finding products in the electric field of a thunderstorm cloud.

Analysis of recent investigations and publications. Studies of corona discharge processes have been carried out for many decades. However, they continue to this day. The reason is that the processes are of a probabilistic nature, and the completeness and reliability of the results of the research depends to a large extent on the means used to measure the electrophysical quantities and the speed of the video recording. Naturally, the information received in recent years, more accurately due to a qualitatively new level of the technology mentioned above.

The operating principle of the ESE terminal is based on the assumption that the occurrence of a streamer passing to the leader of a downstream zipper from the terminal takes place earlier than from a conventional rod lightning detector [1]. Therefore, the lead time value is the main technical characteristic of the ESE terminal. At the same time, the upstream streamer appears against the background of the corona discharge, which is an integral part of the process. Therefore, the solution of the problem in our institute is begun with the study of the regularities of the development of the streamer corona and its transition to the counter leader [2].

To a certain extent, the appearance of the crown adversely affects the protective properties of the lightning receiver its presence hinders the development of a counter leader. Many studies have been devoted to the study of the corona discharge process, including [3-6]. To ignite the corona, the magnitude of the electric field at the tip of the corona electrode should exceed a certain critical value (E_c). This value was first obtained empirically by the Peak for a cylindrical electrode:

$$E_c = 29.8\delta\left[1+\frac{0.3}{(\delta R)^{1/2}}\right], \quad (1)$$

where E_c is the critical value of the field strength, kV/cm; $\delta = N/N_0$; N, N_0 is the gas density under existing and normal conditions, respectively, R is the electrode radius, cm.

The paper [5] presents the formula (2) for an electrode of spherical geometry with radius R

$$E_c = 27.8\left[1+\frac{0.54}{(R)^{1/2}}\right]. \quad (2)$$

A comparison of the results of the estimation with these formulas for electrodes of radius $R \leq 1$ cm, for which the formulas are valid, is presented in Table 1.

Table 1

The values of the critical electric field strength, calculated by Peak and Baselian formula [5]

R, cm	0.1	0.5	1.0
E_c, kV/cm	58.5	42.6	39.0
E_c [5], kV/cm	75.1	48.9	42.8

Obviously, the discrepancy between the values of the critical strength increases with decreasing radius of the electrode.

In the intervals with a high degree of inhomogeneity of the electric field, the plasma region arising from the corona discharge can penetrate into the zone with a low intensity only in the form of a thin channel – a streamer. When the streamer enters the weak field, its speed slows down, it can stop. Such an incomplete process is called an impulse or streamer crown. The propagation continues as long as the electric field strength is greater than the minimum allowable. The average value of the electric field strength E_s along the streamer channel with positive polarity is in the range 450 kV·m^{-1} – 500 kV·m^{-1} [3]. Waters (1987) and Gallimberti (1979) show that increasing the length of the streamer L is directly proportional to the growth of the voltage U_i, as long as L is small compared to the length of the discharge gap. The coefficient of proportionality is equal, respectively, to the mentioned authors: 0.145 cm·kV^{-1} и 0.152 cm·kV^{-1}.

According to the authors of [5], blunt lightning rods are more effective in intercepting lightning than sharp ones. On the contrary, it is stated in [7] that, by varying the radius of the lightning-conductor within rather wide limits (practically significant), it is impossible to influence the magnitude and distribution of the space charge of the corona in its vicinity. This contradiction also requires experimental verification.

The boundary velocity of the rise of the pulse front for a quasi-stationary regime, when the voltage variation during the development of streamers can be neglected, is 50 kV·μs^{-1}. According to formula (2) from [7], it follows that for a linear increase in the electric field strength, the corona current increases linearly, and when E_0 is stabilized, the current decreases with time. The data of experimental studies [6] do not confirm this fact. If the steepness of the front is above the boundary, the streamer moves forward during the entire time of voltage growth at the gap, while its velocity increases.

A strong streamer flash injects so much charge into the gap that the field on the entire anode falls far below the ionization threshold, as a result of which there is a pause in the development of the discharge [7]. If the voltage across the gap does not change or changes slowly, the pause time can be long – about the time of ion drift by a distance comparable to the anode radius (for $r_a \sim 10$ cm and average electric field strength of 5 kV·cm^{-1} $\Delta t \sim 10^{-3}$ s). This phenomenon is characteristic of a rod with an acute conical vertex, because the element that injects the charge has a point size. Consequently, a flat top of the rod should have advantages in creating a stable streamer sequence.

The goal of the paper is investigation of the formation of space charge in the region of the apex of a rod lightning detector under the action of the electric field of a thunderstorm cloud to evaluate the efficiency of elements of lightning protection systems.

Results of theoretical investigations. Obviously, the lightning receiver, the conductor connected to the ground, has a zero potential. As the thundercloud approaches, an electric charge is induced on it, the surface density of which is determined by the strength of the electric field at the top in the region of greatest inhomogeneity. Under certain conditions described above, there is a corona discharge and streamers, which subsequently grow into a leader facing the lightning.

The speed of the lightning detector depends on the degree of ionization of the surrounding airspace. If ionization is active, a cloud of charged particles is formed, complicating the germination of the oncoming leader. This effect is based on the designs of dissipaters, which are combinations of thin conductors. If the ionization is weak, there are no charges necessary for the formation of avalanches. Hence, we can assume that there is a design of the top of the lightning detector, which will provide the corona current optimal for minimizing the formation time of the oncoming leader. This fact is important for the selection of a standard sample of the lightning detector, the need to determine which was initiated in [2] and confirmed by the standard [1].

In order to study the initial phase of the formation of a stationary corona at the apex of a rod lightning detector, the mathematical model is maximally approximated to the real conditions when testing in accordance with the standard [1]. The electrostatic field is formed by two circular disk-like conductive plates, 10 m in diameter each. One of the plates (upper) is assigned a potential of 10 kV, the other is grounded ($U = 0$). The distance between the plates of the model varies in the range from 3 m to 10 m. The value of the potential is chosen in this way for reasons of the electric field strength $E_0 \geq 1$ kV·m^{-1}, characterizing the pre-threat situation. The height of the lightning rod is assumed to be 2 m. The mathematical model of the problem is as follows. In airspace, the electric field is potential, and the potential satisfies the Laplace equation. The boundary conditions of the problem are given by the vanishing of the potential on the lower plate and rod; positive potential of 10 kV on the upper plate; the remaining boundaries correspond to the condition of continuity of the potential.

The aim of the simulation is to determine the ratio of the parameters of the rod lightning receiver, in which an optimum ratio of the maximum field strength near the vertex and the volume of this region (the stressed volume) is obtained, which is favorable for the streamer process.

Calculation of the electric field strength on the surface of the pointed rod is carried out along the generatrix of the cone of its vertex. The degree of sharpness of the vertex of the rod is characterized by the sharpness coefficient (k), which is equal to the ratio of the height of the tip to the radius of the rod. Variants are considered when the coefficient takes the values 1; 2; 3 and 4 for a rod with a radius of 0.05 m. The results of calculating the electric field strength at the tip of a point of a pointed rod 2 m high, found in an electric field of intensity 2 kV·m^{-1}, are shown in Table 2. The calculated values of the field strength factor K at the point under consideration are also given there.

Table 2

The electric field strength at the tip of the point of a pointed rod of 2 m high

k	1	2	3	4
E, kV·m^{-1}	220	600	1020	1250
K	110	300	510	625

The results of the solution of the problem for various variants of the height of the rod (in the range from 1 m to 8 m), the cross section (circle, square, polygons), its size (from 10 mm to 30 mm) and the shape of the vertex (plane, point[8]). The simulation results showed that the maximum value of the electric field strength on the rod surface increases in direct proportion to the rod height. In particular, for a rod of square cross-section, this dependence is described by formula (3) with an error ≤ 5%.

$$E_m(h) = 26.7 \cdot E_0 \cdot h\,, \qquad (3)$$

where $E_m(h)$ is the maximum value of the strength of the E-field on the edge of a vertex of a square rod with a flat vertex, V·m^{-1}; E_0 is the intensity of the electric field in which the rod is placed, V·m^{-1}; h is the rod height, m.

In order to verify the results, a comparison is made with the results of calculations obtained by other researchers: using the formulas given in [4] for the grounded half of a spheroid in an external electric field and the numerical method of work [9]. The intensity of the E-field at the tip of the rod with a radius of 0.05 m with a vertex in the form of a hemisphere is calculated. The input parameters of the model are: H = 5 m, h = 2 m, U = 104 V. According to our estimates, the maximum value of the electric field strength at the top of the rod is $77.2 \cdot 10^4$ V·m^{-1}, that is 36 times greater than $E_0 = 2 \cdot 10^3$ V·m^{-1}. When using graph 10 from [4] for a spheroid with a height-to-radius ratio of 40, the gain is determined close to 30. As a result of the numerical solution in [9], the result is close to 35. Taking into account some difference between the geometric figures used in the calculations, And a not too exact scale on the graph in [4], there are grounds to believe that the results of the numerical method used by us are reliable. An illustration of the stressed volume around a rod of square cross section is shown in Fig. 1.

Fig. 1. The intense volume of the E-field around the rod square section (model rotated 90° to the left)

In order to generalize the results of the investigation of the process of corona discharge formation from rod lightning receivers, computer simulation was carried out on the basis of a multifactor experimental design. As a response function, the value of the intensive volume of space around the vertex of the rod is chosen. The intensive volume is the volume of pace, in which the strength of the external electric field exceeds 30 kV·m^{-1}. Based on the analysis of the results of experimental studies, quantitative and qualitative factors are selected that fully determine the value of the response function. These factors are: the strength of the electric field, the length of the rod, the shape of the cross section, the dimensions of the section, the shape of the vertex. A priori, it is assumed that the significance levels of these factors are comparable. From experience it is known that the response function has several maxima, depending on the shape of the cross-section of the rod. Therefore, the choice of the model zero point is related to the cross-sectional shape of the rod. The functional relationships constructed earlier from the experimental data show that they are analytical and allow one to specify a specific type of dependence of the objective function on each of their chosen factors. This allowed us to confine ourselves to a two-level factorial plan of type 2^k (k is the number of factors). To ensure the possibility of checking the adequacy of the chosen mathematical model and the correctness of the determination of constants, an unsaturated plan was used (the number of experiments exceeds the number of unknown constants in the model). A full factorial experiment is performed on the basis of which the target response function is constructed.

The value of the intensive volume, determined from the established functional dependence, is compared with the value of the number of streamer pulses obtained experimentally. Comparison made it possible to determine the required minimum stressed volume at which the corona discharge process begins. In addition, the value of the length of the initial steamers is determined, depending on the values of the experimental factors.

The main results of theoretical studies are as follows:

– since the zone of increased tension is localized near the ribs of the rod, the «intensive volume» increases with the perimeter of the rod;

– the maximum value of the electric field strength and the magnitude of the stressed volume on the surface of the lightning receptacle, at other things being equal, is achieved when using a rod of square cross-section with a flat top. Such a rod is proposed as a new standard for the document [1].

Results of experimental investigations. At a certain value of the electric field strength into which the lightning detector is placed, streamer flashes with a current of tens of mA occur against the background of a «quiet» corona whose current is not more than hundreds of microamperes. Only a streamer flash can transform into a leader under certain conditions. Therefore, the determination of the critical value of the electric field strength at which streamer flares occur and the nature of their behavior when the level of electric field strength varies is an important task. Modeling was carried out on the high-voltage test bench BBC-1.2 at the NIPKI «Molniya» NTU «KhPI». To estimate the performance of

a particular lightning detector, it is proposed to use the values of streamer parameters that arise when placed in an electric field.

To reveal the relationship between the parameters of streamers and the protective properties of the lightning detector, a set of studies was carried out, including the determination of the characteristics of streamers at a constant and pulsed voltage. Investigations at constant voltage make it possible to evaluate the behavior of the lightning detector when a thunderstorm cloud approaches, while the other part of the study is related to the study of the process of the appearance of streamers when exposed to a pulsed electric field accompanying a growing lightning channel.

The investigations were carried out on rod lightning receivers placed between two parallel metal planes. Dimensions of the planes: lower – 4×6.5 m, upper – 3.6×5.2 m. The scheme of the test setup for studying the characteristics of the current of the corona at a constant and varying voltage and its external view are shown in Fig. 2 and 3 respectively.

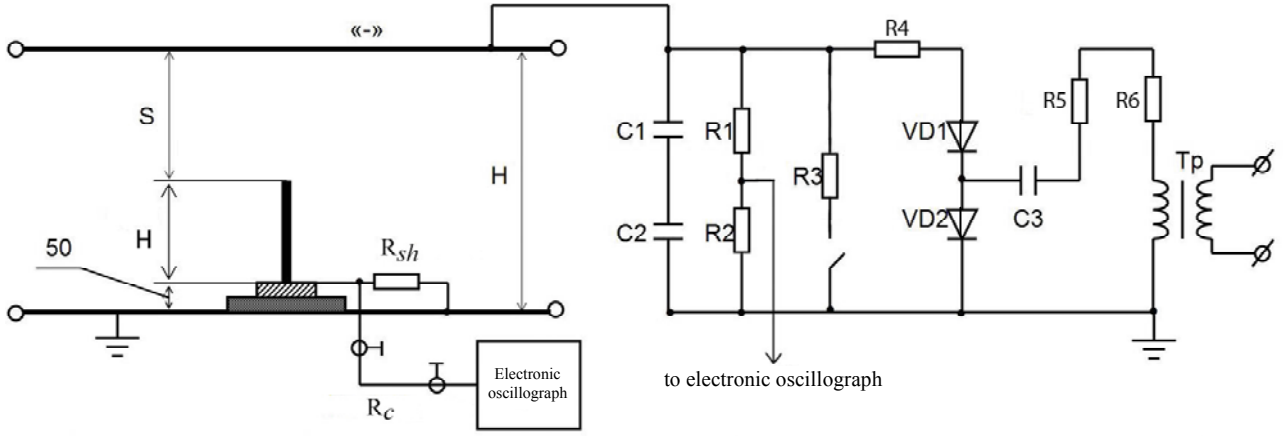

Fig. 2. Circuit of the test bench BBC-1.2
(C1 = 0.381 μF; C2 = 0.385 μF; C3 = 0.4 μF; R1 = 300 MΩ; R2 = 30 kΩ; R3 = 60 kΩ; R4 = 510 kΩ; R5, R6 = 60 kΩ; R_{sh} = 75 Ω; R_c = 75 Ω; Tp – transformer ИОМ 100/25)

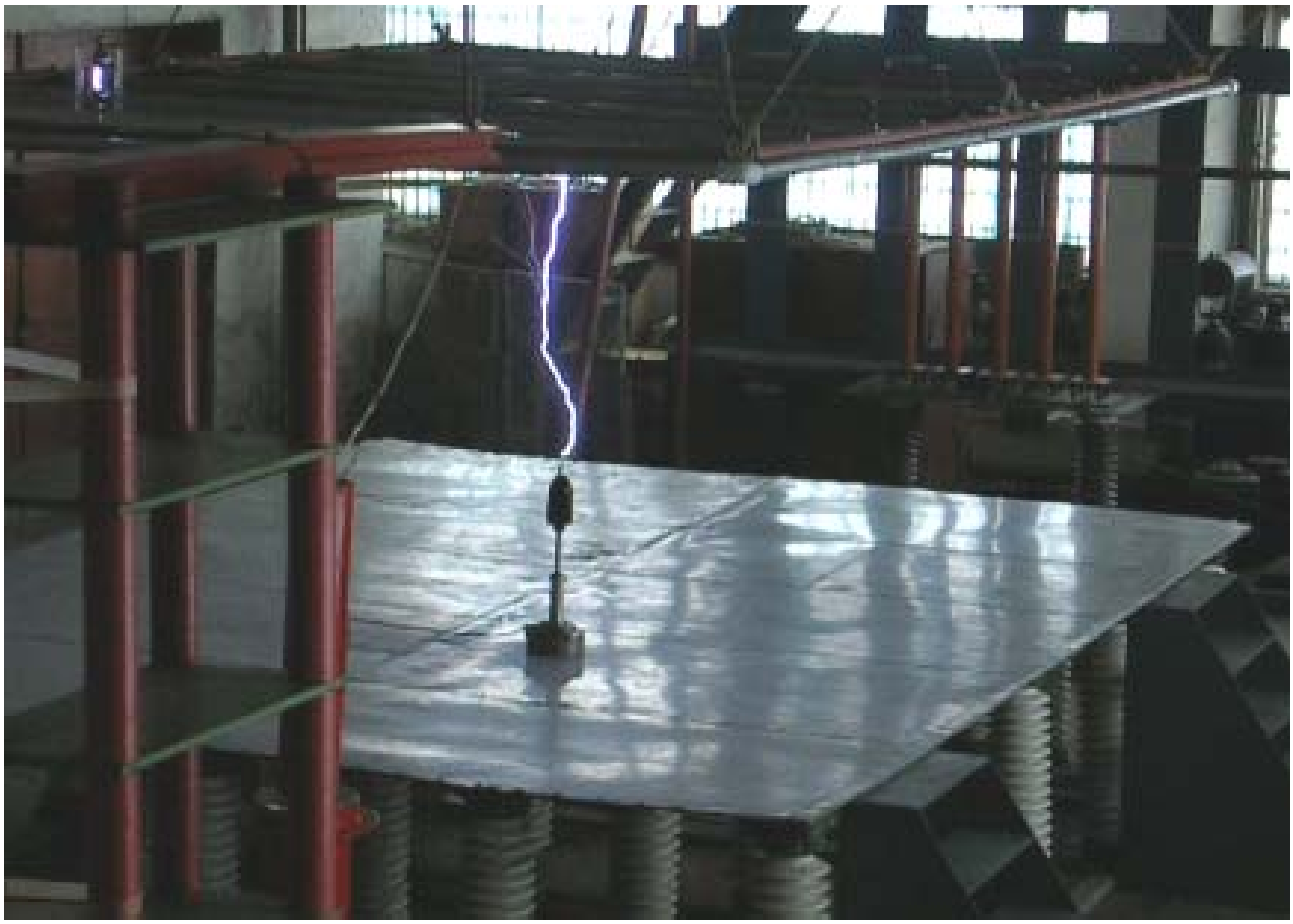

Fig. 3. External view of the test bench BBC-1.2

In this variant, the lower plane is grounded. The upper potential plane – it is supplied with a high voltage of negative polarity. The distance (S) between the vertex of the rod and the potential upper electrode varied in the range from 2.5 m to 0.5 m.

Here, the initial value of the electric field strength in the gap did not change. The results of experimental investigations are presented in detail in [6-8]. A generalization of these results allows us to draw the following conclusions. A typical oscillogram of the current strength of a single streamer is shown in Fig. 4. The charge contained in the streamer is approximately $5.85 \cdot 10^{-9}$ C. For comparison, in [5], measuring the charge of the streamer by an alternative method yielded an average value of $5 \cdot 10^{-10}$ C. Taking into account the difference in the configurations of the vertices of the rods and the heights of the rods, the coincidence of the results is satisfactory.

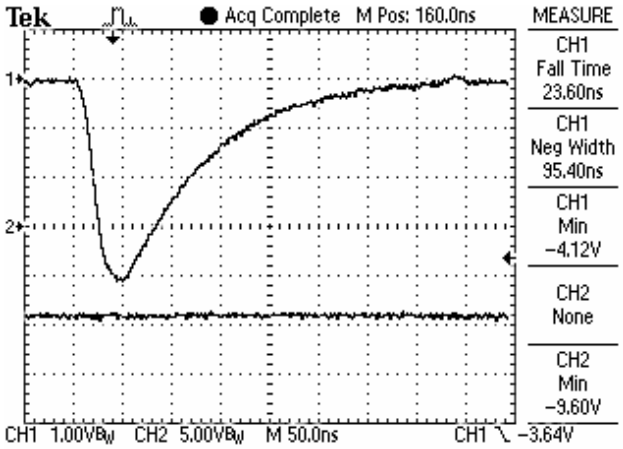

Fig. 4. Oscillogram of a single streamer from a rod of square cross section 12×12 mm^2 with a rod height of 1.7 m, which is in the electric field of intensity 30 kV·m^{-1} (the signal is received from the 75 Ω resistor, charge in the pulse 58.5 10^{-10} C)

The dependences of the average arithmetic number of streamer flares on the electric field strength for the pointed and square rods are shown in Fig. 5.

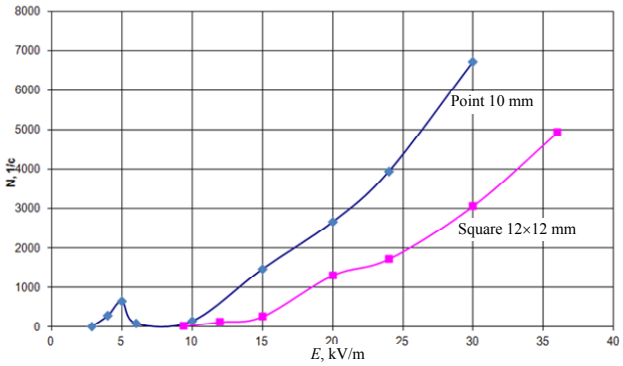

Fig. 5. Dependence of the streamer frequency on the sharpened (diameter 10 mm, sharpness coefficient k = 3) and square (12×12 mm^2) rods on the electric field strength. The length of each rod is 3.4 m

The results of statistical processing of the experimental data are presented in Table 3, 4 for the pointed and square rods, respectively. It should be noted that the time parameters (shape) of the current of a single streamer for all considered cases vary within ± 30 % of the arithmetic mean. Significant changes are observed only for the peak value of the pulse, hence, the value of the charge of the streamer. At each voltage, at least 50 measurements were made. The values of root-mean-square (RMS) deviation presented in the tables unambiguously show a much smaller spread of values for a rod of a square cross-section as compared to a rod with a pointed vertex. This property is characteristic of a rod of any length within the limits considered. It is no accident that the bars of the square section are defined as the elements of the discharge gap for the standard of high voltage value (standard IEC 60062).

Table 3

The results of measurement of the streamer frequency for a pointed rod of circular cross section (diameter 10 mm, sharpness coefficient k = 3, height 3.4 m)

U_0, kV	E_0, kV·m^{-1}	Streamer numbers per second, N	RMS
14.5	2.9	9.16	1.31
20	4	276	7.02
25	5	636	12.58
30	6	78	15.97
50	10	136.6	59.53
75	15	1460	145.60
100	20	2656	322.20
120	24	3940	523.70

From the presented results, it is evident that a «dead» zone (in the range from 6 kV·m^{-1} to 10 kV·m^{-1}) is located near the pointed top. The effect is determined by the point character of the corona element. The presence of such an effect explains the opinion of the authors of [5] mentioned above that blunt lightning rods are more effective at intercepting lightning than sharp ones. It is important to note that this effect is not observed for a rod of square cross section.

Table 4

Results of frequency measurements of streamers for a square rod (12×12 mm^2, height 3.4 m)

U_0, kV	E_0, kV·m^{-1}	Streamer numbers per second, N	RMS
47	9.4	14.7	1.40
60	12	116	4.81
75	15	258	4.74
100	20	1302	20.54
120	24	1720	23.85
150	30	3064	32.77
180	36	4930	93.15

The dependence of the strength of the corona discharge current on the electric field strength, for the rods described above, is shown in Fig. 6. It follows from Fig. 6 that with an electric field strength greater than

15 kV·m^{-1}, the current from the square rod is greater than from the pointed rod, despite the fact that the number of streamers from the pointed rod is about 2 times larger (see Fig. 5). The reason for this is due to the large charge of each streamer from the rod of the square cross section.

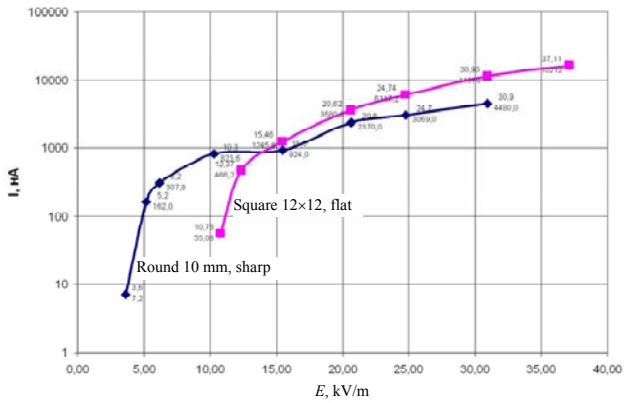

Fig. 6. Dependence of the current of the corona on the strength of the electric field for the pointed (diameter 10 mm, sharpness ratio $k = 3$) and square rods. The length of each rod is 3.4 m

From the presented experimental results, the following conclusions follow:

– the pointed rod (diameter 10 mm, $k = 3$, height 3.4 m) begins to react with an electric field strength of 3 kV·m^{-1}, and a square-section rod (12×12 mm^2) of the same height not earlier than from 9 kV·m^{-1};

– corona discharge from the pointed rod in the E-field intensity range from 6 kV·m^{-1} to 10 kV·m^{-1} stops, which fully corresponds to the results of [5] cited above in the introduction;

– at an E-field strength exceeding 10 kV·m^{-1} the number of streamers from the pointed rod is approximately twice as large as from the square rod;

– the average peak value of the current of an individual streamer is higher for a square rod, for example, at strength $E \approx 10$ kV·m^{-1}, this value is 5 mA for a pointed rod and 60 mA for a square rod;

– the value of the root-mean-square deviation, with other identical conditions for the case of a square rod, is less than for the case of a pointed rod.

Alternative method for measuring the streamer speed. The traditional method of measuring the speed of streamer-leaders is ultra-fast video recording. To implement this method requires the presence of a high-speed video camera, for example, the type FASTCAM SAS (with the option of up to 10^6 frames per second) and a special mode of illumination of the investigated discharge gap. The limitation of the realization of this method is not only the high cost of the camera, but also the fixed sector of the survey, which makes it difficult to use the method effectively when investigating long (more than 3 m) discharge gaps.

An important parameter of the pre-discharge processes is the speed of the oncoming streamer, which is formed from the grounded object. With higher the averaged speed, the probability of lightning entering the object is higher. It is known [10] that the streamer speed depends on the electric field strength in the discharge gap. Thus, in a region where the field strength E exceeds $3 \cdot 10^6$ V·m^{-1}, the streamer speed can reach 10^7 m/s. However, such tension, and, consequently, speed, is possible only in the streamer zone of the head of the lightning leader. It is indicated in [10] that the measured average leader speed is $3.36 \cdot 10^5$ m/s, the minimum is $8 \cdot 10^4$ m/s, and the maximum speed is $2.6 \cdot 10^6$ m s. It is proved that there is a minimum streamer speed, which is 10^3 m/s in air under normal conditions. At lower values, the tape drive stops. Consequently, the range of change of the parameter under study (the streamer-leader speed) is more than four orders of magnitude.

It is known [10] that the ionization wave is formed from the top of the rod and propagates in the interelectrode gap towards the opposite electrode. As a rule, in air gaps up to 5 m long (typical for most laboratory conditions), the streamer-leader has a single-channel structure without significant branching. A weakly conducting cover forms around the channel of the streamer. The streamer model adopted is based on the following assumptions:

– the channel of the critical streamer is single (not branching);

– the diameter of the channel, taking into account the cover, is constant;

– the density of charges in the channel is uniform.

Under these assumptions, the length of the streamer is directly proportional to the charge in the channel (taking into account the cover). The integral value of the charge in the channel is proportional to the streamer current and time by formula (4). In fact, this is the area under the curve $I(t)$, represented on the oscillogram (Fig. 7)

$$Q = \int_0^T I(t)dt\,, \qquad (4)$$

there Q is the charge value in the channel; T is the duration of the process, $I(t)$ is the dependence of current on time since the beginning of the process.

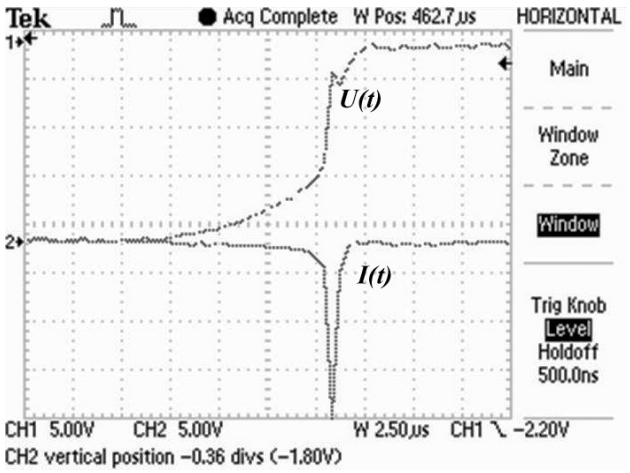

Fig. 7. Oscillogram of the dissemination process of the critical streamer

Denote the channel length of the streamer L_k. It is obvious that at the moment of contact of the opposite electrode L_k is equal to the length of the air gap L, and the streamer charge has the value of Q. This moment is fixed by the abrupt failure of the voltage $U(t)$ applied to the air gap.

It should be noted that the moment of closure of the gap by the streamer cannot be determined from the maximum streamer current, since the maximum value of the current strength is reached after closing the gap and is determined by the magnitude of the discharge voltage in the discharge loop.

Consequently, the result of the experiment gives such initial data:

– total channel charge (Q);

– time interval (T), during which the streamer crosses the air gap;

– the length of the air gap (L).

From these data, it is easy to determine the mean of the streamer speed at an interval by the obvious formula (5).

$$V_A = LT^{-1}. \tag{5}$$

To estimate the instantaneous values of the streamer velocity at various points in the air gap space, we use the above assumptions about the nature of the streamer propagation. The streamer channel, in the form of a cylinder of length L, of a certain radius (whose value for the problem under consideration is not essential) is divided into N equal parts. At each n-th section, the value of the charge (Q_n) is estimated by the formula (6).

$$Q_n = Q/N. \tag{6}$$

Further actions are illustrated in Fig. 8, which shows a typical curve $I(t)$ on an enlarged scale. The area under the curve $I(t)$, giving the value of the charge Q, is determined. This area is divided into N equal parts. The partitioning algorithm for some particular cases will be presented later. The corresponding values of t_k are found. The streamer speed (V_n) at any arbitrarily small segment is determined by the formula (7).

$$V_n = L(N \cdot \Delta t_n)^{-1}, \tag{7}$$

where Δt_n is the value of the n-th time interval.

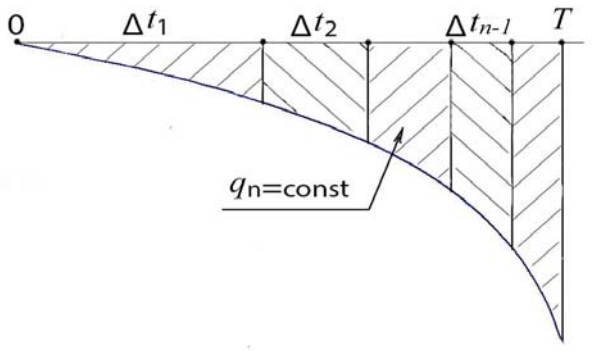

Fig. 8. The principle of subdividing the area under the curve

Results of the calculation estimation. Let us consider particular cases of the functional dependence of the streamer current on the propagation time. If the current does not depend on time, the streamer is distributed with a constant speed. Such an option is hypothetical, since in experiments is not visible.

As a first approximation, the curve of $I(t)$ dependence can be approximated by a straight line passing at a certain slope angle (k). In this case, the functional dependence of the current strength on time is described by formula (8)

$$I(t) = k \cdot t. \tag{8}$$

After substituting (8) into formula (4), for the total charge of the streamer we obtain (9)

$$Q = 0.5k \cdot T^2. \tag{9}$$

The instant of time (t_1) of the first segment passing by the streamer (coincides with the time interval) is found by formula (10)

$$t_1 = \frac{T}{\sqrt{N}}. \tag{10}$$

To calculate the subsequent values of t_n it is not difficult to obtain the recurrence formula (11)

$$t_n^2 = \left(\frac{T^2}{N}\right) + t_{n-1}^2. \tag{11}$$

The character of the curve on the oscillogram (Fig. 7, lower curve) can be described more accurately by an exponential dependence. In this case, it is more convenient to consider the dependence in the inverse time variant, without taking into account the sign, which allows us to introduce the function (12):

$$I(t) = \exp(-\alpha \cdot t), \tag{12}$$

where α is the coefficient determining the decay rate of the function.

The maximum value of the current is set equal to unity, since its absolute value does not affect the further results. The value of the parameter α is easily determined from the curve $I(t)$. For this it is sufficient to find the time moment (t_e) at which the current reaches a value of 0.368. The parameter $\alpha = t_e^{-1}$.

The recurrence relation for finding the values of time (t_n) from the previous value (t_{n-1}), is described by formula (13).

$$t_n = -\left(\frac{1}{\alpha}\right) \cdot \left[\exp(-\alpha t_{n-1}) - \left(\frac{1}{N}\left(1 - \exp(-\alpha T)\right)\right)\right]. \tag{13}$$

This relation makes it easy to find all the values of t_n with any given accuracy determined by the number of partitions N. It should again be pointed out that in this case the count of the time intervals is realized from the maximum of the current strength to the beginning.

In the example shown in Fig. 7, the distance from the top of the lightning collector to the upper potential electrode was 1.2 m. The time of development of the process of germination of the streamer, defined as the

interval from the point of divergence of the curves to the instant of a sharp decrease in voltage, is 9 μs. The number of intervals is chosen equal to 10. The values of the corresponding time intervals are calculated using formula (13). On the basis of the obtained data, taking into account that each segment of the streamer length is equal to 0.12 m, a spatial dependence of the velocity, represented by the graph in Fig. 9.

In the example considered, the streamer speed varied from $1.8 \cdot 10^4$ m/s to $1.1 \cdot 10^6$ m/s. The average value of the streamer speed in the air gap is $1.3 \cdot 10^5$ m/s. The calculated values of the streamer velocity are in good agreement with the data obtained by other methods [10].

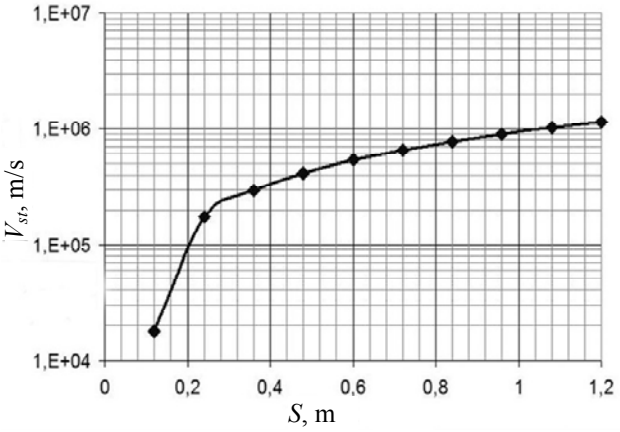

Fig. 9. Graph of the streamer speed change from the path

The proposed algorithm can be described as follows:

– the integral value of the charge Q (the area under the curve of the $I(t)$ curve) is determined;

– the number of partitions is chosen, for reasons of sufficient accuracy;

– the values of the time intervals for which the areas under the curve are equal are equal to and equal to the N-th part of Q;

– the speed at a specific spatial gap is defined as the quotient of the interval length divided by the time it intersects.

The method can supplement the procedure for attestation of lightning receivers according to the standard [1].

Conclusions.

The functional dependences of the streamer frequency with metal rods with a length of 3.4 m of circular cross section with a pointed vertex and a square section with a flat top have been determined experimentally.

It is established that the frequency of the streamer follow-up for the case of a rod of square cross section has a deterministic character: with increasing electric field strength, the repetition frequency increases monotonically with coefficient which is close to 0.25 $s^{-1} \cdot V^{-1} \cdot m$.

The value of RMS, under other identical conditions for the case of a square rod, is several times smaller than for the case of a pointed rod.

It has been established that corona discharge from a sharpened rod in the range of electric field strength from 6 kV/m to 10 kV/m ceases, and the repetition frequency with increasing intensity reaches 6 kHz.

On the basis of the obtained results of the investigation of the features of the formation of a streamer corona from the top of a rod lightning detector with a height of more than 1 m, it is proposed to take as a standard lightning detector for testing ESE terminals in accordance with the standard [1] a square bar (12×12 mm^2) with a flat top with height of 1 m.

Certification of ESE type lightning detectors is recommended to begin with comparative tests with a standard lightning detector, by placing them both in the working volume of the test bed and recording the discharge frequency in each of them when a voltage pulse with a front duration of more than 100 μs is applied to the gap.

A method for estimating the rate of advance of a critical streamer is proposed, based on the synchronous measurement of the voltage across the discharge gap and the streamer current from the lightning detector.

Based on the aggregate of the results obtained, the standard [1] is recommended not to be introduced as a national Standard of Ukraine until the introduction of scientifically justified data into the requirements of the standard.

The results were obtained within the framework of the research work (state registration No. 0115U000611), which was carried out by order of the Ministry of Education and Science of Ukraine in 2015-2016.

The author thanks P.N. Melnikov and S.P. Shalamov for their help in carrying out experimental and theoretical research, and the scientific adviser V.V. Kniazev – for valuable advices and recommendations.

REFERENCES

1. NF C 17-102:2011 (Ed.2) Protection contre la foudre – Systèmes de protection contre la foudre à dispositif d'amorçage. Union Technique de l'Electricité (UTE), 2011. 82 p.

2. Kniazev V.V., Lesnoi I.P., Chernukhin A.Iu. Investigation results of the ESE-terminal and dissipaters' parameters. *Bulletin of NTU «KhPI»*, 2008, no.21, pp. 78-87. (Rus).

3. Ortéga P., Heilbronner F., Rühling F., Díaz R., Rodière M. Charge–voltage relationship of the first impulse corona in long air gaps. *Journal of Physics D: Applied Physics*, 2005, vol.38, no.13, pp. 2215-2226. **doi: 10.1088/0022-3727/38/13/021**.

4. Moore C.B., Rison W., Mathis J., Aulich G. Lightning rod improvement studies. *Journal of Applied Meteorology*, 2000, vol.39, no.5, pp. 593-609. **doi: 10.1175/1520-0450-39.5.593**.

5. Bazelian E.M. The effect of the space charge of the corona in lightning protection. *Trudy IV Rossiiskoi konferentsii po molniezashchite* [Proceedings of the IV Russian Conference on Lightning Protection]. NPO «Strimer», Sankt-Peterburg, 2014, pp. 1-16. (Rus).

6. Chernukhin A.Iu. Parameters of pulse corona on metal roads in strength electric field. *Bulletin of NTU «KhPI»*, 2014, no.50, pp. 155-160. (Rus).

7. Chernukhin A.Iu., Kniazev V.V. A features of streamer crown are from cored air terminals. *Bulletin of NTU «KhPI»*, 2015, no.20, pp. 149-155. (Rus).
8. Kniazev V.V., Chernukhin A.Iu. Effects of corona in pre-discharge conditions. *Trudy IV Rossiiskoi konferentsii po molniezashchite* [Proceedings of the IV Russian Conference on Lightning Protection]. NPO «Strimer», Sankt-Peterburg, 2014, pp.62-70. (Rus).
9. Rezinkina M.M. Simulation of electric fields in the presence of rods with rounded upper ends. *Technical Physics*, 2015, vol.60, no.3, pp. 337-343. **doi: 10.1134/S1063784215030238**.
10. Vernon Cooray. *Lightning Protection*. Ins.Eng.Tech., London, UK, 2010. 1070 p.

Received 24.04.2017

A.Yu. Chernukhin, Research Associate,
Scientific-&-Research Planning-&-Design Institute «Molniya»
National Technical University «Kharkiv Polytechnic Institute»,
47, Shevchenko Str., Kharkiv, 61013, Ukraine,
phone +38 057 7076292,
e-mail: chernukhin@yahoo.com

How to cite this article:
Korobko A.A. Multifrequency algorithms for determining the moisture content of liquid emulsions by the method of resonance dielcometry. *Electrical engineering & electromechanics*, 2017, no.3, pp. 47-56. **doi: 10.20998/2074-272X.2017.3.07.**

UDC 536.242 **doi: 10.20998/2074-272X.2017.3.08**

R.V. Zaitsev

MODELING OF AN ADVANCED HEAT EXCHANGE UNIT WITH MICROCHANNELS FOR A COMBINED PHOTOENERGY SYSTEM

Purpose. Mathematical modeling of the heat exchange unit main parameters for photoenergy system based on general models with forced circulation of heat transfer fluid. Methodology. To determine the coefficient of heat transfer at a given coolant temperature and surfaces temperature necessary to determine the temperature gradient in the wall of the heat exchanger. Temperature gradients can be determined by solving the equation of energy, which depends on the distribution of the flow rate in the flow. In general, a solution of convective heat transfer fluid to flow along the plane comes to solution of the system of differential equations. Results. In the paper features of the selection of theoretical basis and mathematical modeling of thermal processes in the heat exchange unit for combination photoenergy system are presented. As a result of the simulation conducted we improve and develop high-efficiency heat exchange unit with microchannels. Testing of the proposed unit proved its high efficiency through the implementation of turbulent flow of coolant with heat transfer coefficient at 18 kW/(m^2·K). Analytical testing of the heat exchanger allowed showing that heat exchanger unit provides a stable operating temperature at less than 50 °C with the coolant flow rate is less than 0.3 m/s. Originality. Novelty of the proposed heat exchanger is in the optimal design of microchannels to improve the heat transfer coefficient. Practical value. The use of this heat exchanger will improve the quality and uniformity of cooling solar panels and reduce energy costs for circulation of fluid. References 12, figures 4.

Key words: **heat exchanger unit, coolant, solar panels, combined photoenergy system.**

В работе рассматриваются особенности подбора теоретических основ и математическое моделирование тепловых процессов в теплообменном блоке для комбинированной фотоэнергетической установки. По результатам моделирования проведено совершенствование и разработка высокоэффективного теплообменного блока с микроканалами. Апробация предложенного блока подтверждает его высокую эффективность за счет реализации турбулентного режима протекания теплоносителя. Использование такого теплообменника позволить повысить качество и равномерность охлаждения солнечных батарей и уменьшить затраты энергии на циркуляцию жидкости. Библ. 12, рис. 4.

Ключевые слова: **теплообменный блок, теплоноситель, солнечная батарея, комбинированная фотоэнергетическая установка.**

Introduction. Global energy market trends and the associated increase in the consumption of natural energy resources clearly show the need to find additional sources of energy that could compensate for the lack of available resources, and ideally – completely replace them. As the experience of the USA, Japan, Germany, shows one of the ways to solve this problem associated with the conversion of solar energy into electricity using semiconductor photovoltaic cells (solar cells – SC).

The most common type of SC is devices based on the structure of mono- and polycrystalline silicon thickness of 200 μm. The main problem of their widespread use is the high price of electricity they produce, due to high material and energy intensity of the process of manufacture. To reduce the cost of SC promising is the use of systems operating under concentrated solar radiation. The use of mirrors allows hundreds of times lower cost of SC. However, the use of silicon SC based on traditional designs with concentrated solar radiation reduces the efficiency of the order [1, 2]. At the same time, the use of silicon multijunction SC with vertical diode cells with increasing intensity of solar radiation demonstrates the increased efficiency [3, 4].

Developed earlier [5] photoenergy plant based on silicon multijunction SCs with vertical diode cells or SC based on gallium arsenide, which has a positioning and control system, thus increasing the amount of light energy that comes to the surface power plant has many advantages. Such a photoenergy plant will produce not only electricity but also heat water. But along with this, there were severely difficulties in uniform cooling of installed SC that are needed to specifically address [6-8]. The conventional notation [9, 10] is used in this article.

The goal of the work is mathematical modeling of the main parameters of the heat exchange unit for photoenergy plant based on general models of heat transfer at forced circulation of fluid.

1. Investigation technique. In accordance with the general standard requirements for photoenergy plants for industrial equipment, the output voltage of the solar battery (SB) must not exceed U_{NM} = 48 V; load current – I_{NM} = 10.4 A; electric power that SB transits to the load – P_{NM} up to 500 W. Hence, at the $S_{SB} \approx 100$ cm^2 specific electrical power P_{NM} can be calculated, which is given to the load by 1 cm^2 of such SB and which is equal to 5 W/cm^2. However, along with this, at the maximum possible efficiency of SC, for example based on gallium arsenide, at 30%, to provide the necessary parameters, to the SB surface light with power density of at least 16.7 W/cm^2 has come. So the power of 11.7 W/cm^2 is excessive and will come to the SB and the heat exchanger in the form of heat, which will lead to significant and rapid overheating of SB.

The aperture area of the mirror system that concentrates, $S_a \approx 2.4$ m^2. At the solar radiation power P_s = 1000 W/m^2 the energy coming to this area Q_s = 2396 W. By selecting better material for the mirrors, the proportion of energy supplied to the photodetector plate after accounting reflectance of mirrors (r_z = 0.95), and the processes of reflection and absorption system plate – glass, which takes into account absorptive capacity

(τ_α) [9] we have $Q_{s1} = r_z Q_s$ (τ_α) = 1761 W (this corresponds to the effective concentration factor K_{eff} = 386). After conversion of the part of this energy into electrical energy with efficiency η = 30%, giving Q_{s2} = 528 W of electrical energy, into thermal energy $Q_{s3} = Q_{s1}(1-\eta)$ = 1233 W transfer.

To determine the coefficient of heat transfer at given temperature of the coolant and the surface temperature that flowed it is necessary to determine the temperature gradient in the wall of the heat exchanger. Temperature gradient can be determined by solving the equation of energy, which in turn depends on the distribution of the flow velocity in the considered flow region. In general terms, solving the problem of convective heat transfer fluid for fluid flow along the plane comes to solving the following system of differential equations (1) [9]

$$\begin{cases} \frac{1}{\rho}\frac{\partial\rho}{\partial\tau}+\frac{\partial w_x}{\partial x}+\frac{\partial w_y}{\partial y}=0; \\ \frac{\partial w_x}{\partial\tau}+w_x\frac{\partial w_y}{\partial x}+w_y\frac{\partial w_x}{\partial y}=\frac{\mu}{\rho}\left(\frac{\partial^2 w_x}{\partial x^2}+\frac{\partial^2 w_x}{\partial y^2}\right)-\frac{1}{\rho}\frac{\partial\rho}{\partial x}+g_x; \\ \frac{\partial w_y}{\partial\tau}+w_x\frac{\partial w_y}{\partial x}+w_y\frac{\partial w_y}{\partial y}=\frac{\mu}{\rho}\left(\frac{\partial^2 w_y}{\partial x^2}+\frac{\partial^2 w_y}{\partial y^2}\right)-\frac{1}{\rho}\frac{\partial\rho}{\partial y}+g_y; \\ \frac{\partial T}{\partial\tau}+w_x\frac{\partial T}{\partial x}+w_y\frac{\partial T}{\partial y}=\frac{\lambda}{\rho c_p}\left(\frac{\partial^2 T}{\partial x^2}+\frac{\partial^2 T}{\partial y^2}\right); \\ p=\rho RT. \end{cases} \quad (1)$$

Such a system of equations in general defies analytic solution, therefore special cases are considered.

1.1. Heat transfer at the motion of fluid in direct smooth pipes. At moving liquids and gases in pipes and channels there are laminar ($Re_{f,d} \le 2300$), turbulent ($Re_{f,d} \ge 10^4$) and the transition from laminar to turbulent ($2300 < Re_{f,d} < 10^4$) regimes of fluid flow.

Definitive the parameters for calculating the Reynolds criterion: $T_0 = T_f = 0.5\cdot(T_{f,in} + T_{f,out})$ – the average temperature of the fluid in the; $R_o = d_{in}$ – internal pipe diameter; $w_0 = G/(\rho\cdot f)$ – average by the pipe section velocity of the fluid movement.

1.1.1. Heat transfer in laminar fluid flow regime in pipes ($Re \le 2300$). Heat pipes at a stabilized flow and stabilized heat transfer can be calculated at T_w = const and q_w = const by the approximate formula [9]:

$$N_u = 4\varepsilon_t, \quad (2)$$

where the amendment ε_t is calculated by the formula

$$\varepsilon_t = \left(\frac{Pr_{fl}}{Pr_w}\right)^{0.25}. \quad (3)$$

In laminar regime of the movement in the direct smooth pipes and presence of sections of hydrodynamic and thermal stabilization for a more accurate approximation of the experimental data there are two subregimes: laminar viscous and laminar viscous-gravitational. Laminar viscous flow regime occurs when Rayleigh numbers $Ra < 8\cdot10^5$ and laminar viscous-gravitational mode when $Ra \ge 8\cdot10^5$.

Heat transfer at the laminar viscous flow regime in pipes ($Re \le 2300$; $Ra < 8\cdot10^5$). Average by the internal surface of the pipe of length l heat transfer coefficient is calculated by the formula obtained at $l/(Re\cdot d) \le 0.05$ and $0.07 \le \mu_w/\mu_f \le 1500$ [5]:

$$Nu = 1.55\left(Re\cdot d_{in}/l\right)^{1/3}\cdot\left(\mu_f/\mu_w\right)^{0.14}\cdot\varepsilon_l. \quad (4)$$

The value ε_l of amendment taking into account the impact on heat transfer of hydrodynamic flow stabilization in the initial section of heat:

– at:

$$\frac{l}{Re\cdot d} < 0.1 - \varepsilon_l = 0.6\left(\frac{l}{Re\cdot d}\right)^{-\frac{1}{7}}\left(1+2.5\frac{l}{(Re\cdot d)}\right), \quad (5)$$

– at:

$$l/(Re\cdot d) < 0.1 - \varepsilon_l \approx 1. \quad (6)$$

Heat transfer at the laminar viscous-gravitational fluid medium mode in pipes ($Re \le 2300$; $Ra < 8\cdot10^5$). Average heat transfer coefficient at the laminar viscous-gravitational medium mode can be calculated by the M.A. Mikheyev criterion equation [10]:

$$Nu = 0.15\cdot Re_{f,d}^{0.33}\cdot Pr_f^{0.33}\cdot\left(Gr_{f,d}\cdot Pr_f\right)^{0.1}\cdot\varepsilon_t\cdot\varepsilon_l. \quad (7)$$

Correction factor ε_l taking into account the impact on heat transfer of the process of hydrodynamic flow stabilization in the initial section of heat transfer equal to:

– at $l/d < 50$ values of ε_l are founded by experimental data [6];

– at $l/d \ge 50$ – $\varepsilon_l = 1$.

1.1.2. Heat transfer at the turbulent fluid movement mode in pipes ($Re \ge 10^4$). Average heat transfer coefficient at the turbulent fluid flow in direct smooth pipes is calculated by the M.A. Mikheyev formula [10]:

$$Nu_{f,d} = 0.021\cdot Re_{f,d}^{0.8}\cdot Pr_f^{0.43}\cdot\varepsilon_t\cdot\varepsilon_l. \quad (8)$$

Correction factor ε_l taking into account the impact on heat transfer of the process of hydrodynamic flow stabilization in the initial section of heat transfer equal to:

– at $l/d < 50$–$\varepsilon_l \approx 1+2d/l$;

– at $l/d \ge 50$–$\varepsilon_l = 1$.

Values of ε_l depending on the Reynolds criterion are presented in [9].

1.1.3. Heat transfer at the transition fluid flow regime in pipes ($2300 < Re < 10^4$). The transitional flow regime is characterized by mixing laminar and turbulent flows. In this case, the heat transfer coefficient can be calculated by the formula [10]:

$$Nu_{f,d} = K_0\cdot Pr_f^{0.43}\cdot\varepsilon_t\cdot\varepsilon_l, \quad (9)$$

where the complex K_0 depends on the Reynolds number [10], and the amendment ε_l is calculated like at turbulent mode of the fluid flow.

1.2. Heat transfer at the motion of fluid in the channels of arbitrary cross-section. All of the above criterion formula for calculating heat transfer in circular pipe have been used for the calculation of heat transfer during the flow of liquids and gases in channels of other (non-circular) cross-sectional shapes (rectangular, triangular, ring, etc.), the longitudinal washing of pipes beams entered to the channel of arbitrary cross-section, and at the fluid flow that does

not fill the entire cross-section of the channel. Here, as the characteristic size equivalent or hydraulic diameter of the channel should be used:

$$R_0 = d_{ekv} = d_r = 4f / P, \quad (10)$$

where f is the area of the flow cross-section, m^2; P is the wetted perimeter of the channel, m.

1.3. Heat transfer at the turbulent motion of fluid in the curved pipes. At the movement of liquid in curved pipes (laps, coil) there is its additional turbulence and, consequently, increasing the heat transfer coefficient [11]. To calculate the heat transfer in the curved pipes it is necessary to multiply the Nusselt number the on correction factor:

$$\varepsilon_g = 1 + 1.8 \cdot d_{in} / R_g, \quad (11)$$

where d_{in} is the internal pipe diameter, and R_g is the bend radius.

2. Results of investigation and their discussion. As shown earlier [5] to reach acceptable temperatures of SB the intensity of the heat transfer should be increased. You can use either increase of the area of heat transfer through the use of radiator, or try to use turbulent flow of coolant to increase the heat transfer coefficient [12].

Based on the proposed theoretical study, two options for designs that are shown schematically in Fig. 1 are considered. The design shown in Fig. 1,*a* has a large area of the heat exchanger, and the design shown in Fig. 1,*b* has a large coefficient of heat transfer at the heat exchanger area close to the area of the heat receiving plate.

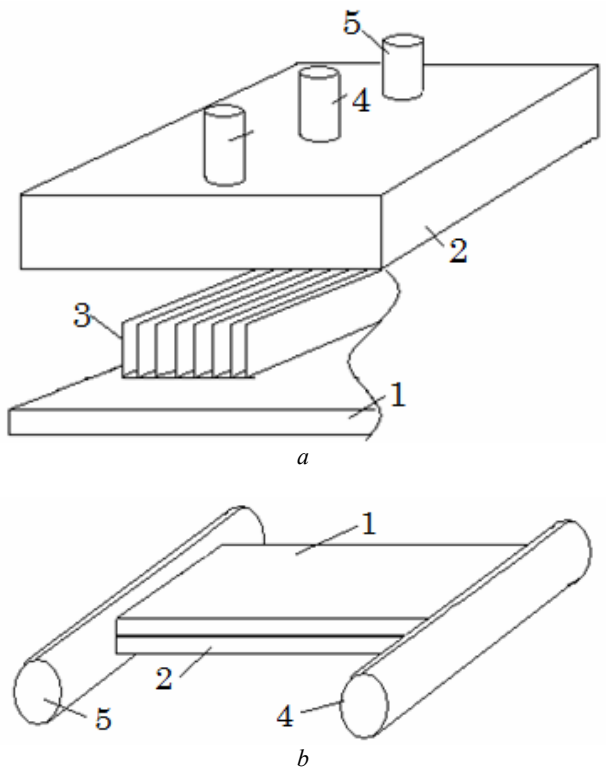

Fig. 1. Schematic representation of the designs of the cooling block with plate radiator (a) and ram with a small gap width between the plates (b): 1 – cover of the cooling block, 2 – the cooling block housing, 3 – radiator plates, 4 – tube for feeding coolant 5 – tube for cooling output

To calculate the heat exchange unit with a radiator with a large area of heat exchange surface (Fig. 1,*a*), and industrial copper radiator used to cool the elements of computer circuits was chosen as a model. It has the following dimensions: 91×91×25 mm, 56 plates, the distance between them is 1 mm, i.e. there are 55 channels for water leaking of the cross section 1×20 mm (including the thickness of the upper plate of 5 mm), but at the central water supply there are efficiently 110 channels. At coolant (water) consumption in the first closed loop of 10 l/min (0.016 kg/s) the flow velocity (w) in gaps between the plates is 0.0682 m/s. At an average temperature of cooling water ~ 50°C kinematic viscosity of water ν = 0,556 10^{-6} m^2/s. Taking into account the effective diameter d_e = 1,9·10^{-3} we obtain Reynolds number $Re = wd_e/\nu = 234$, corresponding to laminar flow. Calculating the Grashof (495) and Rayleigh (1752) numbers we determine that in the selected radiator with indicated coolant consumption the laminar viscous flow regime takes place. Calculation of heat transfer coefficient between the coolant and radiator plates gives Nu = 1.838 W/(m^2·K), which is insufficient for effective heat dissipation, and such a heat exchanger cannot be used in the photoenergy unit.

To calculate the heat exchange unit with radiator with a large heat transfer coefficient (Fig. 1,*b*) it was proposed the following dimensions of the section of the water strait 1×80 mm with length of 60 mm. At such sizes and water consumption as above the flow velocity in gaps between the plates is 1.875 m/s. Taking into account the effective diameter d_e = 1,98·10^{-3} m we obtain the Reynolds number $Re = wd_e/\nu$ = 6661, corresponding to the transition mode of the flow leakage. Calculation of heat transfer coefficient between the coolant and the upper plate of the radiator provides Nu = 13931 W/(m^2·K). Reducing the distance between the plates to critical, in terms of viscosity, 0.5 mm permits to increase the flow velocity to 2.92 m/s, but with less fluid consumptopn, since hydrodynamic resistance increases and the pump can provide consumption of 7 l/min that conserves the flow in transient mode. Here Nu = 18483 W/(m^2·K).

Based on performed calculations, the basic design of the flat heat exchanger has been improved with the introduction to it of microchannels to increase the coefficient of heat transfer. Block of the heat exchanger is designed as a complete unit. Fig. 2 shows the design of the radiator, which is a skirt design. In this design collecting planes with tubes which feed (outlet) coolant, and ribs that form microchannels for coolant provided are provided. The bottom of the radiator is the basis for fixing SB, thus decreasing the thermal resistance «surface – coolant».

Taking into account the presented design and theoretical investigations the mathematical modeling of such a heat exchanger operation at different fluid velocities was conducted. The main criteria for analysis were uniform cooling surface and its temperature at the supply of the above mentioned amount of heat. The corresponding heat pattern is shown in Fig. 3.

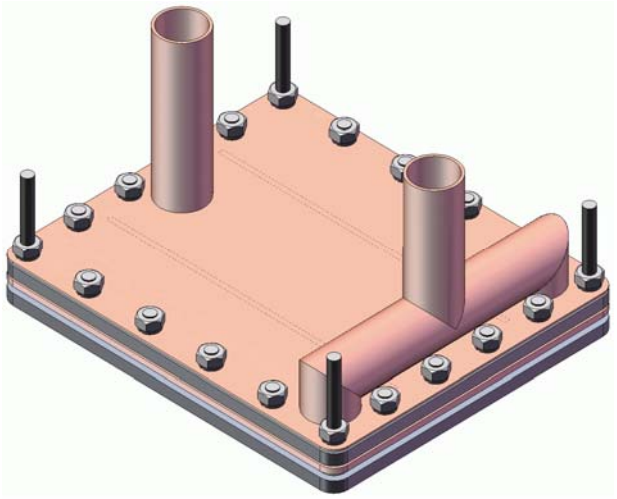

a

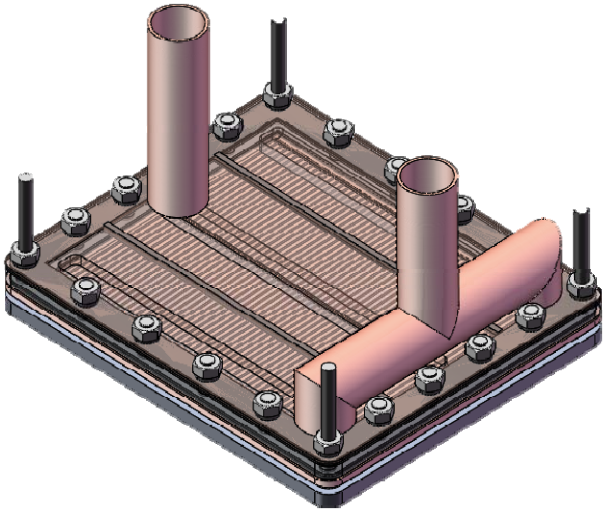

b

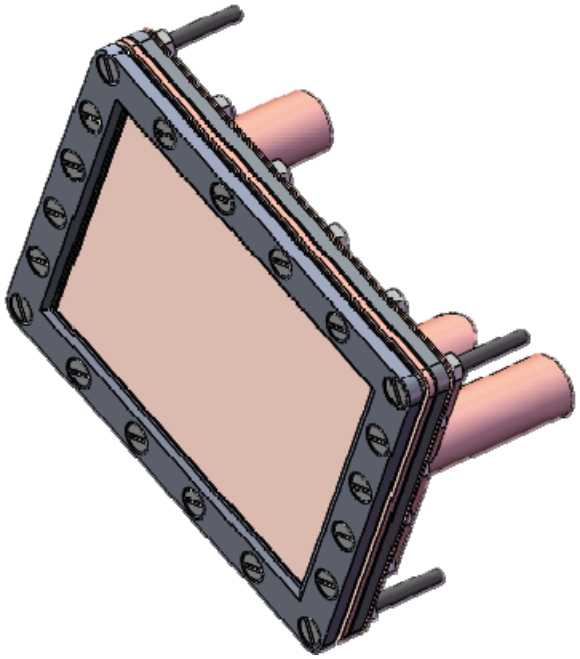

c

Fig. 2. Pictures of a flat heat exchanger: general (*a*) cross-section in microchannels (*b*) and from the heat transfer plane (*c*)

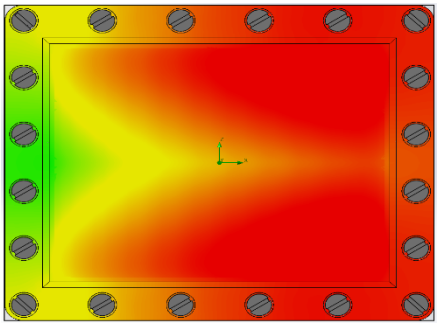

a

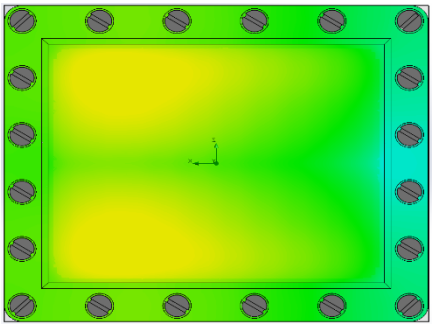

b

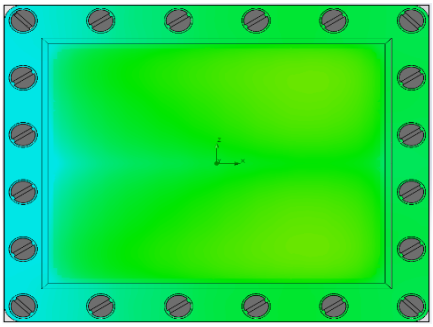

c

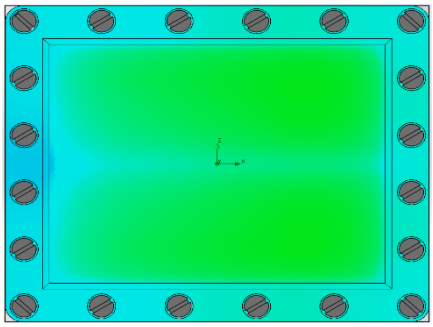

d

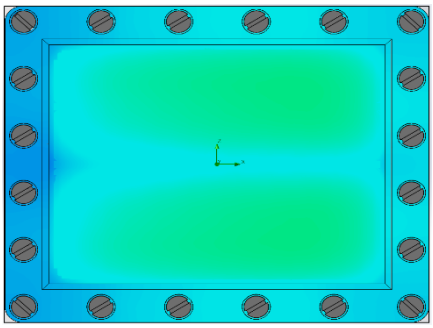

e

Fig. 3. Thermal patterns of the heat exchanger at following modeling conditions: *a* – w = 0.1 m/s, maximal surface temperature T_{max} = 63.25 °C; *b* – w = 0.2 m/s, T_{max} = 48.27 °C; *c* – w = 0.3 m/s, T_{max} = 43.38 °C; *d* – w = 0.5 m/s, T_{max} = 39.18 °C; *e* – w = 1.0 m/s, T_{max} = 35.72 °C

Analysis of the thermal patterns leads to the conclusion that even when the fluid flow velocity of 0.3 m/s for the proposed design of the heat exchanger sufficient cooling surface uniformity is reached (Fig. 3,*c*). Here, the maximum temperature does not exceed 43.5 °C, that is enough for SB effective operation without reducing efficiency. At the same time, reduce of the speed of fluid leads to loss of uniformity of cooling and to significant increase in the surface temperature to more than 60 °C that is unacceptable.

It should also be noted that the required heat exchange parameters are achieved at the speed of 0.3 m/s, which is much less than 2.92 m/s, which were obtained for the classic flat heat exchanger. Here, further increase in the speed of the fluid does not substantially improve uniformity and reduce the temperature, but will require additional energy losses to create flow.

Reducing the effective fluid flow compared with the classic flat heat exchanger indicates higher efficiency of heat transfer. This is possible only during the transition from the transitional regime of fluid flow in a classic flat heat exchanger to the turbulent regime in the proposed design.

To confirm the mode change of fluid flow mathematical modeling of fluid flow in the channels of the heat exchanger was conducted, the pictures are shown in Fig. 4.

The analysis of fluid flow confirmed the movement in turbulent regime, which allows maximum heat transfer coefficient and consequently achieves uniformity of cooling and low temperature at minimum energy consumption to create the fluid flow.

Conclusions.

1. The theoretical calculations and modeling of heat transfer processes in converting solar energy in the manufactured heat exchange unit of the photoenergy plant are conducted, which showed that the most efficient is a plate heat exchanger equipped with the implementation in it of turbulent fluid flow, which achieves heat transfer coefficient of about 18 kW/(m^2·K).

2. Based on calculations an improved heat exchange unit with microchannels is developed and requirements correction to specifications of the photoenergy plant based on it is carried out.

3. Analytical verification of the heat exchanger permitted to determine that at selected parameters of the photoenergy plant, the heat exchanger unit provides stable operating temperature less 50 °C with the coolant flow velocity less than 0.3 m/s. The indicated temperature is optimal for solar battery operation at minimum energy consumption to create liquid flow.

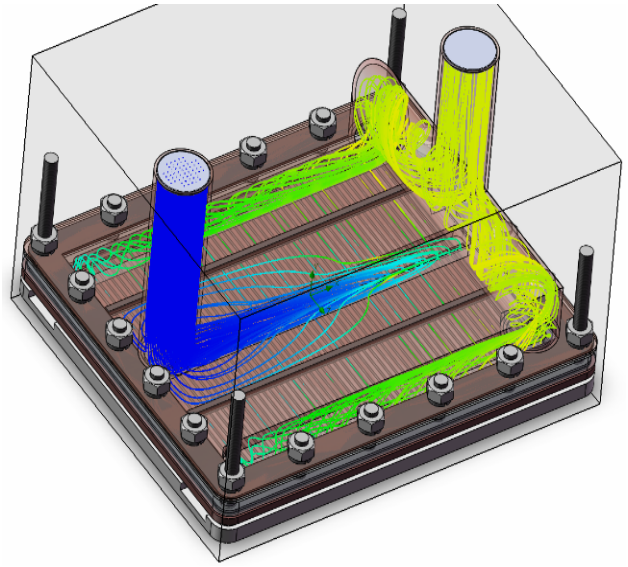

a

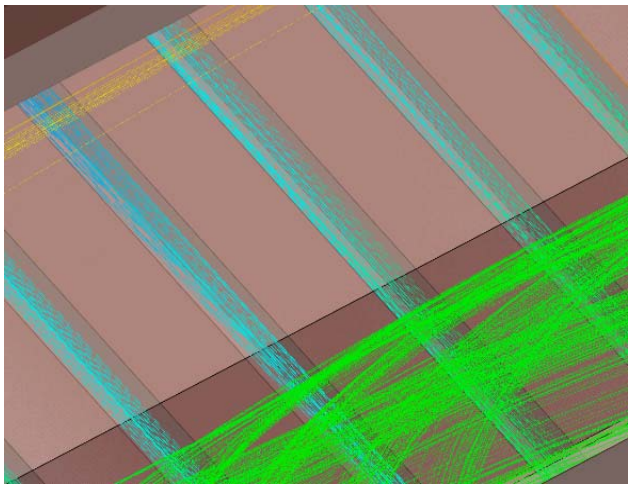

b

Fig. 4. Images of fluid flow modeling pictures in the heat exchanger as a whole (*a*) and in its microchannels (*b*)

REFERENCES

1. Jones A.D., Underwood C.P. A thermal model for photovoltaic systems. *Solar Energy*, 2001, vol.70, iss.4, pp. 349-359. **doi: 10.1016/S0038-092X(00)00149-3.**

2. Tuomiranta A., Marpu P., Munawwar S., Ghedira H. Validation of thermal models for photovoltaic cells under hot desert climates. *Energy Procedia*, 2014, vol.57, pp. 136-143. **doi: 10.1016/j.egypro.2014.10.017.**

3. Sokol E. *Rozroblennya fotoenerhetychnoyi ustanovky na osnovi bahatoperekhidnykh kremniyevykh sonyachnykh elementiv z vertykal'nymy diodnymy komirkamy. Zvit pro NDR (zaklyuchnyy; № derzhreyestratsiyi 0111U007628)* [Development of the energy picture settings based on multijunction solar cells with silicon-governmental vertical diode cells. Report on R&D (final; state registration number 0111U007628)]. Kharkiv, NTU «KhPI», 2012. (Ukr).

4. Strebkov D.S. *Matrichnye solnechnye elementy: Monografija v 3-h tomah. Tom 1* [Matrix solar cells: Monograph in 3 volumes. Vol. 1]. Moscow, GNU VIESH Publ., 2009. 120 p. (Rus).

5. Sokol E.I., Kopach V.R., Zaitsev R.V. Physical and technical features and practical limits of the photonenergy module of the new generation on the territory of Ukraine. *Renewable energy*, 2011, no.2(25), pp. 18-28. (Rus).

6. Reddy K.S., Premkumar D., Vikram T.S. Heat transfer modeling and analysis of solar thermo-chemical reactor for hydrogen production from water. *Energy Procedia*, 2014, vol.57, pp. 570-579. **doi: 10.1016/j.egypro.2014.10.211.**

7. Steinfeld A. Solar thermochemical production of hydrogen – a review. *Solar Energy*, 2005, vol.78, iss.5, pp. 603-615. **doi: 10.1016/j.solener.2003.12.012.**

8. Modi A., Buhler F., Andreasen J.G., Haglind F. A review of solar energy based heat and power generation systems. *Renewable and Sustainable Energy Reviews*, 2017, vol.67, pp. 1047-1064. **doi: 10.1016/j.rser.2016.09.075.**

9. Isachenko V.P., Osipov V.A., Sukomel A.S. *Teploperedacha* [Heat transfer]. Moscow, Enegroizdat Publ., 1981. 488 p. (Rus).

10. Mikheyev M.A. *Osnovy teploperedachi* [Fundamentals of heat transfer]. Moscow-Leningrad: Gosenergoizdat Publ., 1960. 208 p. (Rus).

11. Shokri R., Ghaemi S., Nobes D.S., Sanders R.S. Investigation of particle-laden turbulent pipe flow at high-Reynolds-number using particle image/tracking velocimetry (PIV/PTV). *International Journal of Multiphase Flow*, 2017, vol.89, pp. 136-149. **doi: 10.1016/j.ijmultiphaseflow.2016.06.023.**

12. Shirvan K.M., Ellahi R., Mirzakhanlari S., Mamourian M. Enhancement of heat transfer and heat exchanger effectiveness in a double pipe heat exchanger filled with porous media: Numerical simulation and sensitivity analysis of turbulent fluid flow. *Applied Thermal Engineering*, 2016, vol.109, Part A, pp. 761-774. **doi: 10.1016/j.applthermaleng.2016.08.116.**

Received 21.01.2017

R.V. Zaitsev, Candidate of Technical Science, Associate Professor,
National Technical University «Kharkiv Polytechnic Institute»,
2, Kyrpychova Str., Kharkiv, 61002, Ukraine,
phone +38 068 8888246,
e-mail: zaitsev.poman@gmail.com

How to cite this article:
Zaitsev R.V. Modeling of an advanced heat exchange unit with microchannels for a combined photoenergy system. *Electrical engineering & electromechanics*, 2017, no.3, pp. 57-62. **doi: 10.20998/2074-272X.2017.3.08.**

UDC 621.316.99 **doi: 10.20998/2074-272X.2017.3.09**

D.G. Koliushko, S.S. Rudenko

A COMPUTER PROGRAM FOR INTERPRETATION OF THE DATA OF VERTICAL ELECTRICAL SOUNDING VEZ-4A

Purpose. Creating a computer program for interpreting the results of vertical sounding the soil in the form of multilayer model most typical for Ukraine. Methodology. The algorithm of the program is constructed on determination the soil structure with the help of the method of point source current, method of analogy and method of equivalent. The option of automatic interpretation based on Hook-Jeeves method. The program is implemented in the programming language Delphi. Results. The computer program «VEZ-4A» has a possibility of the interactive and automatic interpretation sounding results in the multi-layered geoelectrical model. Originality. In first time the computer program for analyzing and interpreting results of the soil sounding by Wenner configuration was created on the base of the analytical solution for field of current point source located in four-, three- or two-layer structure . In paper the review is presented and basic functions of our program are analyzed. Practical value. The program «VEZ-4A» is created and adapted for use in the electromagnetic diagnostics of grounding of existing power plants and substations. References 7, tables 1, figures 3.

Key words: **vertical electrical sounding, grounding, soil, Wenner installation.**

В работе был предложен алгоритм работы программы для интерпретации результатов вертикального электрического зондировании грунта в рамках диагностики состояния заземляющих устройств. Математический аппарат для реализации алгоритма построен на базе методов точечного источника тока, наименьших квадратов, Хука-Дживса и эквивалентирования. Приведено описание и основные функции разработанной программы. Библ. 7, табл. 1, рис. 3.

Ключевые слова: **вертикальное электрическое зондирование, заземление, грунт, установка Веннера.**

Introduction. One of the main objectives of the first phase of the electromagnetic diagnostics of grounding device [1, 2] of electrical voltages of different classes is vertical electric sounding (VES) of soil. The quality of the interpretation of results of VES and definition of the soil structure greatly affect the accuracy of the calculation of normalized electrical parameters: resistance of the grounding device, touch voltage and voltage on the grounding device.

Currently a number of specialized software for 1D, 2D and 3D interpretation of VES are known. The basis for the method of their construction is Dar Zarruk [3] method or analytical method based on optical analogy to solve the problem of the electric field of a point power source located on the surface of the geoelectric structure. Here, this source of constant, stationary or quasistationary current is considered [4, 5]. However, mathematical tools and specialized programs that define the structure of multilayer soil based on VES data, serve to resolve narrow-geological problems and is not adapted for use in the diagnosis of grounding systems and the use of existing universal pallets and method modules are expensive and ambiguous [6]. In the frame of the electromagnetic diagnosis of grounding devices state programs are used to interpret the VES as two- and three-layer geoelectric structures, such as «VEZ-2Auto» and «VEZ-3», which do not allow to cover all existing in Ukraine soils.

The statistical distribution of soils according to the number of layers in the locations of power Ukraine shows that the vast majority of soils have a three-layer structure – 72.7%, about 17% is four-layer and only 8.3% – two-layer [2]. Thus, development of the software to interpret the results of the VES with number of layers at least four will cover 98% of soils in Ukraine in the placements of power objects.

The goal of the work is development of a software for interpreting the results of the vertical electrical sounding of the four-layer soil.

Materials of investigations. The most common for VES is the Wenner installation, which is a four-electrode symmetrical system (Fig. 1). Interelectrode distance is equal between all neighboring electrodes also affects the size L. Probing depth is half the distance between the current electrodes AB or $1.5 \cdot L$ [3]. Thus, increasing the interelectrode distance increases the depth of sensing by the installation.

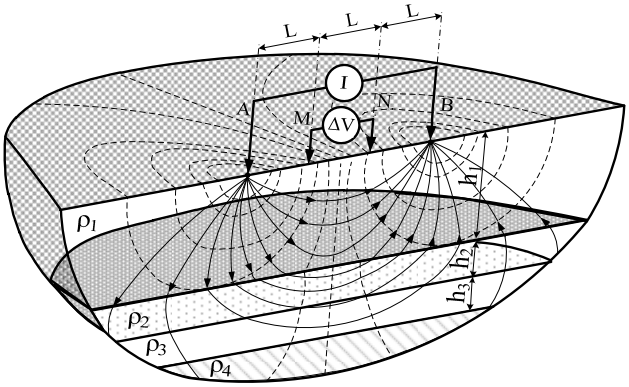

Fig. 1. Soil sounding by using the Wenner installation

The result of measurement is the dependence of imaginary specific electrical resistance (SER) ρ_y on the interelectrode distance, determined by the known expression [4, 7]

$$\rho_y = 2\pi L \frac{U_{VES}}{I_{VES}}, \quad (1)$$

where L is the distance between electrodes; U_{VES} is the voltage measured during VES; I_{VES} is the current measured during VES.

For the interpretation as the basis of program the embedded expressions for imaginary SER ρ_y is used as a function of the value L in multilayer medium with plane-parallel outside the division during VES by using the Wenner installation:

– at the two-layer structure [7]:

$$\rho_y = \rho_1 \left\{ 1 + 4 \sum_{n=1}^{\infty} K_{2,1}{}^n \left[\frac{L}{\sqrt{L^2 + (2nh)^2}} - \frac{L}{\sqrt{4L^2 + (2nh)^2}} \right] \right\}, \quad (2)$$

where h is the depth of the layer division in the two-layer model and the common measure in the three-layer model; $K_{2,1} = (\rho_2 - \rho_1)/(\rho_2 + \rho_1)$ is the heterogeneity rate; n is the number of the member of the series; L is the distance between nearest electrodes;

– at the three-layer structure:

$$\rho_y = \rho_1 \left\{ 1 + 4 \sum_{n=1}^{\infty} q_n^n \left[\frac{L}{\sqrt{L^2 + (2nh)^2}} - \frac{L}{\sqrt{4L^2 + (2nh)^2}} \right] \right\}, \quad (3)$$

where q_n is the coefficient of expansion of the integrand function [4].

Formulas (2) and (3) are obtained by using the expression for the electric field potential of the point source current in multilayer environment [4], at the placement of it and the observation point on the ground surface. In this case, (3) was obtained using the method of undetermined coefficients.

In the frame of improving the method of electromagnetic diagnosis of the grounding device based on the analytical solution of the problem of the electric field of a point power source located on the surface of the four-layer conducting half-space with plane-parallel boundaries of division, the authors have developed mathematical apparatus [5] for the interpretation of results of sounding and equivalentiation [2] of multilayer structures in the computational models.

To enable the software development, the authors used the earlier solution [5] of the stated the problem, provided the location of the observation point on the surface of the four-layer soil. In that case, the imaginary SER will look like:

$$\rho_y = \rho_1 + \rho_1 \sum_{j=1}^{3} \left(4K_{j+1,j} \cdot \sum_{n=0}^{k_{ur}} \left[\frac{K_n L}{\sqrt{L^2 + (2h_j + 2n)^2}} - \frac{K_n L}{\sqrt{4L^2 + (2h_j + 2n)^2}} \right] \right), \quad (4)$$

where $K_{j+1,j}$ is the heterogeneity rate determined as $K_{j+1,j} = \dfrac{\rho_{j+1} - \rho_j}{\rho_{j+1} + \rho_j}$; K_n is the factors obtained as a resilt of the expansion of the function characterizing the multilayer medium; n is the number of the member of the series; k_{ur} is the total number of the members of the series.

A function characterizing the multilayer medium has a form [5]:

$$F'_Z(\lambda) = \frac{1}{F_Z(\lambda)}, \quad (5)$$

where $F_Z(\lambda)$ is determined as follows:

$$F_Z(\lambda) = 1 - K_{2,1}e^{-2\lambda h_1} - K_{3,2}e^{-2\lambda h_2} - K_{4,3}e^{-2\lambda h_3} + K_{2,1}K_{3,2}e^{-2\lambda(h_2 - h_1)} + K_{2,1}K_{4,3}e^{-2\lambda(h_3 - h_1)} + K_{3,2}K_{4,3}e^{-2\lambda(h_3 - h_2)} - K_{2,1}K_{3,2}K_{4,3}e^{-2\lambda(h_3 - h_2 - h_1)}.$$

The value of K_n from the expression (4) is founded at the solution by the method of least squares of the system of equations, developed for the function approximation characterizing the multilayer medium (5), by the method given in [5], taking into account the number of layers of soil and h_n=2·n.

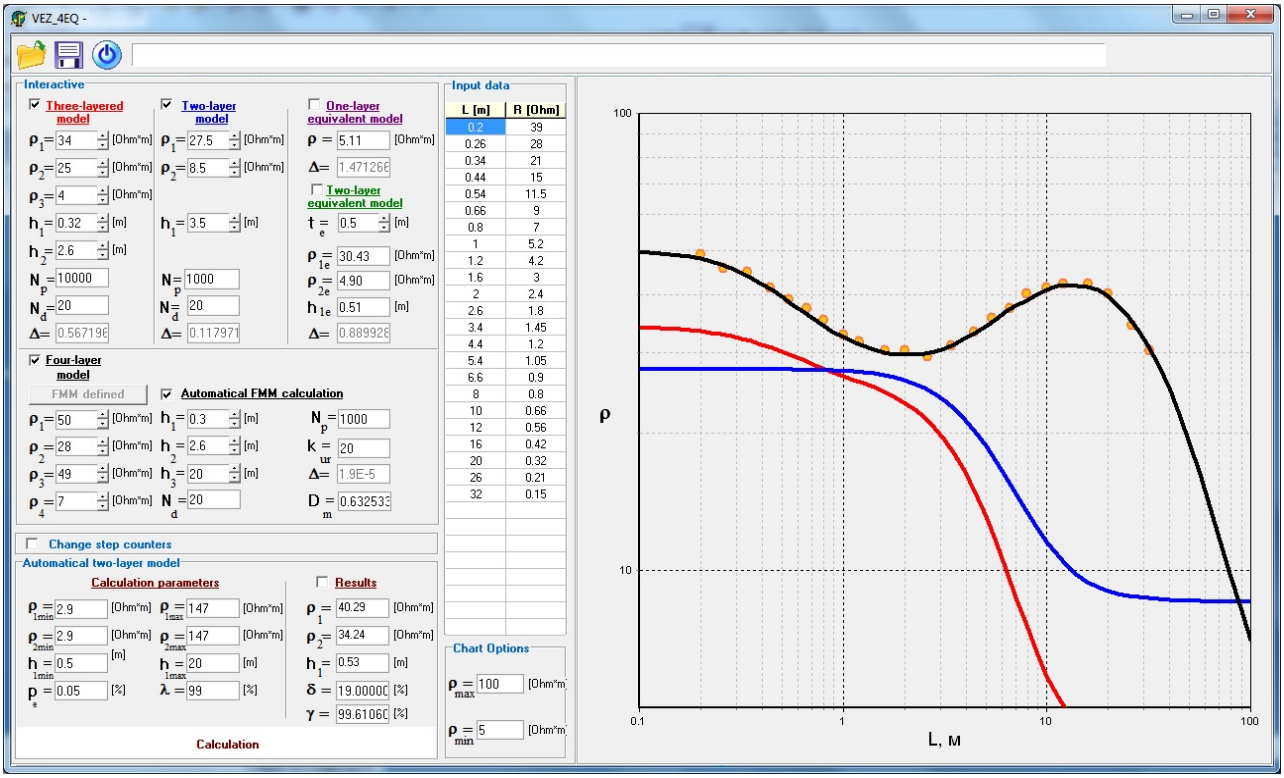

Fig. 2. A working window of the software for multi-layer soils interpretation «VEZ-4A»

Based on expressions (1) – (4) and using the method of least squares for the approximation of the function that characterizes the multilayer soil, in the software environment Delphi developed has developed a program

for interpreting the results of VES as four-layer geoelectric structure «VEZ-4A», which interface is shown in Fig. 2.

The developed program permits to perform both interactive and automatic interpretation of VES results.

When approximating functions characterizing multilayer medium we should consider the change of the interval of the dimensionless parameter $\lambda \in [0; \infty]$. The required number of members of series k_{ur} is determined by the relative error of approximation D_m of the output function (5), recommend value of it (see Fig. 2) is not more than 1%. Here, $F'_Z(\lambda) = 1$ at $\lambda \to \infty$.

The feature of the program is that in addition to the standard algorithm also contains the following blocks (see Fig. 3):

– automatic interpretation block in the form of a two-layer model Block 1;

– interactive interpretation block in the form of a two-layer model Block 2;

– interactive interpretation block in a three-layer model Block 3;

– interactive interpretation block as a four-layer model Block 4.

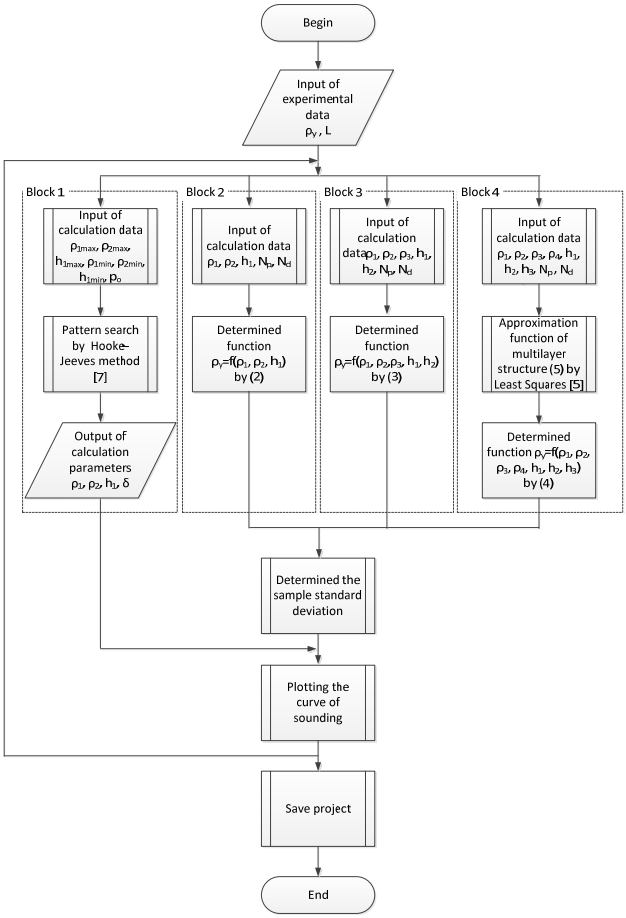

Fig. 3. An algorithm of the software operation

The standard blocks include the following:

– Input of experimental data ρ_y, L;

– Determined the sample standard deviation;

– Plotting the curve of sounding;

– Save project.

Methods and expressions for the block of equivalentiation (not specified in the algorithm) that were used in the program are given in [2].

Start of calculation and graphical display of VES takes place when selecting the appropriate models (Block 1 – Block 4).

By varying parameters of the models – SER of layers and their thicknesses – the largest compliance of the VES curve with experiment is reached. Here, the control of compliance is carried out in two ways:

1) by visual comparison of experimental points and calculated VES curve on the graph;

2) by analysis of the value of the standard medium deviation Δ (its lowest value corresponds to the maximum precision).

Change the settings of models is also possible in two ways:

1) direct input of the parameter value to the field;

2) to change by the step by step method using the the component of Delphi «UpDown».

Step of the specified component is floating and depends on the absolute value of the parameter.

For automatic interpretation of the results of VES in the block «Automatic calculation of two-layer model» in the «Calculation options» we have to set limiting parameters of the search (at the beginning they are automatically set according to the minimum and maximum values of the experimental VES curve, in the future they can be changed by the user), the probability of errors p_e (default value 0.05) and reliability of the calculation λ (default value 99%). It should be noted that with decreasing p_e and increasing λ the calculation time will increase.

Start of the procedure occurs when you click «Calculation» button or «Space» on the keyboard, and graphical display of the VES curve – when selecting the corresponding component «CheckBox» for each model of soil.

In the block «Results» the software displays obtained values of model parameters calculation (ρ_1, ρ_2 and h_1), and maximum deviation of calculation results from the experimental data δ and the reliability of the model γ (accepted values of these parameters are selected under the terms of the problem solved, recommended values are $\delta \le 10$ % and $\gamma \le 95$ %). If you obtained too much value of δ or low γ, then the options to improve the accuracy of calculation are:

– to increase limiting values of the search parameters in the section «Calculation options»;

– reducing the probability of error p_e and (or) to increase the reliability of the calculation λ;

– to delete clearly erroneous error point from the block «Initial data» if it does not meet the trends of placement of the experimental VES curve.

Conclusions.

1. The authors developed the algorithm of the software operation the feature of it is the possibility of interpreting the VES results interactively or automatically as two-, three- and four-layer soil.

2. The program is implemented for interpretation of the VES results based on a mathematical model to determine

the potential of the electric field of a point current source located in a four-layer half-space.

3. The developed program «VEZ-4A» can cover about 98% of soils in the locations of energy facilities in Ukraine.

The program for interpreting the results of the VES has been successfully used in the conducting electromagnetic diagnosis of grounding systems state for 10 substation of the voltage class of 150 kV, 20 substations of the voltage class 110 kV and substation ВРП-750 kV of the Rivne NPP in 2015-2016.

REFERENCES

1. *Natsional'nyy standart Ukrayiny. SOU 31.2-21677681-19:2009. Viprobuvannya ta kontrol' prystroyiv zazemlennya elektroustanovok. Tipova instruktsiya.* [National Standard of Ukraine SOU 31.2-21677681-19:2009. Test and control devices, electrical grounding. Standard instruction]. Kyiv, Minenergovugillya Ukrayiny Publ., 2010. 54 p. (Ukr).

2. Koliushko D.G., Rudenko S.S., Koliushko G.M. Analysis of electrophysical characteristics of grounds in the vicinity electrical substation of Ukraine. *Electrical engineering & electromechanics*, 2015, no.3, pp. 67-72. (Rus). **doi: 10.20998/2074-272X.2015.3.10.**

3. Shevnin V.A., Kolesnikov W.P. Rating depth VES for the uniform and layered medium. *Electronic Journal «GEORazrez»*, 2011, no.1(8), pp. 1-9. Available at: http://www.georazrez.ru/download/2011/08/Shevnin-Otcenka_glubinnosti_VEZ.pdf (Accessed 10 November 2013). (Rus).

4. Burgsdorf V.V., Yakobs A.I. *Zazemlyayushchie ustroystva elektroustanovok* [Grounding device of electrical installations]. Moscow, Energoatomizdat Publ., 1987. 400 p. (Rus).

5. Koliushko D.G., Rudenko S.S. Interpretation the results of the vertical electrical sounding as the geoelectrical half space with four layer. *Bulletin of NTU «KhPI»*, 2015, no.12(1121), pp. 324-329. (Rus).

6. Koliushko G.M., Koliushko D.G., Rudenko S.S. On the problem of increasing computation accuracy for rated parameters of active electrical installation ground grids. *Electrical engineering & electromechanics*, 2014, no.4, pp. 65-70. (Rus). **doi: 10.20998/2074-272X.2014.4.13**.

7. Petkov A.A., Koliushko D.G., Link I.Y. Determination of parameters two-layer model of ground on the results for the vertical electric sounding conducted in the vicinity of substation. *Electrification and automation of agriculture*, 2004, no.2(7), pp. 3-11. (Ukr).

Received 06.04.2017

D.G. Koliushko[1], *Candidate of Technical Science, Senior Research Associate*
S.S. Rudenko[1], *Research Associate,*
[1] National Technical University «Kharkiv Polytechnic Institute», 2, Kyrpychova Str., Kharkiv, 61002, Ukraine,
e-mail: nio5_molniya@ukr.net

How to cite this article:
Koliushko D.G., Rudenko S.S. A computer program for interpretation of the data of vertical electrical sounding VEZ-4A. *Electrical engineering & electromechanics*, 2017, no.3, pp. 63-66. **doi: 10.20998/2074-272X.2017.3.09.**

UDC 621.311 **doi: 10.20998/2074-272X.2017.3.10**

Y.I. Sokol, Yu.A. Sirotin, T.S. Ierusalimova, O.G. Gryb, S.V. Shvets, D.A. Gapon

NETWORK-CENTRIC TECHNOLOGIES FOR CONTROL OF THREE-PHASE NETWORK OPERATION MODES

Purpose. The development of the control system for three-phase network is based on intelligent technologies of network-centric control of heterogeneous objects. The introduction of unmanned aerial vehicles for monitoring of three-phase network increases the efficiency of management. Methodology. The case of decomposition of the instantaneous capacities of the fixed and variable components for 3-wire system. The features of power balance for the different modes of its functioning. It should be noted that symmetric sinusoidal mode is balanced and good, but really unbalanced, if the standard reactive power is not zero. To solve the problem of compensation is sufficient knowledge of the total value of the inactive components of full power (value of the inactive power) without detail. The creation of a methodology of measurement and assessment will require knowledge of the magnitudes of each inactive component separately, which leads to the development of a unified approach to the measurement and compensation of inactive components of full power and the development of a generalized theory of power. Results. Procedure for the compensation of the current of zero sequence excludes from circuit the source, as the active component of instantaneous power of zero sequence, and a vector due to a current of zero sequence. This procedure is performed without time delay as it does not require integration. Only a 3–wire system with symmetrical voltage eliminates pulsations and symmetrization of the equivalent conductances of the phases of the task. Under asymmetric voltage, the power is different, its analysis requires the creation of a vector mathematical model of the energy processes of asymmetrical modes of 3–phase systems. Originality. The proposed method extends the basis of the vector method for any zero sequence voltages and shows that the various theories of instantaneous power three wired scheme due to the choice of a basis in a two-dimensional subspace. Practical value. The algorithm and software implementation for the decomposition of the zero sequence current, which allocated the procedure of obtaining null-balanced vectors of phase and interfacial voltage, calculation of active and inactive instantaneous power is zero balanced mode. The simulation results obtained in the software package Matlab by the method of visual programming in Simulink. References 9, figures 5.

Key words: **network-centric control, unmanned aerial vehicle, losses, quality, monitoring, instantaneous power.**

Интеграция интеллектуальных и сетецентрических технологий в процесс управления режимами работы трехфазной сети обеспечивают оперативность компенсации нелинейностей в системе за счет ортогонального разложения тока и использования метода базисных функций для минимизации потерь. Библ. 9, рис. 5.

Ключевые слова: **сетецентрическое управление, беспилотный летательный аппарат, потери, качество, мониторинг, мгновенная мощность.**

Introduction and problem definition. System processes of intellectualization of Ukrainian electric power system are based on the introduction of Smart Grid technologies. The value of this technological transformation is to redistribute the demand for electric power at the moments of maximum load, to reduce additional investments in the reorganization of the power system in order to increase its productivity [1]. Multilevel development of the control system of the operation modes of a three-phase network implies the use of the principle of network-centricity – the control of heterogeneous objects of the energy system infrastructure in a single information and communication management space due to the formation and maintenance of a single integrated contextual information environment for all tiers [2].

The concept of network-centric control of the modes of operation of a three-phase network implies the formation and maintenance in the actual state of a single image of the real state in the most understandable and simple form for the whole system. One of the ways to achieve these management objectives is to introduce into the system of operational maintenance of the power system [1], in addition to the distributed subsystem of digital measuring modules, a group of unmanned aerial vehicles (UAV) for monitoring the state of a three-phase network [3]. Multi-agent technologies for the collection and transmission of information using UAVs ensure the continuity of acquisition and the relevance of the contextual information image of the three-phase network.

Reactivity, asymmetry and nonlinearity of load in a three-phase system lead to the presence of inactive components of the total power and causes not only additional losses of electricity, but also causes the appearance of pulsations of instantaneous power (IP) – the energy non-equilibrium of the system. This causes a decrease in the efficiency, it contributes to the occurrence of dangerous resonance phenomena during the operation of the equipment.

Analysis of recent investigations and publications. The efficiency of the use of electric energy is determined mainly by the creation of such conditions for its consumption, under which the required quality of electric energy supply is provided with minimal losses [4, 5]. The quality of electricity supply can significantly affect the power consumption, reliability of the power supply system [6]. Exceed of the quality indicators of electric energy above the permissible leads to a reduction in the service life of the equipment, a decrease in its efficiency and a violation of the technological process. Minimization of losses in the 3-phase system is significantly associated with the possibility of reducing additional losses that are caused by consumption nodes with asymmetric and non-linear loads [7].

The goal of investigations is the development of methods for compensating the inactive component of instantaneous power in the presence of an asymmetric load under conditions of network-centric control of the operating modes of a three-phase network.

Main materials of investigations. A 3-wire circuit is a special case of the 4-wire circuit. The introduced definitions of unbalanced (balanced, really balanced) and unbalanced (balanced) modes remain valid for the 3-wire scheme. However, IP of 0-balanced processes are used to classify modes.

In a 3-wire circuit:

– the active instantaneous power is fully determined by 0-balanced current and voltage processes

$$p(t) = p_!(t) = i_!^{\bullet} u_!,$$

– the vector IP coincides with its 0-component

$$q(t) = q_0(t) = q_0(t)e_0$$

and is fully determined by $q_0 = q_0(t) = [i \times u]^{\bullet} e_0$ algebraic projection of the vector IP onto the unit vector e_0 which we call a scalar inactive IP.

The decomposition of instantaneous powers into constant and variable components for:

– active IP:

$$\overline{p}_! = \frac{1}{T}\int_{\tau}^{\tau+T} p_!(t)dt; \quad p_!(t) = \overline{p}_! + \widetilde{p}_!(t), \tag{1}$$

where $\tau \geq 0$ is the arbitrary number;

– inactive (scalar) IP:

$$\overline{q}_0 = \frac{1}{T}\int_{\tau}^{\tau+T} q_0(t)dt; \quad \widetilde{q}_0(t) = q_0(t) - \overline{q}_0, \tag{2}$$

classify processes in a 3-wire circuit.

If active IP has no variable (pulsed) component $\widetilde{p}_!(t) \equiv 0$, then mode is balanced. In the general caseB общем случае $\widetilde{p} = p(t) - \overline{p} \neq 0$ and the mode is unbalanced.

As $q(t) = q_0(t) = q_0(t)e_0$, then the mode:

– at which inactive IP has no variable component $\widetilde{q}_0 = \widetilde{q}_0(t) \equiv 0$ is balanced;

– at which the inactive IP is identically equal to zero $q_0(t) \equiv 0$ is really balanced.

Note that the symmetric sinusoidal mode is balanced and balanced, but it is really unbalanced if the standard reactive power is not zero.

Decomposition of current in a 4-wire network with the isolation of zero sequence (ZS). For a 4-wire circuit, the decomposition of the current $i=i_0+i_!$ is valid The basis curves $w_1(t)$, $w_2(t)$ of processes in 3-wire circuit which are used for the decomposition of the current components, are complemented by the unit vector of the ZS.

The voltage vector u (measured with respect to an arbitrary reference point) defines two orthogonal 0-balanced vectors:

– the vector of phase voltages (using a projector matrix $u_! = D_! \times u$) and

– the vector of phase-to-phase voltages (using a skew-symmetric matrix $u_{||} = K^{\bullet} \times u_!$).

At each moment of time, the triple of vectors: $w_1(t)$, $w_2(t)$, e_0 forms an orthonormal basis of the space $S^{(3)}$, since the following orthonormality condition is valid:

$$\begin{bmatrix} w_1^{\bullet} \\ w_2^{\bullet} \\ - \\ e_0^{\bullet} \end{bmatrix} \times [w_1 w_2 \mid e_0] = \begin{bmatrix} w_1^{\bullet} w_1 & w_1^{\bullet} w_2 & w_1^{\bullet} e_0 \\ w_2^{\bullet} w_1 & w_2^{\bullet} w_2 & w_2^{\bullet} e_0 \\ e_0^{\bullet} w_1 & e_0^{\bullet} w_2 & e_0^{\bullet} e_0 \end{bmatrix} = \begin{bmatrix} 1 & 0 & 0 \\ 0 & 1 & 0 \\ 0 & 0 & 1 \end{bmatrix}. \tag{3}$$

The orthogonal current decomposition is valid:

$$i(t) = \underbrace{i_1 w_1 + i_2 w_2}_{i} + \underbrace{i_0 w_0}_{i_0} = \underbrace{(i^{\bullet} w_1)}_{i_1} w_1 + \underbrace{(i^{\bullet} w_2)}_{i_2} w_2 + i_0(t) e_0 \tag{4}$$

because $i=i_!+i_0$, and $i_0 \perp u_!$; $i_0 \perp u_{||}$, then for the decomposition (4) coefficients is valid the following:

$$i_1 = i^{\bullet}\, w_1 = (i_! + i_0)^{\bullet} \times \frac{u_!}{|u_!|} = \frac{i_!^{\bullet} u_!}{|u_!|} = \frac{p_!}{|u_!|}; \tag{5}$$

$$i_2 = i^{\bullet}\, w_2 = (i_! + i_0)^{\bullet} \times \frac{u_{||}}{|u_{||}|} = \frac{i_!^{\bullet}(u_! \times e_0)}{|u_!|} = \frac{e_0(i_! \times u_!)^{\bullet}}{|u_!|} = \frac{q_0(t)}{|u_!|}; \tag{6}$$

$$i_0(t) = i^{\bullet} e_0. \tag{7}$$

Therefore, the decomposition (4) is obtained from the decomposition for the 3-wire circuit

$$i_0 = i_1 + i_2 = \frac{p_!(t)}{u_!} w_! + \frac{q_0(t)}{u_!} w_{||}, \tag{8}$$

by additional term (7) . This gives decomposition of the current for a 4-wire circuit (Fig. 1) in vector-matrix form:

$$i(t) = i_1 + i_2 + i_0 = \begin{bmatrix} w_! & w_{||} & e_0 \end{bmatrix} \times \begin{bmatrix} p_!(t)/u_! \\ q_0(t)/u_! \\ i_0(t) \end{bmatrix}, \tag{9}$$

$$u_! \neq 0.$$

Decomposition is valid at any voltage $u_0(t)$ of 0-sequence.

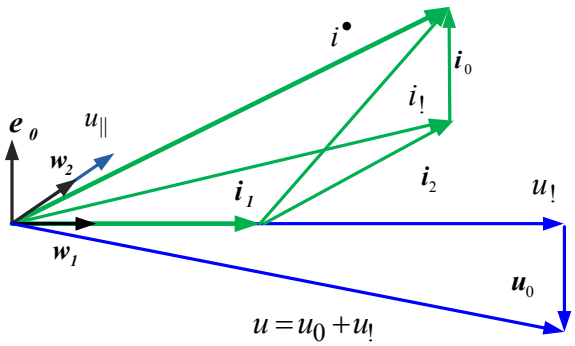

Fig. 1. Current and voltage decomposition in the 4-wire system ($u_0||e_0$)

As $p_0=u_0 \cdot i_0$, then compensation of current of 0-sequence always compensate power of 0-sequence ($i_0=0 \Rightarrow p_0=0$). The converse is not true. In addition, the part of the vector IP is also compensated.

The proposed basis method expands the vector method [8, 9] for any ZS voltage $u_0(t)$ and shows that the different theories of the IP of the 3-wire circuit are due to the choice of basis in the 2-dimensional subspace $L_!^2$.

Features of compensation by the method of basis functions. Before the compensation, the current in the

load network is equal to the current of the source $i_S(t)=i_L(t)=i(t)$ and can contain the 0-sequence current regardless of the presence ($u_0 \neq 0$) or the absence ($u_0 = 0$) of the voltage displacement.

Compensation of the current of the 0-sequence i_0 excludes from the source circuit:

– the active IP of the 0-sequence (both its constant and the variable components at any 0-sequence voltage);

– the vector IP component due to the ZS.

Moreover, this procedure is performed without delay in time, since it does not require integration. Integration and compensation of the 0-balanced current component i_2 (collinear phase-to-phase voltage) which determines the inactive IP, due to 0-balanced current and voltage processes, does not require integration. Compensation of currents $i_0(t)$ and $i_2(t)$ is equivalent to compensation of the vector IP and 0-component of active power (if $u_0 \neq 0$) and is carried out without delay in time. Compensation of active current:

$$\widetilde{i}_1 = \frac{\widetilde{p}_!(t)}{u_!} w_! = (p_!(t) - P_!)\frac{u_!}{u_!^2} \qquad (10)$$

is associated with the pulsating component of the active IP and will require integration. In addition, the expansion coefficients determine the connection of the current vector in the $\alpha\beta$ coordinates of the orthonormal basis in the 2-dimensional subspace and instantaneous powers and can be found without intermediate calculations directly using the measured instantaneous currents $i(t)$ and instantaneous stress values $u(t)$.

Algorithm and implementation of the current decomposition program

$$i(t) = \frac{p_!(t)}{u_!(t)} w_!(t) + \frac{q_0(t)}{u_!(t)} w_{||}(t) + i_0(t)e_0 \qquad (11)$$

ss determined by the following procedures:

– calculation of 0-balanced vector of phase and phase-to-phase voltage:

$$u_!(t) = D_! u(t), \quad u_{||}(t) = K^{\bullet} u(t); \qquad (12)$$

– calculation of active IP and inactive IP of 0-balanced mode:

$$p_!(t) = i^{\bullet} u_! = i^{\bullet} D_! u, \qquad (13)$$

$$q_0(t) = i^{\bullet} u_{||} = i^{\bullet} K^{\bullet} u. \qquad (14)$$

By the Simulink visual programming method the program in the Matlab package is implements. The Matlab package constructs a block diagram of the program using a palette of mathematical model components of various specified electrical power devices. The developed program also implements the current decomposition (15), the first component of which provides power supply with constant power:

$$i = \frac{P}{u_!} w_! + \underbrace{\frac{\widetilde{p}_!(t)}{u_!} w_! + \frac{q_0(t)}{u_!} w_! + i_0(t)e_0}_{\text{compensated current}}. \qquad (15)$$

– The simulation results (Fig. 2-5) represent qualitatively the energy processes in the 4-wire circuit of power supply, in particular, confirm (Fig. 2) the theoretically known behavior of the active and inactive current of pq-theory in the sine-wave mode with symmetrical voltage: the active current realizing the active IP and the reactive current realizing the vector IP (second and third pallets from above) contain a harmonic of the 3-order.

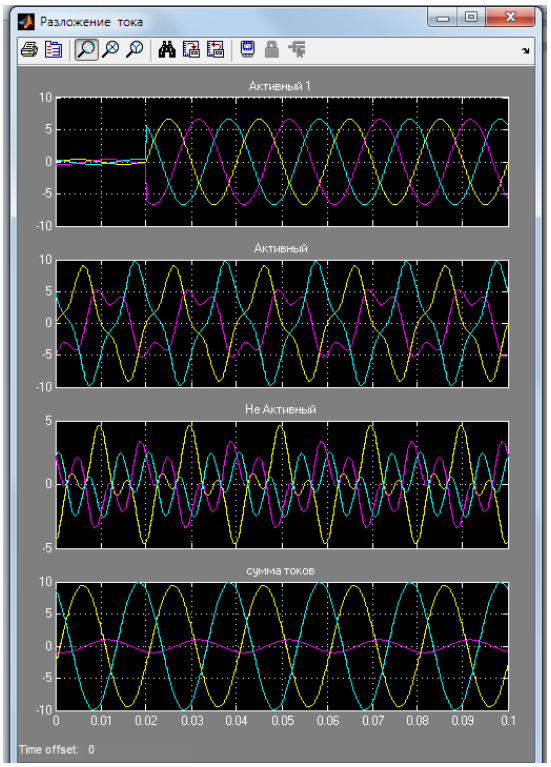

Fig. 2. Oscillograms of total current decomposition onto components

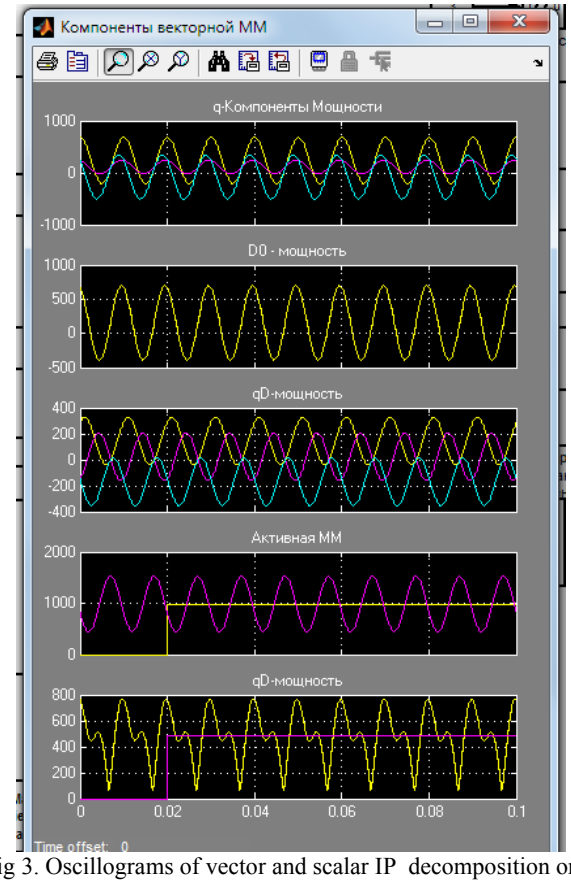

Fig 3. Oscillograms of vector and scalar IP decomposition onto components

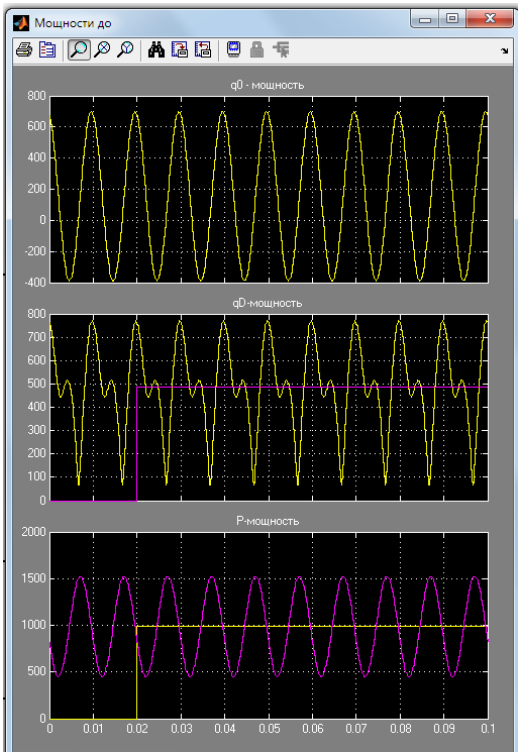

Fig. 4. Oscillograms of scalar IP and components of vector IP before compensation

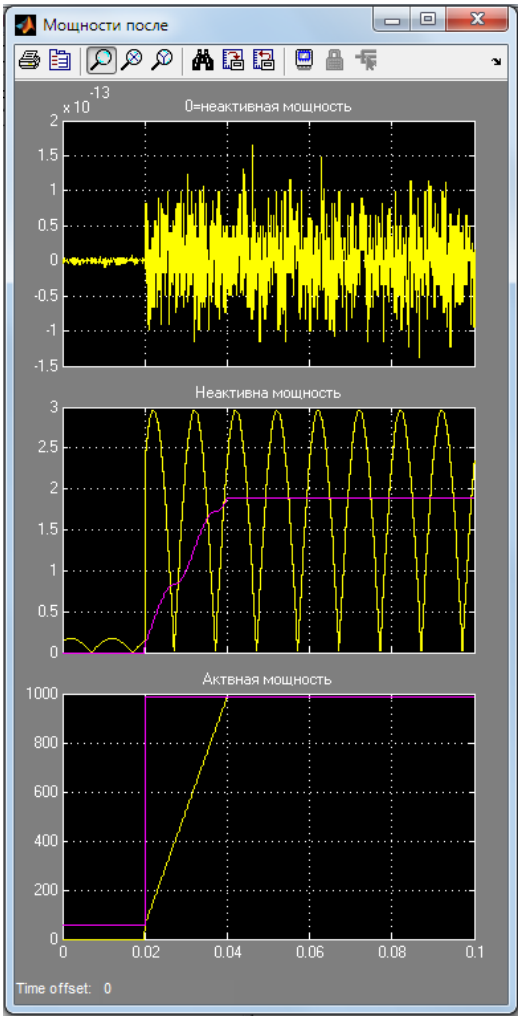

Fig. 5. Oscillograms of scalar IP and components of vector IP after compensation

The active current which realizes the integral active power:

$$i_S = u_1 \left(\frac{P}{u_1^2} \right), \qquad (16)$$

(Fig. 5, bottom pallet) and provides a mode of consumption with current in the source circuit at which:

– current is 0-balanced $i_0(t) \equiv 0 \Leftrightarrow q'(t) \equiv 0$ (middle pallet in Fig. 5);

– the mode is really balanced $q_0(t) \equiv 0$ (top pallet in Fig. 5);

– the mode is balanced $p_1(t) \equiv \overline{p}_1 = P_1$ (bottom pallet in Fig. 5).

Conclusions. Network-centric technologies for controlling the operating modes of a three-phase network using multi-agent methods for collecting and transmitting information using UAVs ensure the continuity of acquisition and the relevance of the contextual information image of the state of the power system.

The case of the decomposition of instantaneous powers into a constant and a variable component for a 3-wire system is considered. The peculiarities of the power balance for different modes of its functioning are singled out. It should be noted that the symmetric sinusoidal mode is balanced, but it is really unbalanced if the standard reactive power is not zero.

The zero sequence current compensation procedure excludes from the source circuit both the active component of the instantaneous power of the zero sequence and the vector component caused by the zero sequence current. This procedure is performed without delay in time, since it does not require integration.

To solve the compensation problem, it is enough to know the total value of the inactive components of the total power (the value of inactive power) without its detailed elaboration. The creation of a measurement and accounting methodology will require knowledge of the values of each inactive component separately, which necessitates the development of a unified approach to measuring and compensating inactive components of full power and developing a generalized theory of power. Only in a 3-wire system with symmetrical voltage, the elimination of pulsations and the symmetrization of phase conductivities are equivalent problems (the power of pulsations and the power of asymmetry of phase conductivities are equal). With unbalanced voltage these powers are different, their analysis for electrical systems requires the creation of a vector mathematical model of the energy processes of asymmetric regimes of 3-phase systems.

Unbalanced loads, which, in addition to additional losses, lead to asymmetry in the voltage and pulsation of the energy flow, cause much greater harm to the power supply than the symmetry of the reactive phase conductivities (reactive power).

REFERENCES

1. Sokol Y.I., Gryb O.G., Shvets S.V. The structural and parametrical organization of elements of a power supply system in the conditions of network centrism. *Electrical engineering &*

electromechanics, 2016, no.2, pp. 61-64. (Rus). **doi: 10.20998/2074-272X.2016.2.11.**

2. Sokol Y.I., Gryb O.G., Shvets S.V. Network centrism optimization of expeditious service of elements of the power supply system. *Electrical engineering & electromechanics*, 2016, no.3, pp. 67-72. (Rus). **doi: 10.20998/2074-272X.2016.3.11.**

3. Shvets S.V., Voropai U. G. Mariechantal aspects of the use of unmanned aerial vehicles. *Bulletin of Kharkiv Petro Vasylenko National Technical University of Agriculture*, 2016, no.176, pp. 33-34. (Ukr).

4. Denisyuk S.P. Optimization of power consumption for energy saving in systems with converters. *Problems of energy saving*, 1994, no.2-3, pp. 81-88. (Rus).

5. Prakhovnik A.V. Energy saving: unconventional look and a different strategy. *Energetic and electrification*, 2008, no.4, pp. 30-33. (Rus).

6. Shidlovsky A.K., Kuznetsov V.G. *Povyshenie kachestva elektroenergii v elektricheskikh setiakh* [Increase the power quality in electric networks]. Kyiv, Naukova Dumka Publ., 1985. 286 p. (Rus).

7. Zhezhelenko I.V., Saenko Yu.L. *Voprosy kachestva elektroenergii v elektroustanovkakh* [Issues of power quality in electrical installations]. Mariupol, PSTU Publ., 1996. 173 p. (Rus).

8. Tenti P., Mattavelli P., Tedeschi E. Compensation techniques based on reactive power conservation. *7th Int. Workshop on Power Definitionsand Measurements under Non-Sinusoidal Conditions*, Cagliari, Italy, July 2006, pp. 84-90.

9. Sirotin Yu.A. Unbalanced current and the pulsating current at asymmetrical voltage. *Tekhnichna elektrodynamika*, 2012, no.2, pp. 42-43.

Received 25.04.2017

Y.I. Sokol[1], *Doctor of Technical Science, Professor, Corresponding Member of the National Academy of Science of Ukraine,*
Yu.A. Sirotin[1], *Doctor of Technical Science, Professor,*
T.S. Iierusalimova[1], *Candidate of Technical Science,*
O.G. Gryb[1], *Doctor of Technical Science, Professor,*
S.V. Shvets[1], *Candidate of Technical Science, Associate Professor,*
D.A. Gapon[1], *Candidate of Technical Science, Associate Professor,*
[1] National Technical University «Kharkiv Polytechnic Institute», 2, Kyrpychova Str., Kharkiv, 61002, Ukraine,
phone +38 057 7076551,
e-mail: Ierusalimovat@mail.ru, dima12345ml@mail.ru, se_sx@bk.ru

How to cite this article:
Koliushko D.G., Rudenko S.S. A computer program for interpretation of the data of vertical electrical sounding VEZ-4A. *Electrical engineering & electromechanics*, 2017, no.3, pp. 67-71. **doi: 10.20998/2074-272X.2017.3.10.**